

N71-20269



GE-SSO-70SD4286
FEBRUARY 1, 1971

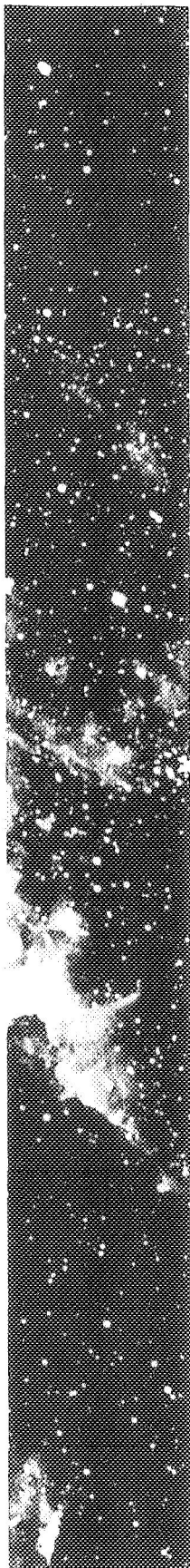
FINAL REPORT

ROLLUP SUBSOLAR ARRAY

Prepared for: Jet Propulsion Laboratory
Prepared Under: Contract 952314

CASE FILE
COPY

VOLUME I
PROGRAM SUMMARY



GENERAL  ELECTRIC

DDC
RECEIVED
APR 1971
REGISTERED
C

Report No. 70SD4286
Date: February 1, 1971

FINAL REPORT

DESIGN AND DEVELOPMENT OF
A THIRTY WATT PER POUND 250
SQUARE FOOT ROLL-UP SOLAR ARRAY

VOLUME I PROGRAM SUMMARY


Prepared for

JET PROPULSION LABORATORY
CALIFORNIA INSTITUTE OF TECHNOLOGY
4800 OAK GROVE DRIVE
PASADENA, CALIFORNIA

Prepared Under: Contract 952314
Contracting Officer: R. G. Curry
Project Manager: W. A. Hasbach

Prepared by:
N. Shepard
P. Perez
K. Hanson

Approved by:


K. L. Hanson
Project Manager

THIS WORK WAS PERFORMED FOR THE JET
PROPULSION LABORATORY, CALIFORNIA
INSTITUTE OF TECHNOLOGY AS SPONSORED
BY THE NATIONAL AERONAUTICS AND SPACE
ADMINISTRATION UNDER CONTRACT NAS7-100

GENERAL  ELECTRIC

SPACE SYSTEMS ORGANIZATION

Valley Forge Space Center

P. O. Box 8555 • Philadelphia, Penna. 19101

"This report contains information prepared by the General Electric Co., Space Systems Organization, under JPL Sub-contract. Its content is not necessarily endorsed by the Jet Propulsion Laboratory, California Institute of Technology, or the National Aeronautics and Space Administration."

ABSTRACT

This report summarizes the results of a program to develop the technology of the rollup solar array concept. A detailed design of a 250 square foot unit providing 31.3 watts per pounds was developed and supporting analysis completed. A full scale engineering development unit was fabricated and subjected to a series of system tests consisting of deployments, deployed dynamics, stowed vibration, stowed pyrotechnic shock, stowed acoustic, and stowed and deployed thermal vacuum. Components tests of the deployable boom, thermal bending of the boom, structural tests of the blanket elements, the boom, and the bearing assembly were carried out.

TABLE OF CONTENTS

<u>Section</u>	<u>Page</u>
1.0 SUMMARY	1-1
2.0 INTRODUCTION	2-1
3.0 TECHNICAL DISCUSSION	3-1
3.1 Description of System	3-1
3.1.1 General Description	3-1
3.1.2 Array Blankets	3-2
3.1.3 Solar Panel Actuator	3-13
3.1.4 Slip Ring Assembly	3-15
3.1.5 Structural Components	3-15
3.1.6 Mass Properties Summary	3-22
3.2 System Performance	3-26
3.2.1 Predicted Electrical Performance	3-26
3.2.2 Performance During System Test Cycle	3-29
3.3 Systems Tests	3-47
3.3.1 Deployed Dynamics Test	3-47
3.3.2 Environmental Tests	3-51
3.3.3 Bi-Stem Life Demonstration	3-79
3.4 Development Tests	3-80
3.4.1 Bi-Stem Thermal Bending Test	3-80
3.4.2 Module Thermal Cycling Test	3-84
3.4.3 Blanket Tracking With A Lateral Offset	3-88
3.4.4 Array Structural Load Deflection Test	3-88
3.4.5 Dummy Cell Module Stiffness Evaluation	3-97
3.5 Problems and Lessons Learned	3-101
4.0 CONCLUSIONS	4-1
5.0 RECOMMENDATION	5-1
6.0 NEW TECHNOLOGY	6-1
7.0 REFERENCES	7-1

LIST OF ILLUSTRATIONS

	<u>Figure</u>	<u>Page</u>
1-1	Rollup Solar Array Configuration (coordinate System Shown)	1-4
1-2	Overall Program Schedule	1-6
3.1-1	RA 250 Assembly	3-3/4
3.1-2	RA 250 Prototype Test Model	3-5
3.1-3	Module Details	3-7/8
3.1-4	Active Module Locations on Prototype Blankets	3-10
3.1-5	Array Blankets	3-11
3.1-6	EOS Module Mounted on -Y Blanket Assembly	3-11
3.1-7	Heliotek (near) GE No. 2 (middle) and Boeing (far) Modules Mounted on -Y Blanket Assembly (VF70127E)	3-12
3.1-8	GE No. (left) and Centralab No. 1 (right) Modules Mounted on -Y Blanket Assembly (VF70127C)	3-12
3.1-9	Solar Panel Actuator	3-14
3.1-10	The BI-STEM Principle	3-17
3.1-11	Slip Ring Assembly (VF70731)	3-17
3.1-12	Inboard End Cop Assembly	3-19
3.1-13	Outboard End Support (VF7015C)	3-19
3.1-14	Center Support	3-23
	a. Component (VF7068)	
	b. Assembly (VF70157B)	
3.2-1	Nominal Subsolar Array I-V Curve	3-27
3.2-2	Damage in J6 Module	3-34
3.2-3	Damage in H1 Module	3-35
3.2-4	Fractured Cell at Foot in G7 Module	3-37
3.2-5	Electrical Performance (From Ryan Solar Array Program Report)	3-39
3.2-6	BI-STEM Limit Switch Actuator Problem	3-43/44
3.3-1	Deployed Dynamics Test Set-Up	3-50
3.3-2	Deployed Dynamics Test Data Flow	3-52
3.3-3	Mode Shape - First Mode Out-Of-Plane Symmetric Excitation	3-55
3.3-4	Predicted Response at Outboard Edge of Blanket (80% Span) Out-Of-Plane Symmetric Excitation	3-58
3.3-5	Results of Narrow Band Frequency Sweep	3-59
3.3-6	Shock Pulse	3-61
3.3-7	Comparison of Various Spacecraft Separation Shock Spectra With the RA 250 Specification and Realized Shock Spectra	3-63
3.3-8	Deployed Transient Temperature History	3-66
3.3-9	Outboard End Support Showing Fractured Separation Nut Mounting Base (VF 70244B)	3-68
3.3-10	Both Separation Nuts with Fractured Mounting Bases (VF70244C)	3-69
3.3-11	Stowed Transient Temperature History	3-71

<u>Figure</u>	<u>Page</u>
3.3-12 View of the Rollup Solar Array Installed in the Acoustic Chamber (C70-0115-A)	3-73
3.3-13 Spectrogram of Input Acoustic Field During Run 3	3-74
3.3-14 Specified Qualification Level Vibration Environments (from Reference 1.2)	3-76
3.4-1 Thermal Bending Test Set-Up (NASA G-69-4536)	3-81
3.4-2 Idealized Tip Deflection Patterns	3-83
3.4-3 Extrapolated Absolute Zero-G Thermal Bending at 33.5 ft ²	3-84
3.4-4 Thermal Cycling Module Test Set-Up	3-86
3.4-5 Typical Active Module Temperature Profile	3-87
3.4-6 Schematic of Tracking Demonstration Test Set-Up	3-89
3.4-7 Rewrap Against Edge Guide	3-90
3.4-8 Load Deflection Tests	3-91
3.4-9 Test Arrangements	3-92
3.4-10 Results of Test 1A, Symmetric Loading in X-Direction	3-93
3.4-11 Results of Test 2A, Antisymmetric Loading in X-Direction	3-93
3.4-12 Results of Test 3A, Symmetric Loading in Z-Direction	3-94
3.4-13 Results of Test 4A, Antisymmetric Loading in Z-Direction	3-94
3.4-14 Solar Cell Module Deflection Test Set-Up	3-96
3.4-15 Face Down Deflection Test - Active Solar Cell Module No. 1 with 5 Gram Load	3-98
3.4-16 Face Up Deflection Test - Active Solar Cell Module No. 1 with 15 Gram Load	3-98
3.4-17 Load Deflection Curves	3-99
3.4-18. Load Deflection Curves - Transverse Curvature	3-100

SECTION 1

SUMMARY

This document contains a detailed summary of the work performed under JPL Contract 952314, Design and Development of a Thirty Watt Per Pound 250 Square Foot Rollup Solar Array. The program objective was to develop the technology of the rollup solar array concept by preparing a detailed design, performing the associated analyses, fabricating an engineering development model, and subjecting the engineering model to a comprehensive test program consisting of both environmental and development tests. The design concept was based on the results of feasibility studies described in Reference 1-1. The environmental and test requirements are given in JPL Specification No. SS501407, Revision E. (Reference 1-2).

This final report has been organized into two volumes for the reader's convenience. The first volume contains a summary of the total program and the most significant results. The second volume contains a detailed discussion of the last four months of the program which included the final assembly of the engineering unit and the system test program. Detailed discussion of the initial portion of the program was given in the quarterly reports, References 1-3, 1-4, 1-5 and 1-6. As an aid to the reader the major contents of the quarterly reports are as follows:

1. Quarterly Report No. 1 (Reference 1-3)
 - a. Design Requirements Summary
 - b. Electrical Performance of the Array
 - c. Bearing, Lubricant, and Spring Motor Selection
 - d. Results of Thermal Cycling Tests of Array Segments

2. Quarterly Report No. 2 (Reference 1-4)
 - a. Detail Design Description of System and Components
 - b. Thermal Analysis and Results
 - c. Deployed Dynamics Analysis (Out of Plane)
 - d. Stowed Structural Analysis (Initial)
 - e. Magnetic Field Analysis
 - f. Reliability Analysis
 - g. Blanket Stiffness Measurements
 - h. Formulation of a Mathematical Model for Deployed Array Blankets
 - i. Stress Analysis Data Sheets

3. Quarterly Report No. 3 (Reference 1-5)
 - a. Design Details for Engineering Prototype
 - b. Out of Plane Deployed Dynamics Analysis Results
 - c. Test Equipment Design Descriptions
 - d. Structural Element Models of the Solar Array Blanket for In Plane Dynamics Analysis

4. Quarterly Report No. 4 (Reference 1-6)
 - a. Description of Active Solar Cell Modules on Test Blankets
 - b. Results of Deployed Dynamics Analysis for Test Condition (1g field)
 - c. Development Test Results
 - (1) Bi-Stem Thermal Bending
 - (2) Module Thermal Cycling
 - (3) Array Structure Load Deflection Test
 - (4) Test Planning

In general, details presented in the quarterly reports are not repeated in this final report, but are referenced. However, it is intended that sufficient information be included in this final report so that it be a complete report and that access to the quarterly reports is not required to determine the general results. The goal of the report is to provide the reader with an assessment of the state of the art achieved by the program and to include data which can be used to extrapolate the design to meet new requirements with respect to size, dynamic characteristics, envelope restrictions and environments. Recommendations with respect to system testing and vehicle integration are given. Problems, both solved and unsolved, are discussed.

The goal of the program was to advance the state of the art of solar arrays for future space missions in which the power requirement is greater than present scientific spacecraft and lighter weight and decreased stowed volume are needed. The configuration was developed in the feasibility study and is shown in Figure 1-1. The unit is made up of two storage drums mounted on a center support structure. Each drum has a bearing system, a slip ring assembly for the transfer of power and signals, and a Negator spring motor that provides a constant tension in the solar array blanket. A deployable boom is mounted on the center support and attached to a leading edge member. The solar array blanket consists of an interconnected assembly of cells mounted on a flexible substrate to form a solar array blanket. A blanket is rolled onto each drum, with the outboard edge attached to the leading edge member. The system is deployed by extending the boom. The deployed boom and the leading edge member comprise the primary structure. Each blanket is under tension from the Negator springs. Outboard end supports are provided in the launch configuration and are pyrotechnically released before deployment. The model spacecraft used as a baseline for the feasibility study was an interplanetary vehicle with a square cross section as shown. Four arrays were mounted on the vehicle

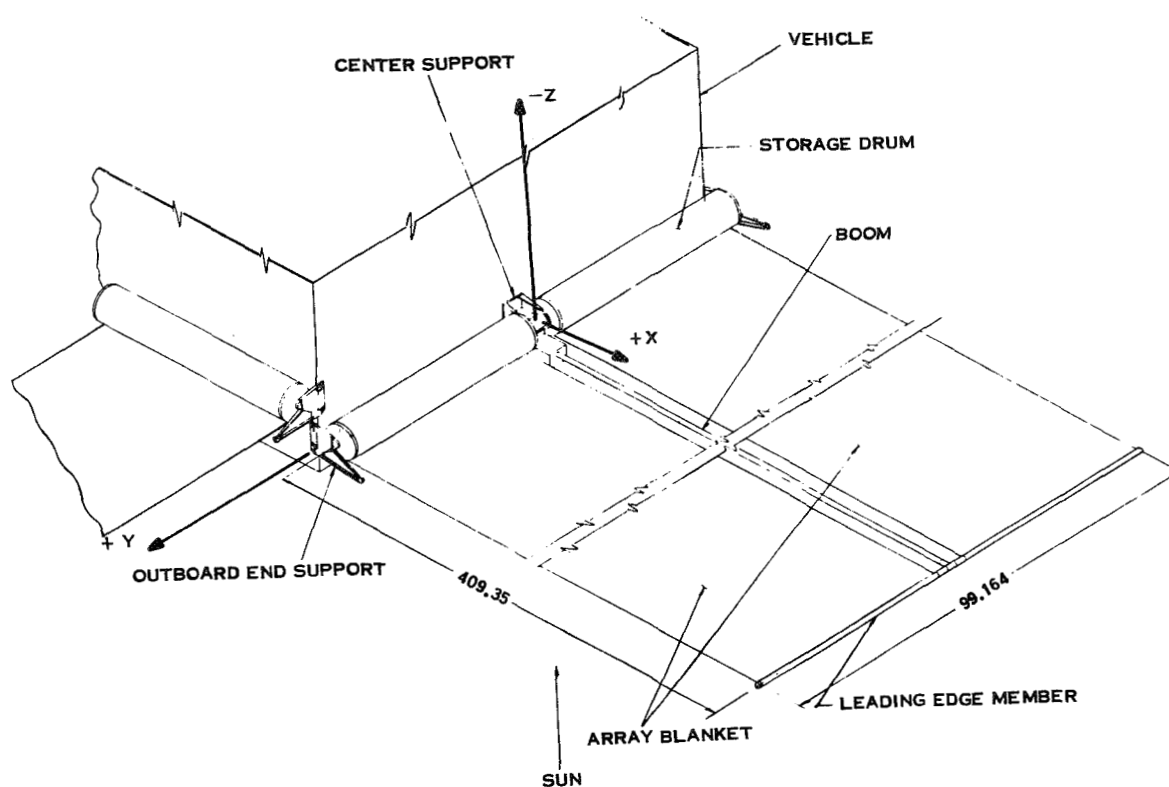


Figure 1-1. Rollup Solar Array Configuration (Coordinate System Shown)

which was oriented with respect to the sun. The vehicle concept was for reference only and the array design is intended to be adaptable to a variety of vehicle configurations and missions. Weight was a primary consideration in all design decisions and tradeoffs.

A summary program schedule is shown in Figure 1-2. The first activities in the program were to prepare a detailed design for a flight system and a design for test blankets approximately 10 percent covered with live solar cells. The design effort was supported by analysis as required. The vibration environment was more severe than had been used in the Feasibility Study and an intensive design and analysis effort was required to accommodate the environment and meet the program weight goal. Test planning and design of the test equipment was initiated at about the mid-point of the array design period. Compensation for gravity forces, measurements of the

low frequency vibration of the deployed array in a vacuum chamber, and the thermal vacuum test involving array deployment resulted in unusual test requirements so significant effort was devoted to test planning and test equipment design. Supporting analysis was provided to aid test planning and predict test results. The test program was initiated with an inspection and performance test designed to evaluate the status of the system. This test, denoted a health check, was performed after each major test.

The major tests were:

1. Deployed Dynamics
2. Pyrotechnic Shock
3. Thermal Vacuum
4. Acoustic Environment
5. Stowed Vibration

The final test activity was a 42-cycle deployment/retraction sequence intended to demonstrate the capability of the system to perform multiple deployments in a mission. Development tests of the components and other system elements were performed as required during the mission.

Overall program results are summarized in Section 4 CONCLUSIONS. The weight goal of a baseline performance of 30 watts per pound was exceeded. The engineering unit was fabricated and tested. The array survived the environmental test program although there were anomalies. These are discussed in the body of the report.

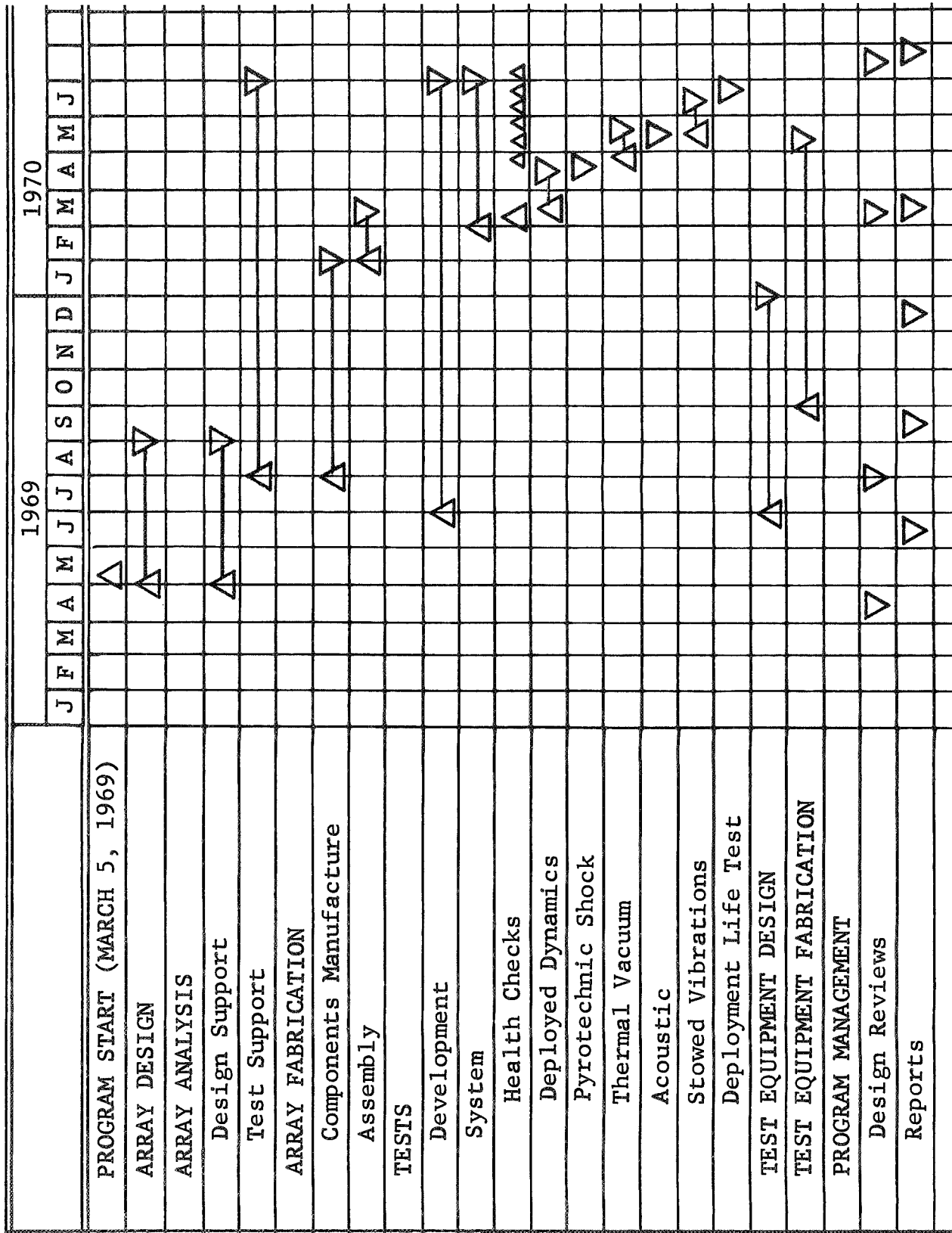


Figure 1-2. Overall Program Schedule

SECTION 2
INTRODUCTION

The results of the program to develop the technology of a 250 square foot rollup solar array are summarized in Volume I. It includes a description of the system design, and describes system performance, both before and after the system test program. The systems and development test program results are described. Summary results such as conclusions and recommendations are included.

Volume 2 includes a detailed discussion of the system test program. The tests are treated in the order they were run and test equipment and special test procedures are included as appropriate. Comparisons of experimental and analytical results are included.

SECTION 3

TECHNICAL DISCUSSION

3.1 DESCRIPTION OF SYSTEM

3.1.1 GENERAL DESCRIPTION

The Rollup Subsolar Array which was designed, fabricated and tested during the program provides 250 square feet of deployed solar cell module area which is stored on drums during launch. Hereinafter this unit is referred to as the RA250. The schematic arrangement of the system in the deployed configuration is shown in Figure 3.1-1. Solar cells are mounted on two flexible substrates of Kapton-H film (each panel is 46 by 402 inches). Tension in each substrate is utilized to maintain the desired single plane geometry and to establish the natural frequency of the deployed system above the required 0.04 Hz. Six major elements make up the RA250 system:

1. Array blankets
2. Single BI-STEM solar panel actuator
3. Storage drums
4. Center support
5. Leading edge member
6. Outboard end supports

Figure 3.1-1 shows the assembly of these various components to form the system.

The RA250 engineering test model is representative of a flight-type design, except for the limited solar cell coverage. A total of 4000 solar cells were bonded

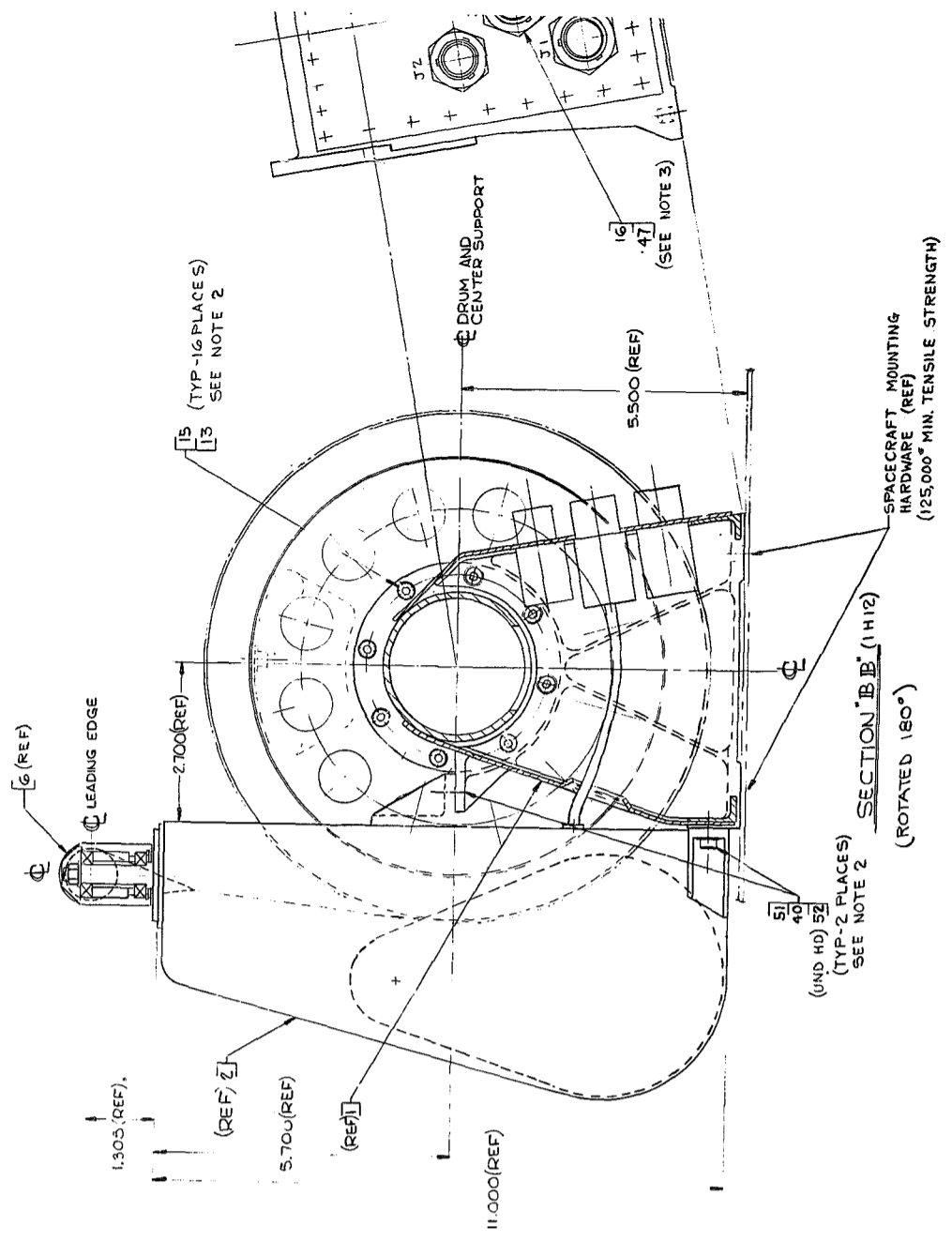
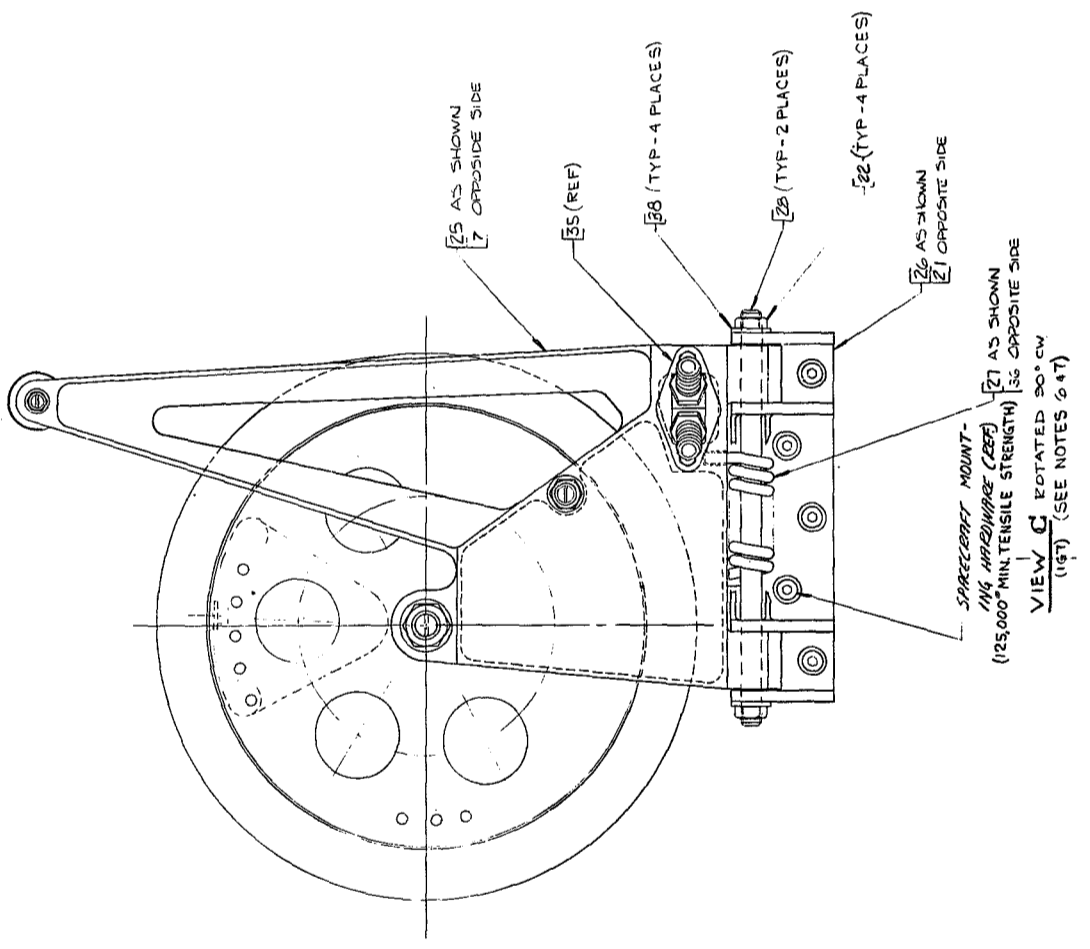
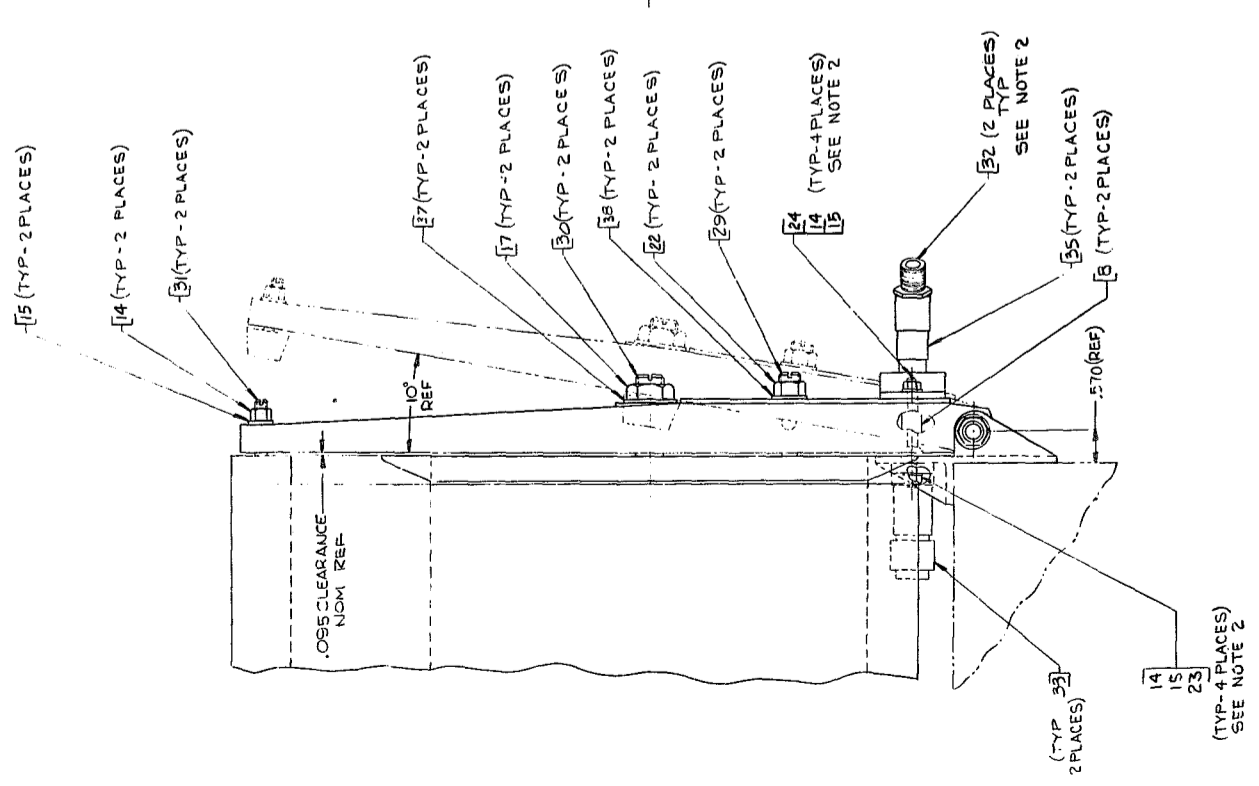
to the substrates with the remaining area occupied by glass platelets which simulated the solar cell mass and interconnect bending stiffness.

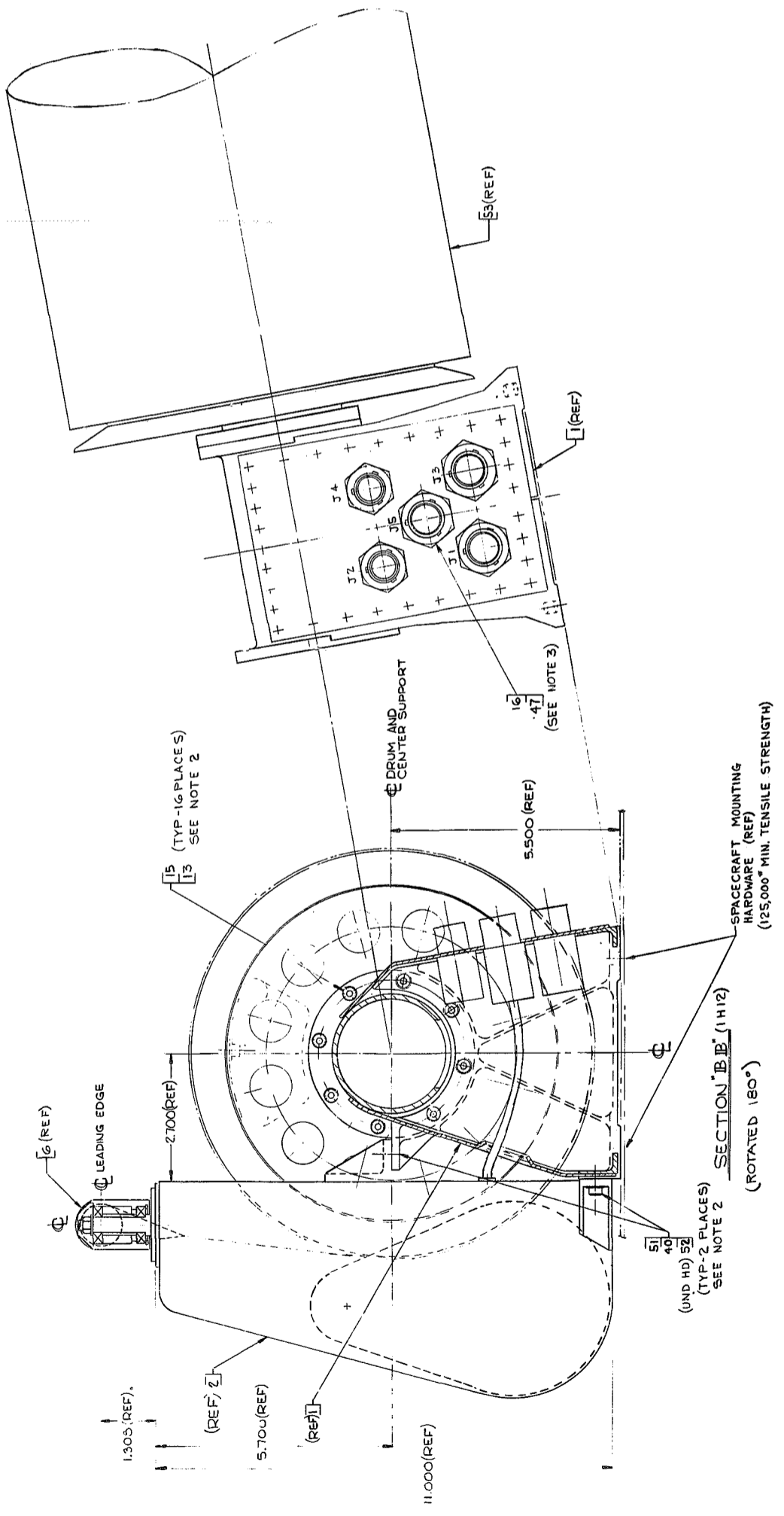
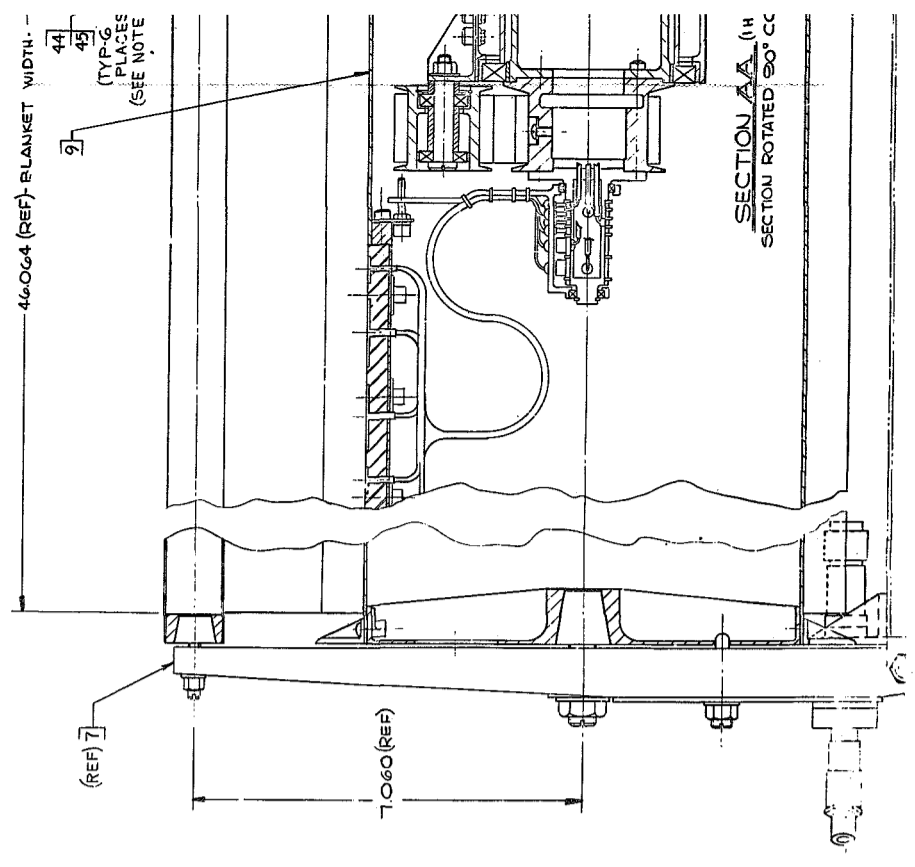
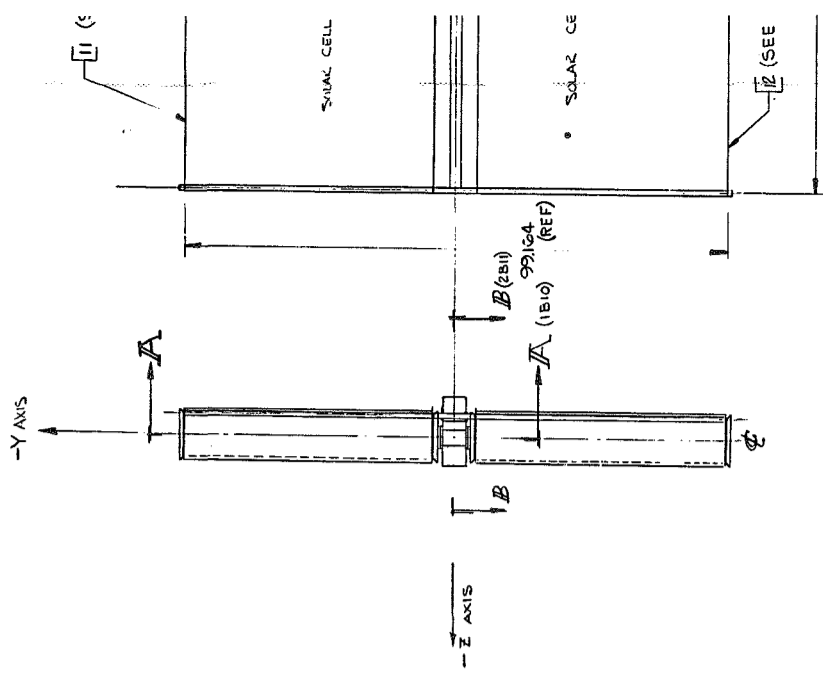
Figure 3.1-2 pictures this model in both the stowed and the fully deployed configuration.

3.1.2 ARRAY BLANKETS

The RA250 flight design consists of two blankets each 46 inches wide by 402 inches long, with end leaders extending beyond the cells at both ends. Each blanket carries six circuits each of 242 cells in series by 19 cells in parallel. Each circuit is composed of twelve series-connected modules (eleven with 20 series by 19 parallel and one with 22 series by 19 parallel). These modules are bonded to a 2 mil Kapton-H film substrate. This substrate is fabricated from copper-clad Schjel-Clad L-7510 which is etched to form a conductor bus strip river-tributary system, with each circuit feeding into the main positive and negative bus which in turn connects to the power feedthrough at the drum. Additional bus strip runs were added to the substrate to enable installation of high-and-low temperature range thermistors on the panel. These also connect to the feed-through section of the drum and the signal slip rings. All connections from the cell side of the substrate to the bus strip system are made around the edges rather than through holes in the substrate. These connections are made with Schjel-Clad L-7510 which is bonded to the Kapton substrated with SMRD-745* adhesive and soldered to the solar cell modules on the front and the bus strips on the rear. The exposed copper bus strips on the rear side of the substrate are covered with Kapton silicone adhesive pressure sensitive tape. Foamed RTV 560 cushioning buttons are deposited on the rear side of the

* SMRD-745 is a flexible epoxy formulated by General Electric Co., Space Systems. It is available from Space Systems on a special order basis.





AS SHOWN OPPOSITE SIDE
 (REF)
 8 (TYP-4 PLACES)
 28 (TYP-2 PLACES)
 22 (TYP-4 PLACES)
 100N
 25N1E SIDE

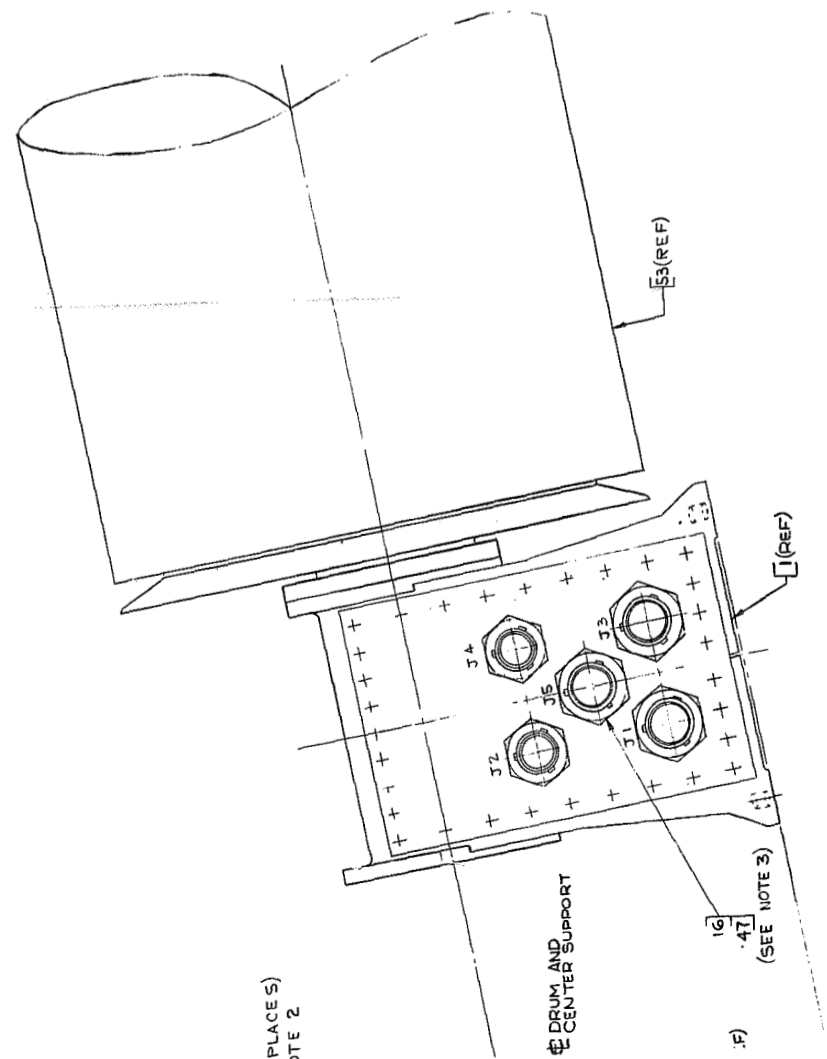
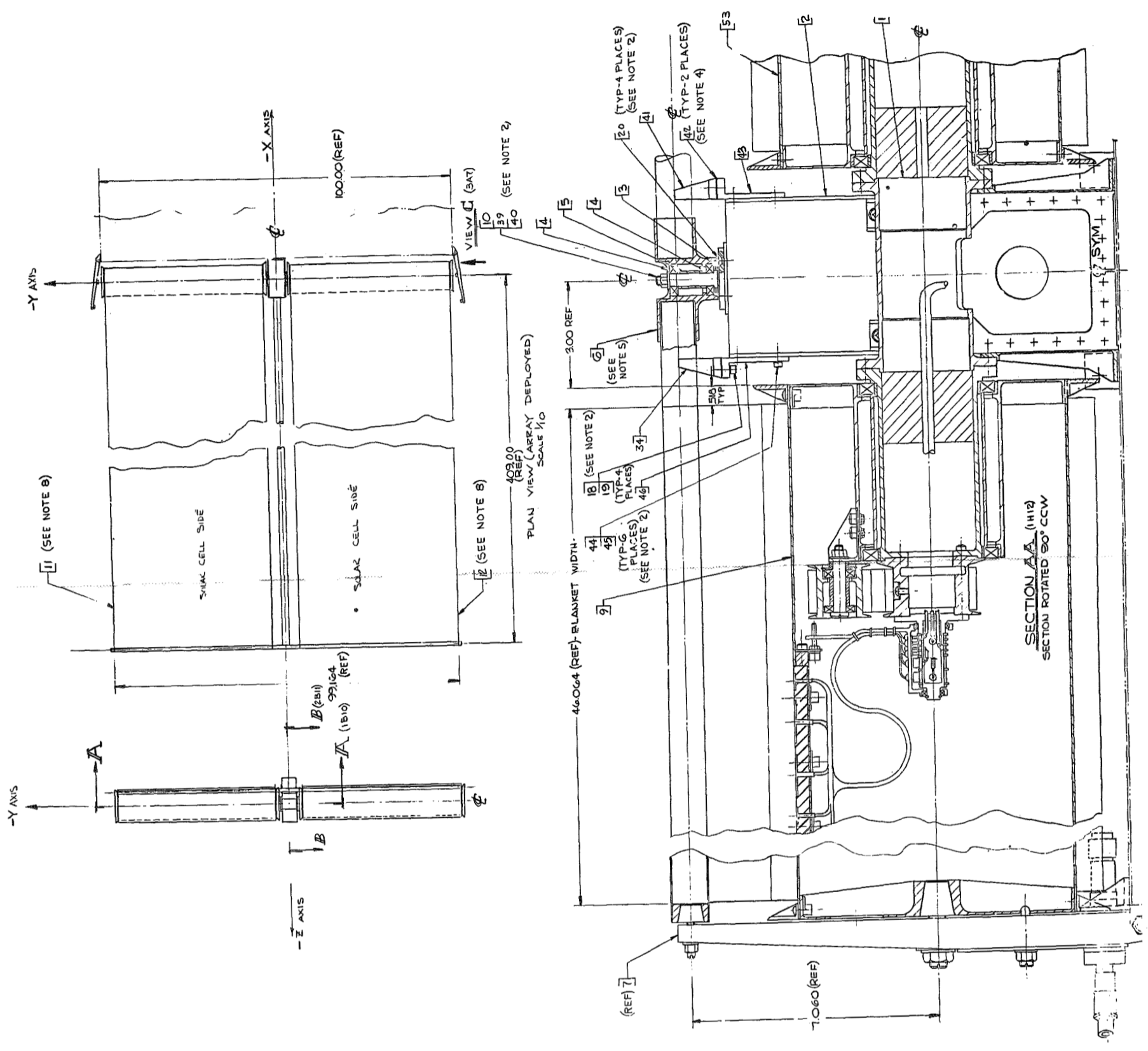
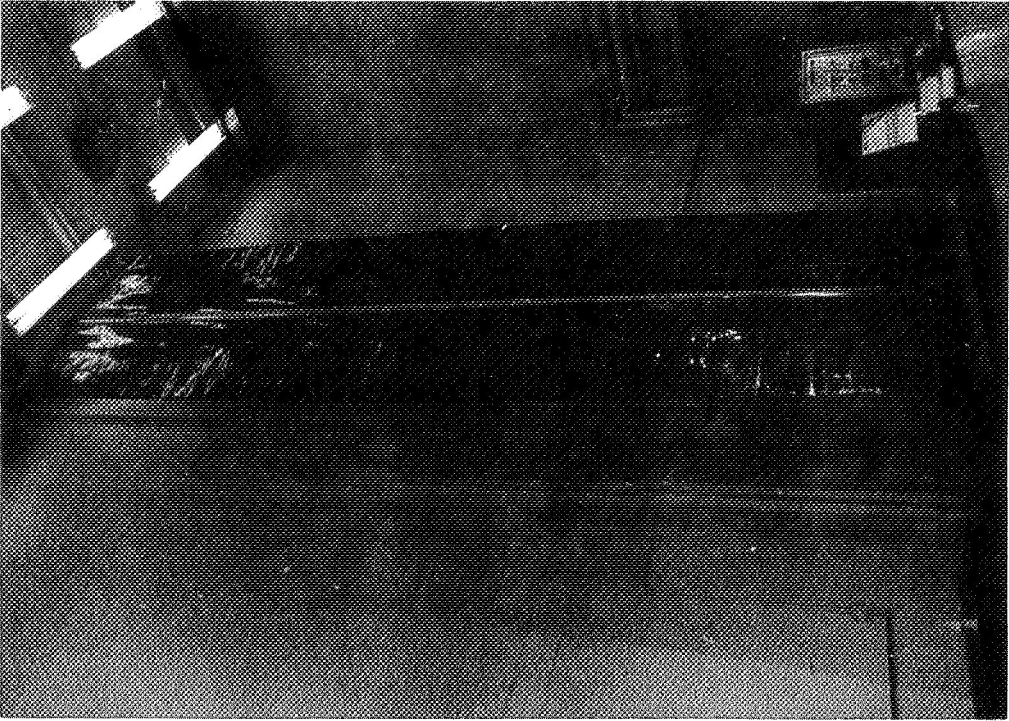


Figure 3.1-1 RA250 Assembly 3-3/4

2

2



(b) Fully Deployed(VF70228D)



(a) Stowed (VF70409B)

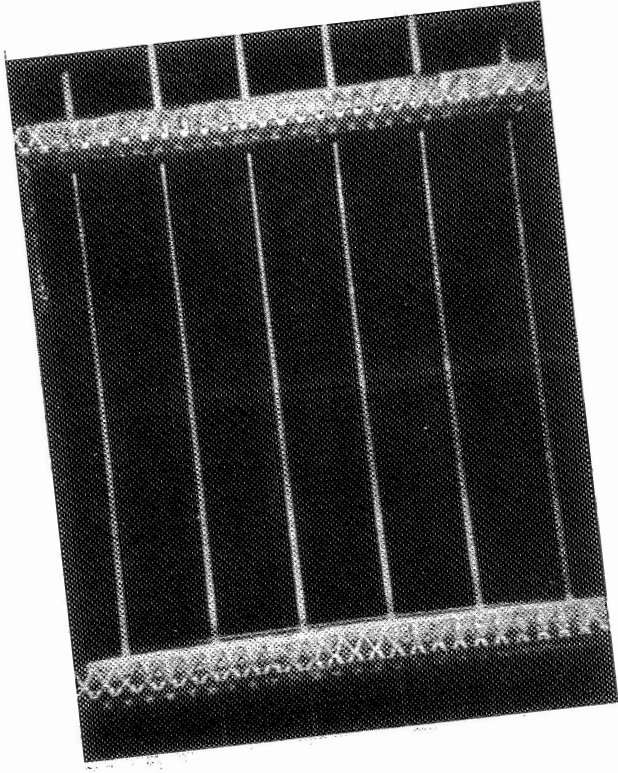
Figure 3.1-2. RA250 Prototype Test Model

substrate at the corners of each solar cell. These buttons supply interlayer cushioning in the stowed configuration.

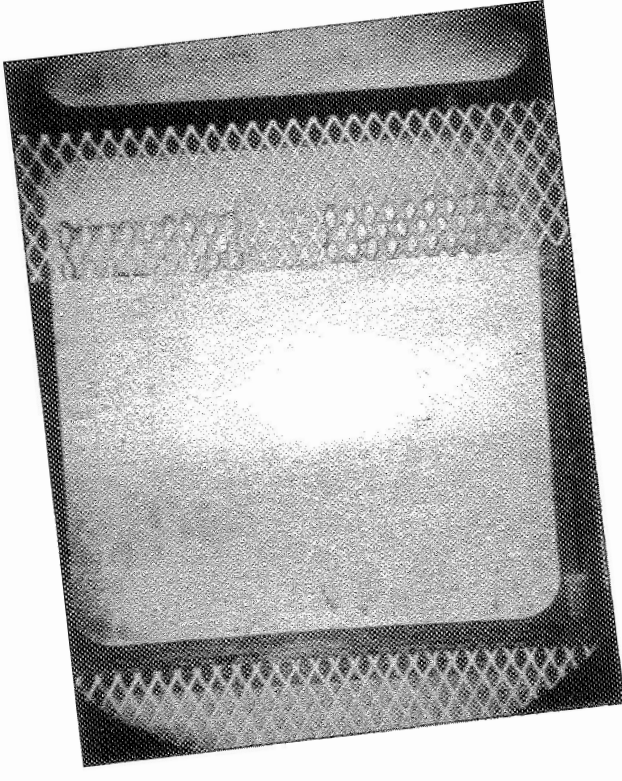
For economic reasons, the RA250 engineering test model was fabricated with partial solar cell coverage. The remaining area was covered with dummy glass modules fabricated from 0.011 x 0.750 x 0.750 in. pieces of Corning 0211 Microsheet joined together with strips of 1/4 in. wide Kapton silicone adhesive pressure sensitive tape. The glass platelet modules provided an accurate mass simulation of the solar cell modules with the tape providing a simulation of the bending stiffness of the actual solar cell interconnections.

In order to incorporate a representative sampling of various interconnection approaches, several recognized solar array fabricators were invited to supply sample modules fabricated with established production techniques. Table 3.1-1 lists each of these modules along with the overall dimensions in the series and parallel direction. The weight of each module reflects the basic difference in the interconnect design. The weight differential column represents the total weight differential if that particular module configuration were used for a flight array (based on a nominal 19p x 20s module weight of 111 grams). The photo-etched interconnect designs would add significant weight to a flight array. The solderless interconnect approach furnished by Boeing is slightly lighter than the baseline GE module. Figure 3.1-3 shows a close-up photograph of the front and rear sides of a typical solar cell within each of the module configurations described in Table 3.1-1. Figure 3.1-4 shows the layout of these active solar cell modules on the engineering test model blankets. These modules were bonded to the substrates with SMRD-745. Figure 3.1-5 shows the completed blankets before attachment to the storage drums. Close-up photographs of several of the modules on the -Y blanket are shown in Figures 3.1-6 through 3.1-8. Figure 3.1-8 also shows the method of

GE Module (19p x 20s)

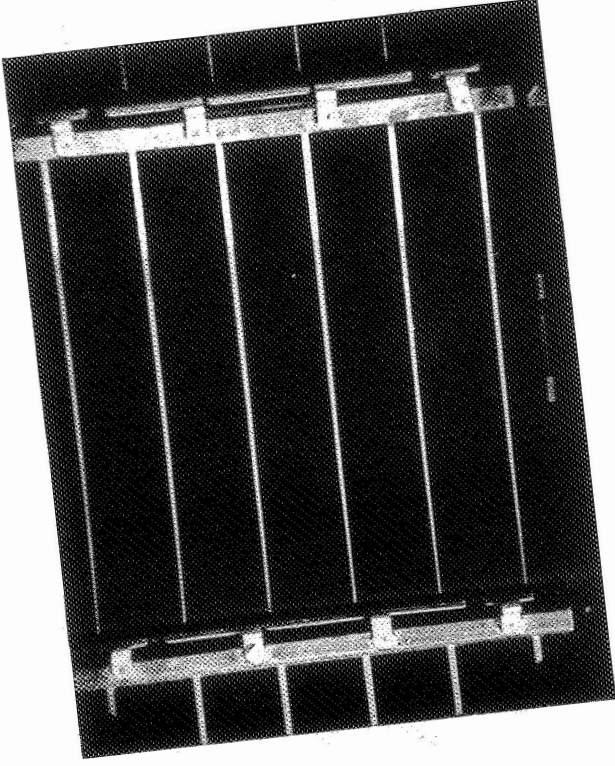


(a) Front Side

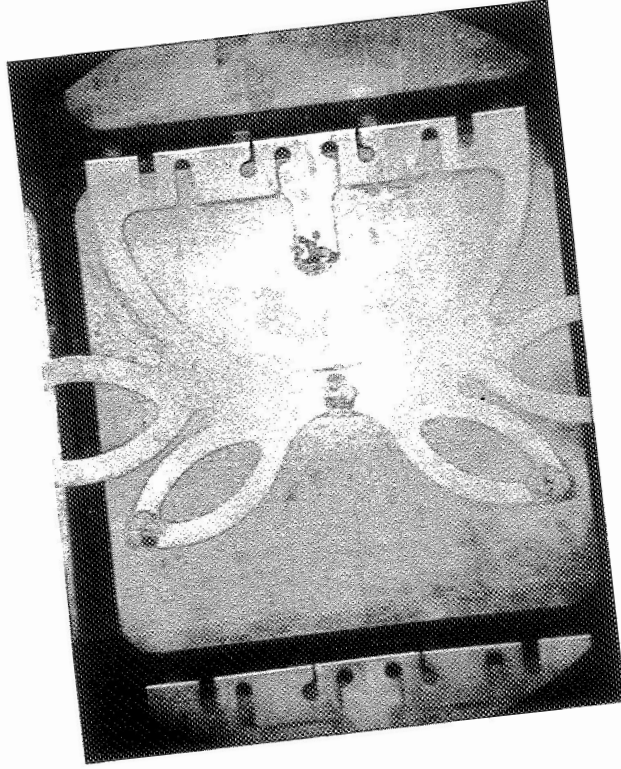


(b) Rear Side

Spectrolab Module (12p x 20s)

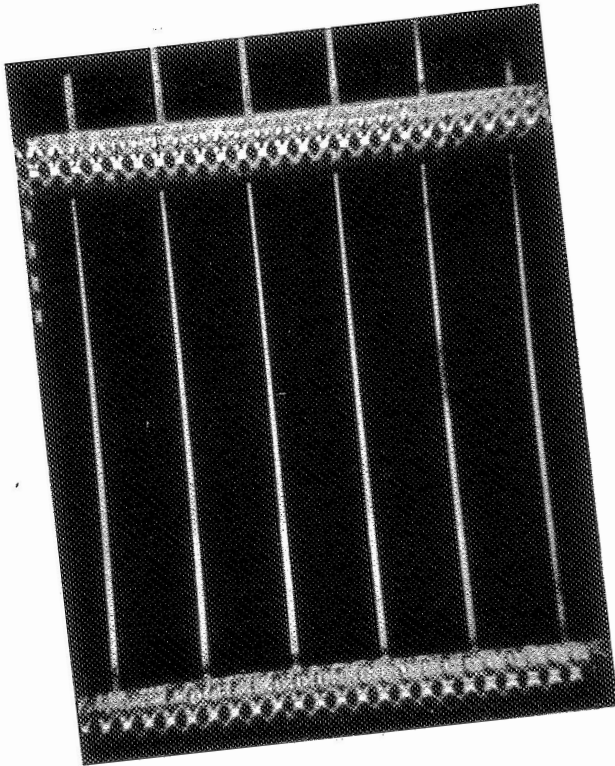


(a) Front Side

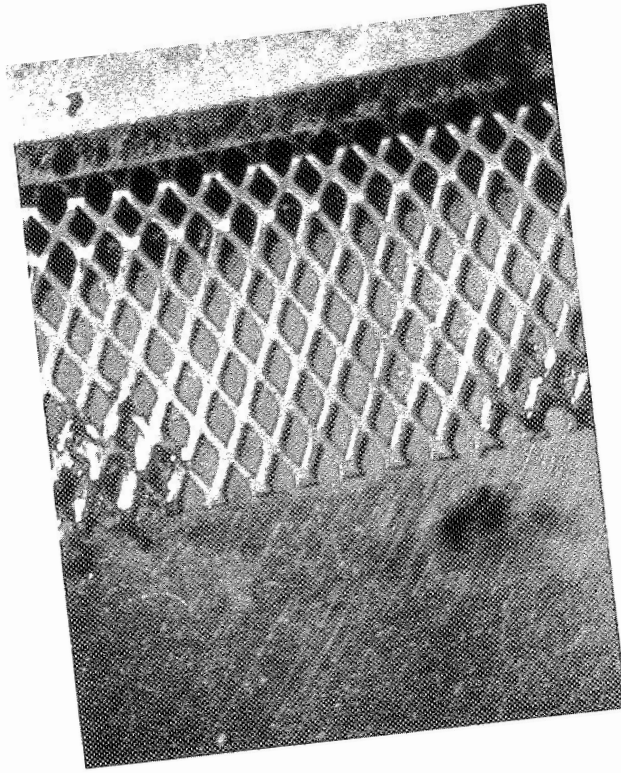


(b) Rear Side

Centralab Module (19p x 20s)

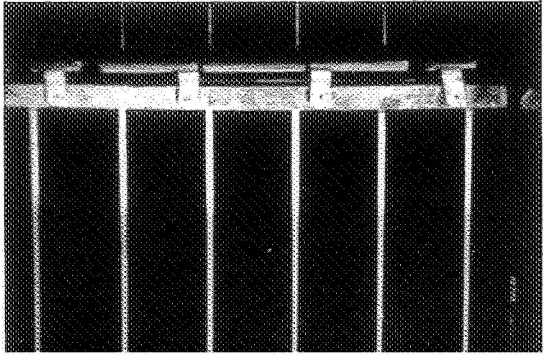


(a) Front Side

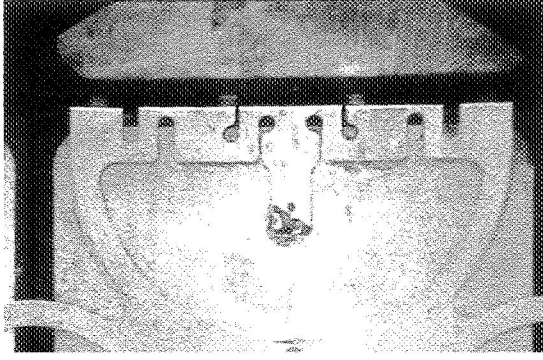


(b) Rear Side

Module (12p x 20s)

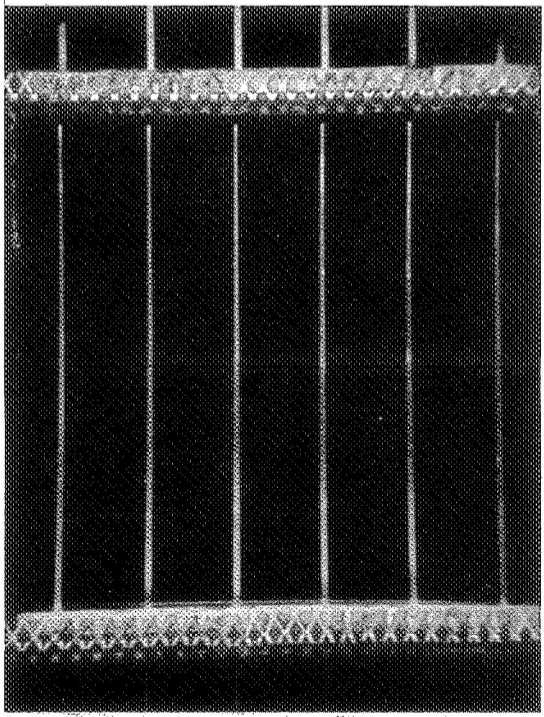


Front Side

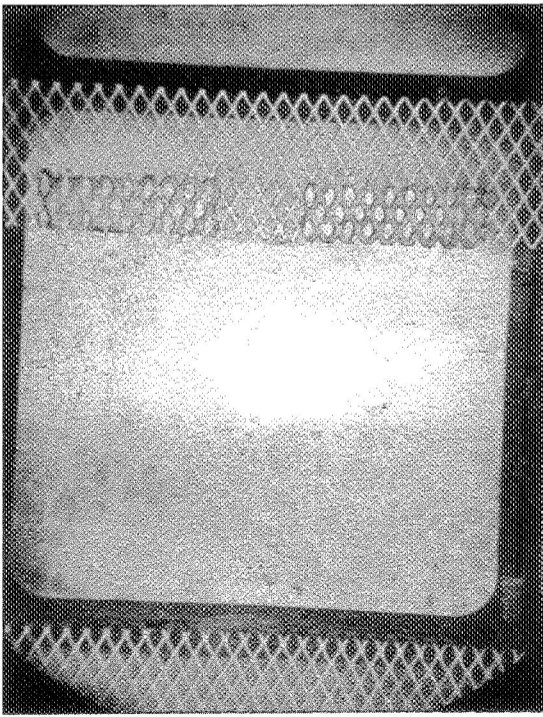


Rear Side

GE Module (19p x 20s)

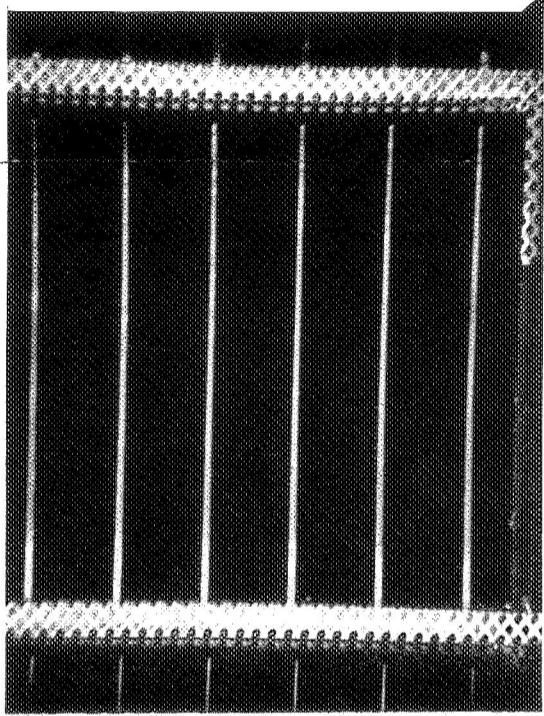


(a) Front Side

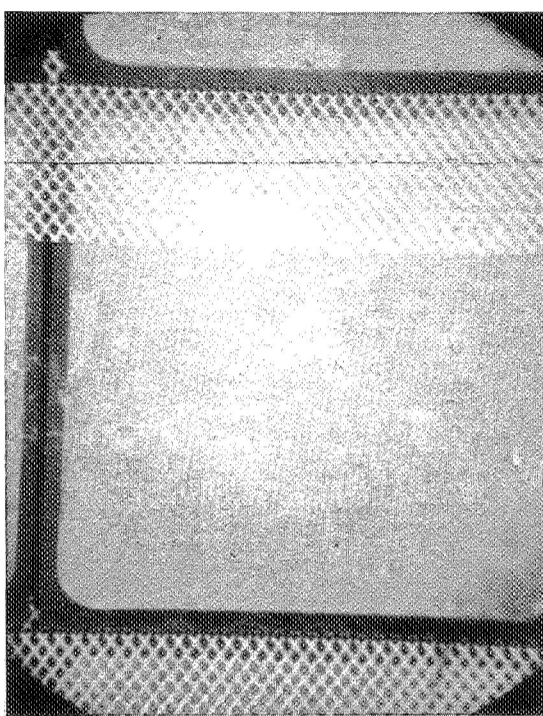


(b) Rear Side

Boeing Module (18p x 20s)

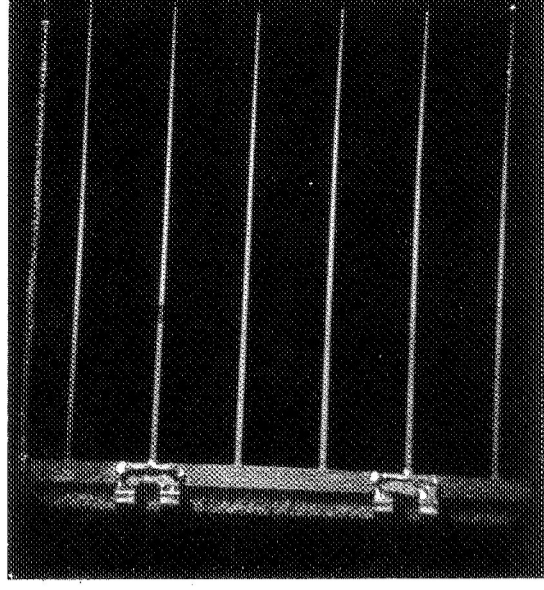


(a) Front Side

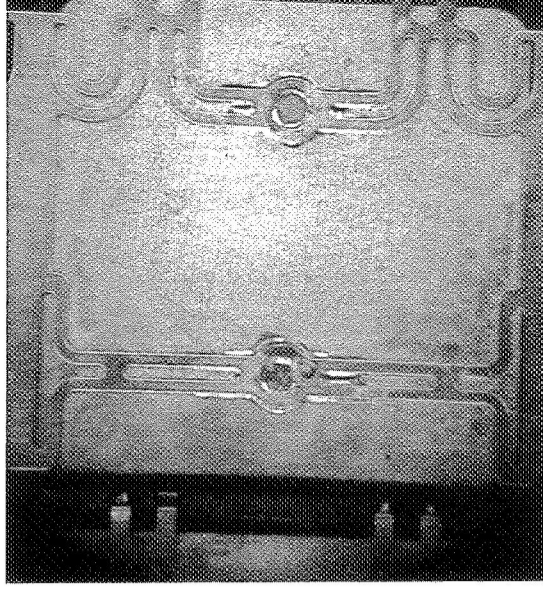


(b) Rear Side

EOS Module (18p x 20s)



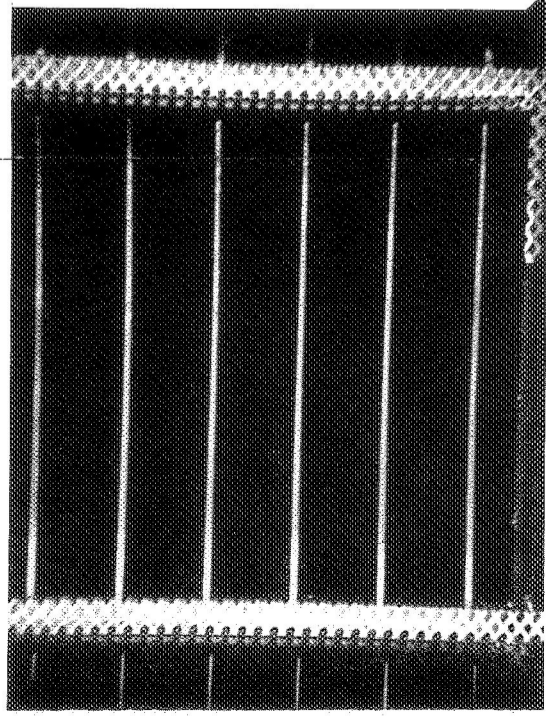
(a) Front Side



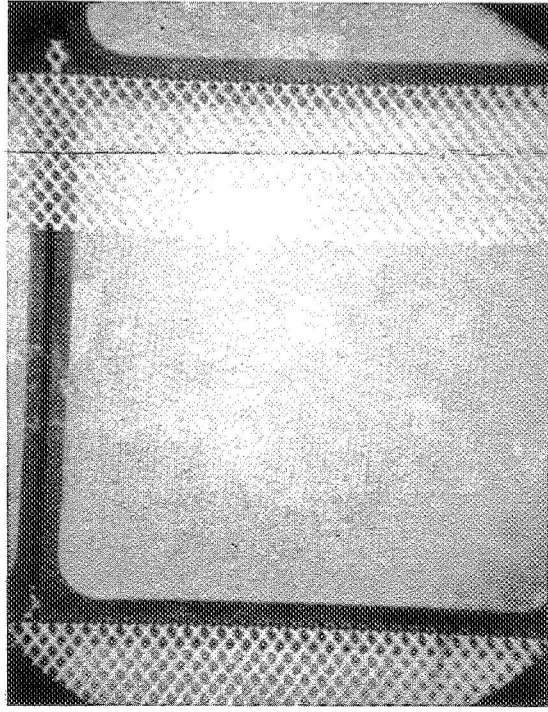
(b) Rear Side

2

Boeing Module (18p x 20s)

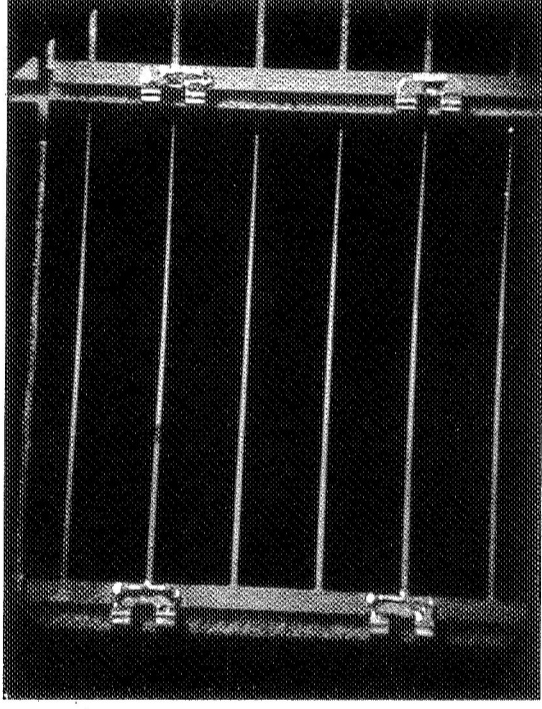


(a) Front Side

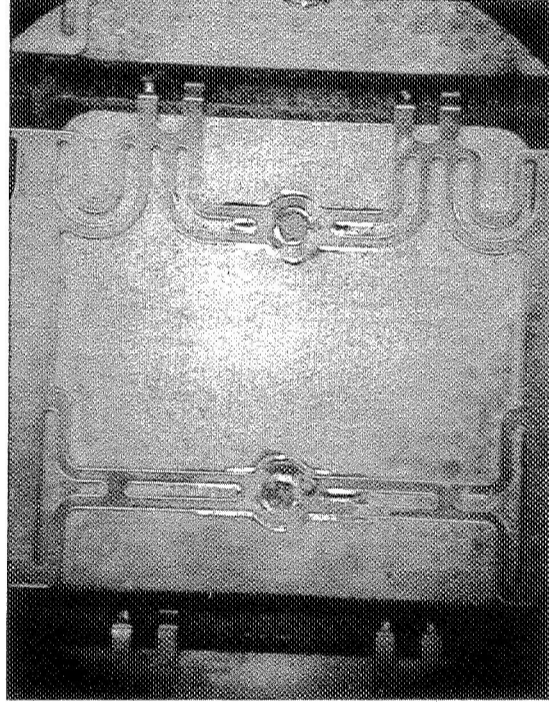


(b) Rear Side

EOS Module (18p x 20s)

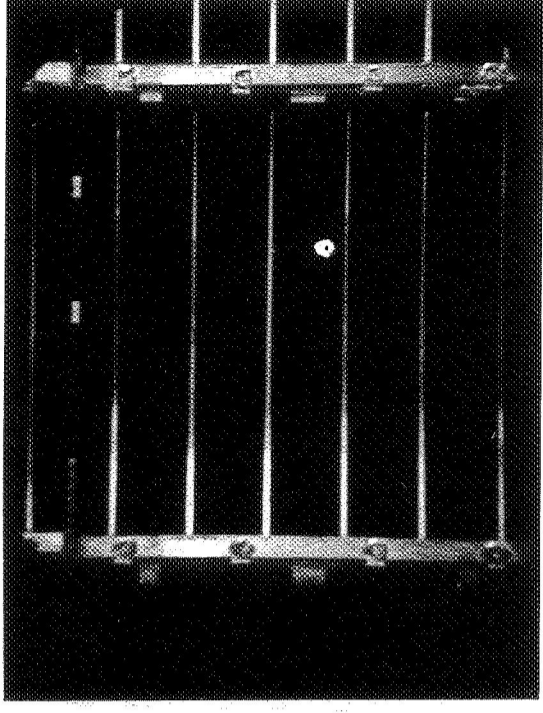


(a) Front Side

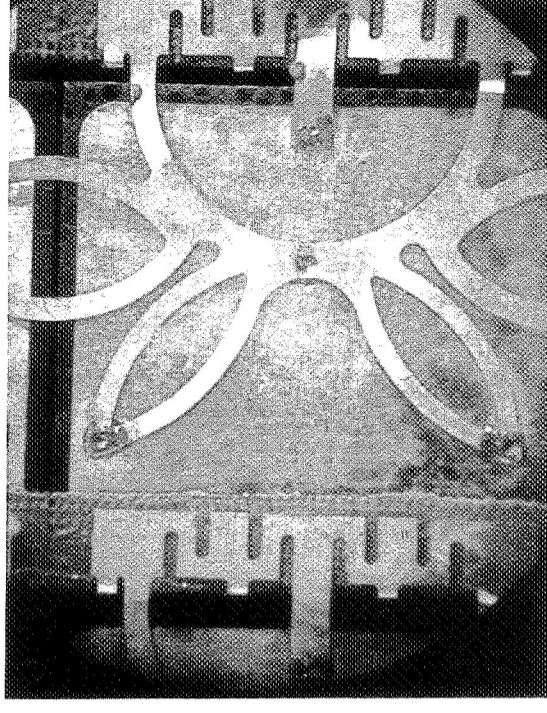


(b) Rear Side

Heliotek Module (19p x 20s)



(a) Front Side



(b) Rear Side

Figure 3.1-3 Module Details

2

2

Table 3.1-1. Solar Cell Module Summary

Module Designation	Size	Dimension Series Direction (in.)	Dimension Parallel Direction (in.)	Weight (gm)	Weight per Cell (gm)	Total* Weight Differential (lb)	Interconnect Material	Interconnect Plating	Height of Strain Relief Loop Above "P" Contact Surface (in.)	Bend Radius of Strain Relief Loop (in.)	Soldering (or Joining) Process
GE No. 1	19p x 20s	16.28	15.17	112.5	0.2961	+0.49	Ag expanded metal, 0.002 in. thick	None	0.021	0.005	IR reflow soldering, Sn 62
GE No. 2	19p x 20s	16.30	15.17	108.5	0.2855	-0.80					
GE No. 3	19p x 20s	16.25	15.22	113.5	0.2987	+0.80					
Heliotek	19p x 20s	16.33	15.24	135.5	0.3566	+7.85	Cu, 1/2 hard, 0.002 in. thick	Ag, 150 μ in.	None, Wrap-around Contact	0.005	Proprietary
Spectrolab	12p x 20s	16.31	9.63	81.0	0.3375	+5.52	Cu, 1/2 hard, 0.002 in. thick	Ag, 150 μ in.	0.040	0.005	Proprietary
Boeing	18p x 20s	16.14	14.56	99.5	0.2764	-1.91	Ag expanded metal	None	**	**	**
EOS	18p x 20s	16.34	14.55	122.8	0.3411	+5.96	Kovar	Ag	**	**	**
Centralab No. 1	19p x 20s	16.56	15.25	121.0	0.3184	+3.20	Kovar expanded metal 0.002 in. thick	Ag, 50 to 100 μ in.	0.032 ± 0.004	0.010	Resistance soldering Sn 62
Centralab No. 2	19p x 20s										
Centralab No. 3	19p x 20s										
Centralab No. 4	19p x 20s										

* Total array weight increase (or decrease) if this module configuration were used on the flight array (based on nominal 19p x 20s module weight of 111 gm)

** Data not supplied by fabricator

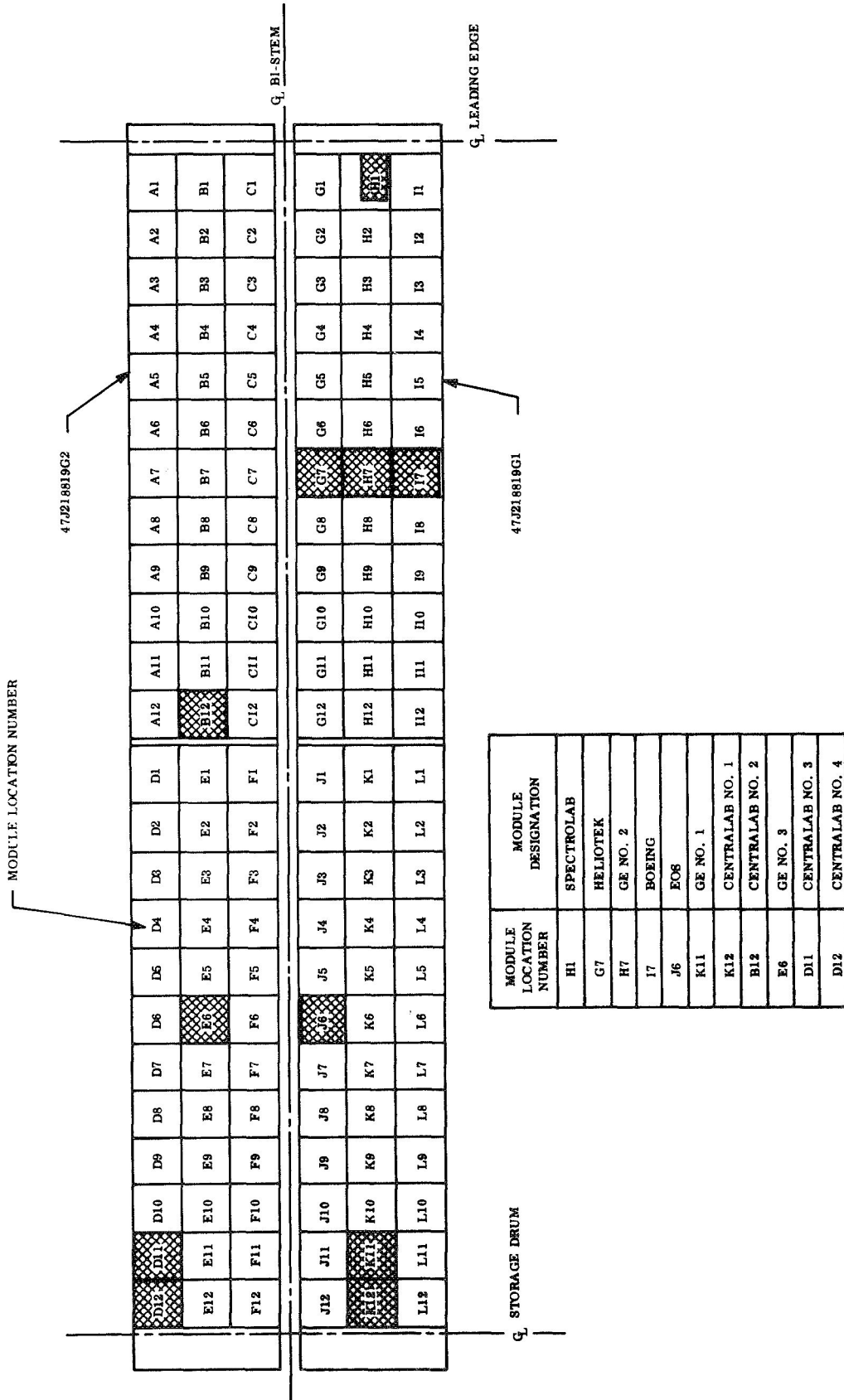
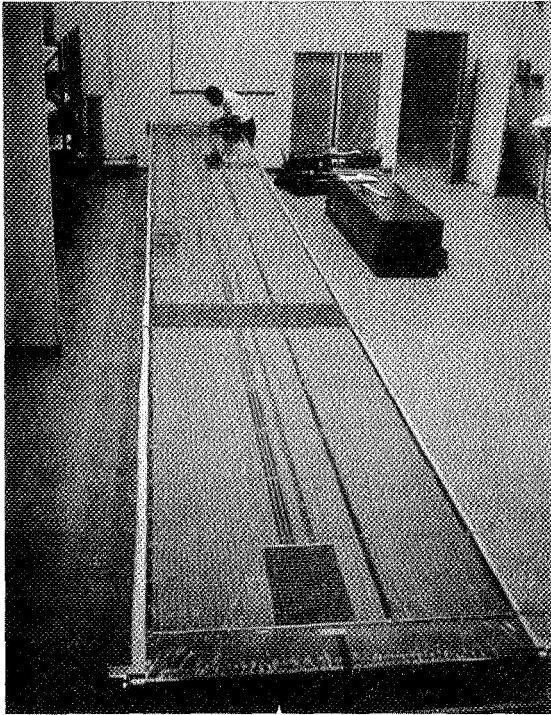
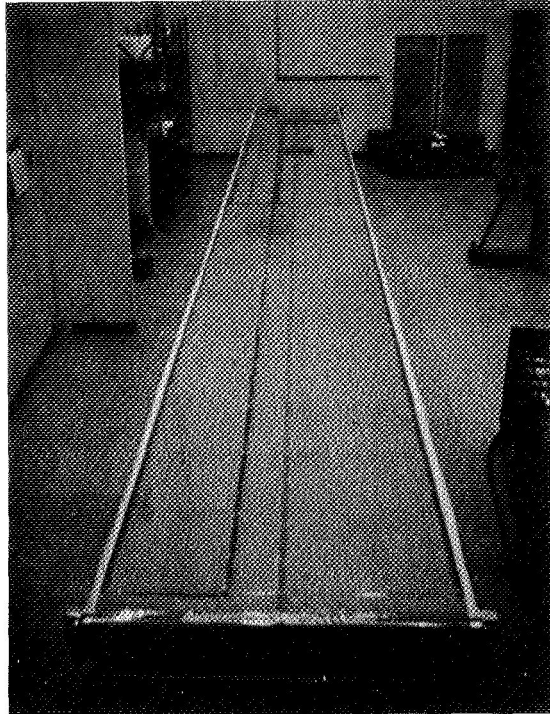


Figure 3.1-4. Active Module Locations on Prototype Blankets



(a) -Y Blanket



(b) +Y Blanket

Figure 3.1-5 Array Blankets

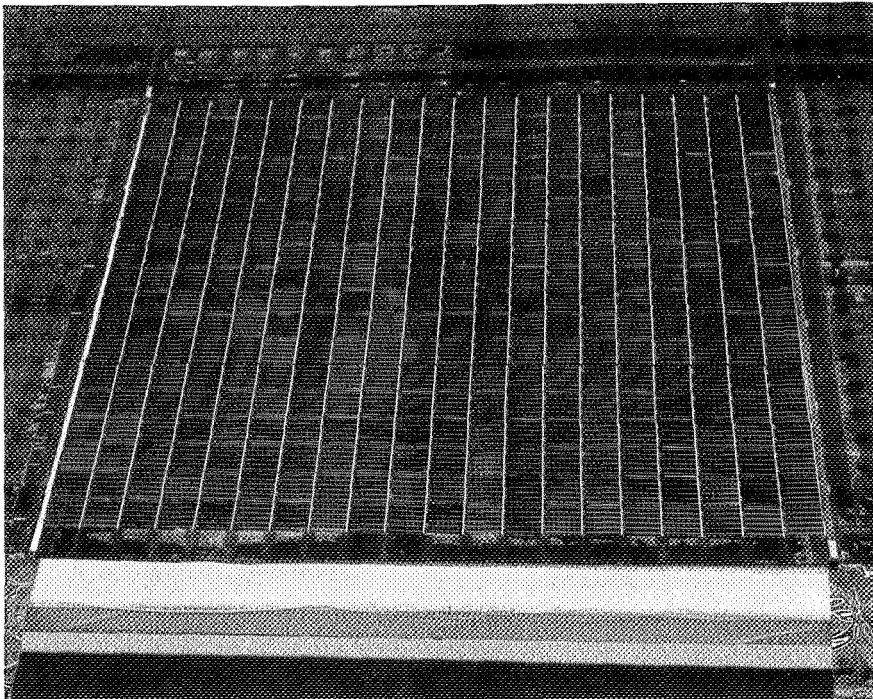


Figure 3.1-6 EOS Module Mounted on -Y Blanket Assembly

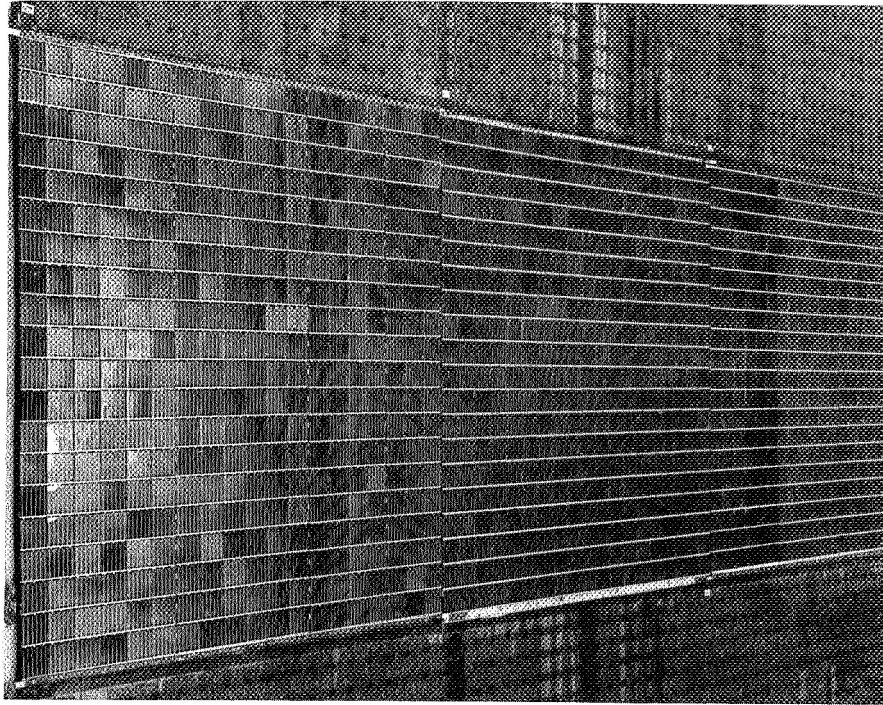


Figure 3.1-7 Heliotek (near) GE No. 2 (middle) and Boeing (far) Modules Mounted on -Y Blanket Assembly (VF 70127C)

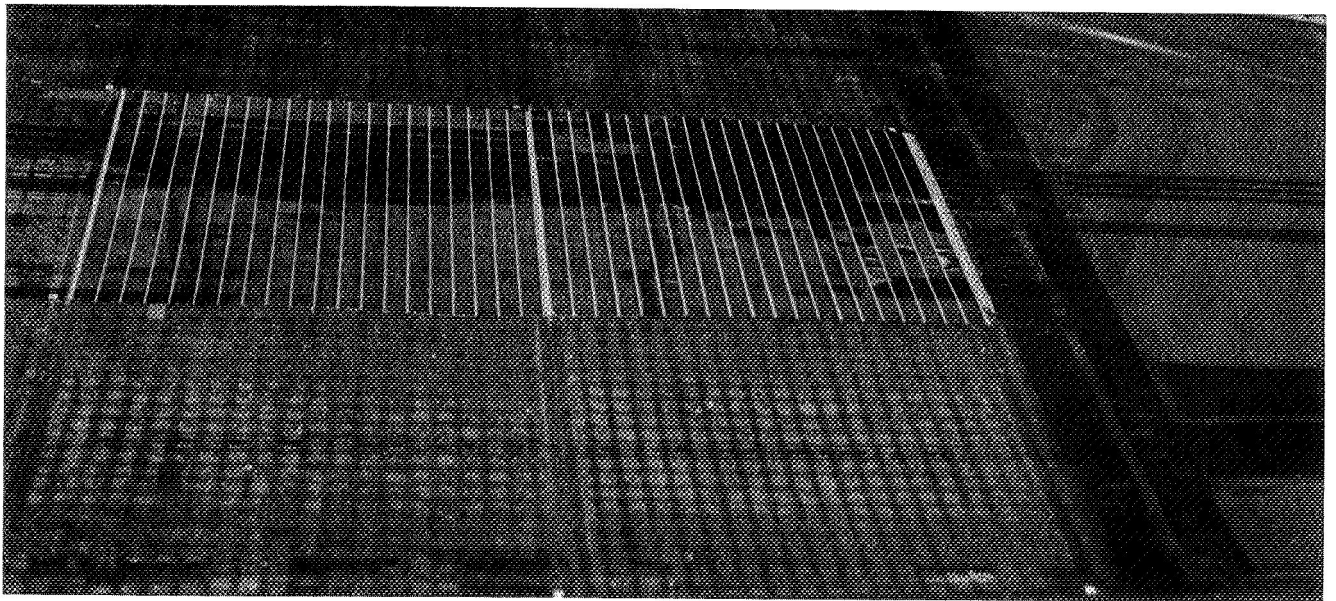


Figure 3.1-8 GE No. 1 (left) and Centralab No. 1 (right) Modules Mounted on -Y Blanket Assembly (VF70127C)

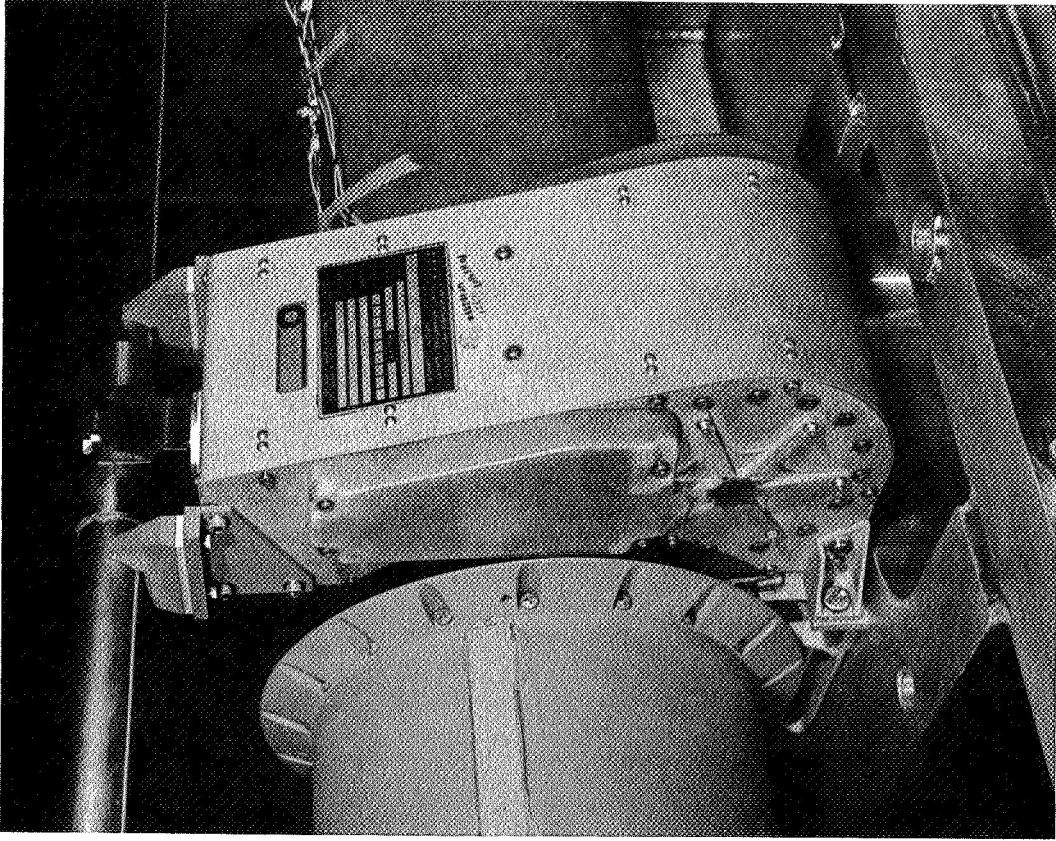
connecting two modules in the series direction. The two main bus strips at the drum end of the blanket are visible through the substrate.

3.1.3 SOLAR PANEL ACTUATOR

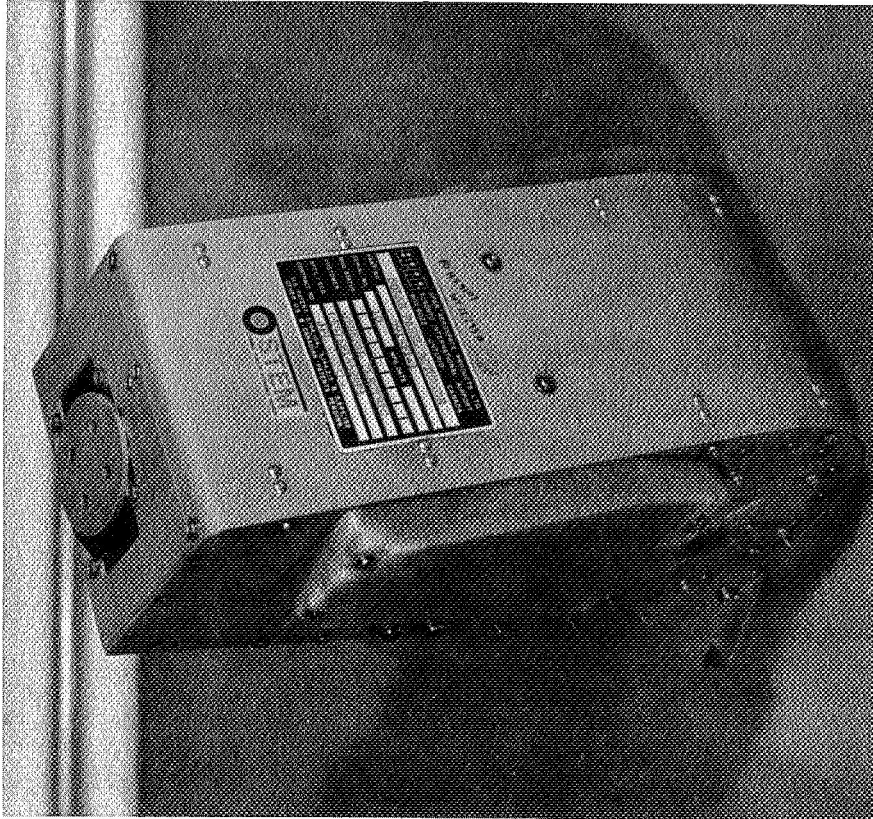
The solar panel actuator is a BI-STEM deployable boom designed and developed by SPAR Aerospace Products, Ltd. Figure 3.1-9 shows this component isolated and mounted on the center support structure between the drums. The boom element of the BI-STEM unit, the component which provides the actuation force for deployment and forms the primary structure in the deployed configuration, has a nominal diameter of 1.34 inches. It is made up of two 301 stainless steel strips, wide and 0.007 inch thick, which are prestressed to form an overlapped tube in the deployed position. The BI-STEM principle is shown schematically in Figure 3.1-10. The boom is silver-plated on its outside surfaces to reduce the temperature gradients in the boom when one side is exposed to solar radiation and the other side is in the shadow. Properties of the boom element (as supplied by the vendor) are given in Table 3.1-2.

Table 3.1-2. Properties of 1.34-Inch BI-STEM Element (Vendor Supplied)

Weight per Unit Length	(lb/in.)	0.01624
Bending Stiffness (EI)	(lb-in ² min)	332,000
Bending Stiffness (EI)	(lb-in ² max)	370,000
Column Torsional Instability	(lb)	22
Self Extension Force	(lb)	12.15



(b) Mounted on Center Support
(VF70136C)



(a) Bi-Stem Component
(VF70136D)

Figure 3.1-9 Solar Panel Actuator

The motor gearhead is an Airesearch unit that has been used in space. The solar panel actuator has been subjected to both component level random and sinusoidal vibration testing on two occasions before installation into the rollup array system. Responses were measured during vibration; amplifications of approximately four were noted.

3.1.4 SLIP RING ASSEMBLY

The slip ring assembly was designed and fabricated by Poly-Scientific Division of Litton Precision Products, Inc. A photograph of this component is shown in Figure 3.1-11. A summary of the pertinent design data is listed in Table 3.1-3. Each storage drum contains a slip ring assembly which functions to transfer array power and signals across the rotary joint between the drums and the center support. The storage drums rotate approximately 15 turns to deploy or retract the array.

There are two power rings per assembly as well as four signal rings. Three of these rings are used to return the signals from two thermistors, while the fourth is used to monitor the array bus voltage on the drum side of the slip rings.

3.1.5 STRUCTURAL COMPONENTS

3.1.5.1 Storage Drum

The two storage drums in the system form the primary structure for the stowed configuration. Each drum assembly includes a shell, outboard end cap, inboard end cap, and edge guides. Two different drum configurations were designed for this application: one utilizing a beryllium monocoque shell and the other fabricated with a magnesium semimonocoque shell. For economic reasons, the magnesium shell

Table 3.1-3. Slip Ring Data

• Power rings per assembly	2
• Signal rings per assembly	4
• Structural material	303 stainless steel
• Ring material	Coin silver
• Ring diameter	0.60 in.
• Brushes per signal ring	2
• Brushes per power ring	4
• Brush material	Silver/copper/niobium diselenide/ graphite
• Brush spring material	Ney Paliney 7
• Rated current per ring	15.0 amp dc
Power	1.0 amp dc
Signal	
• Brush contact force	
Power	0.33 lb + 10%
Signal	0.12 lb + 10%
• Starting torque	
Air	0.7 in. -lb
Vacuum	0.4 in. -lb
• Signal ring static contact resistance	0.065 ohm
• Power ring static contact resistance	0.020
• Rated current density/ring	
Power	188 amp/in. ²
Signal	83 amp/in. ²
• Anticipated power loss/assembly	6 watts
• Weight/assembly	0.617 lb

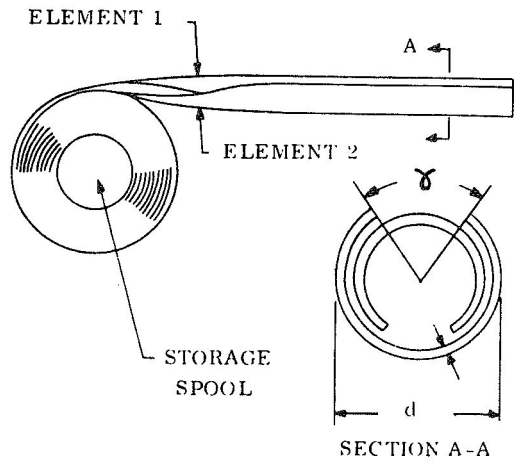


Figure 3.1-10 The BI-STEM Principle

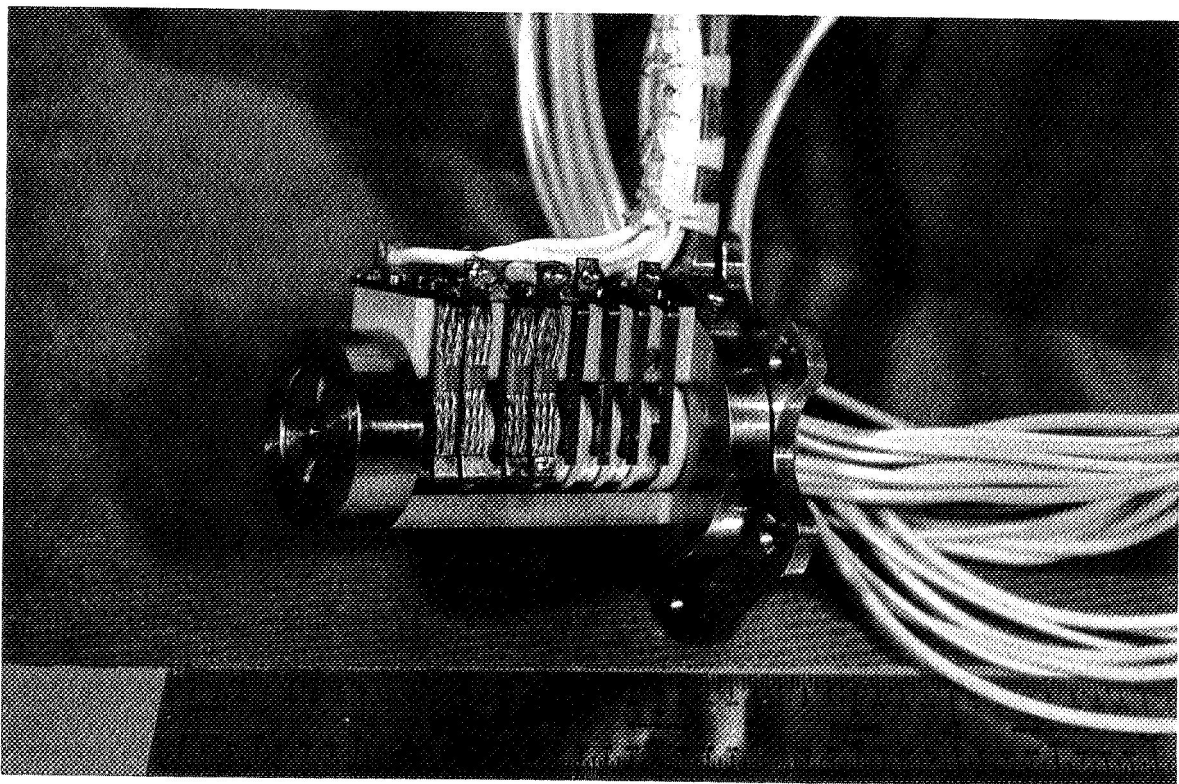


Figure 3.1-11 Slip Ring Assembly (VF70731)

design was selected for use on the engineering test model even though a total weight penalty of 2.0 lb was incurred.

The magnesium drum shells are 47.10 inches long, 0.032-inch thick sheet magnesium rolled into an 8-inch diameter cylinder, which is closed with a lap-butt joint utilizing a 0.75-inch-wide strip of magnesium bonded with Epon 934.

The inboard end cap assembly, pictured in Figure 3.1-12 houses the two main bearings which allow the storage drum to rotate with respect to the support shaft. The constant torque Negator spring motor, which provides the blanket preload force, is mounted on the inboard end cap with the output spool coaxial with the main bearings. The slip ring assembly is then mounted to the inboard end of this output spool. The brushes of the slip ring assembly are wired to the drum shell power feed-through as shown in Figure 3.1-12.

The outboard end cap serves as the supporting interface for the drum outer end during launch. It contains a tapered hole which mates with a tapered plug in the outboard end support.

Two edge guide flanges are mounted on each storage drum to provide control forces to the blanket edge during retraction. If, for any reason, the blanket should tend to rewrap against either flange, that guide should apply corrective forces to prevent the blanket from extending past the end of the drum.

3.1.5.2 Leading Edge Member

The leading edge member (LEM) is the structural element at the outermost edge of the blanket. In the deployed configuration, this member transmits the 4-pound blanket preload force from the array substrates to the boom. In the stowed configuration,

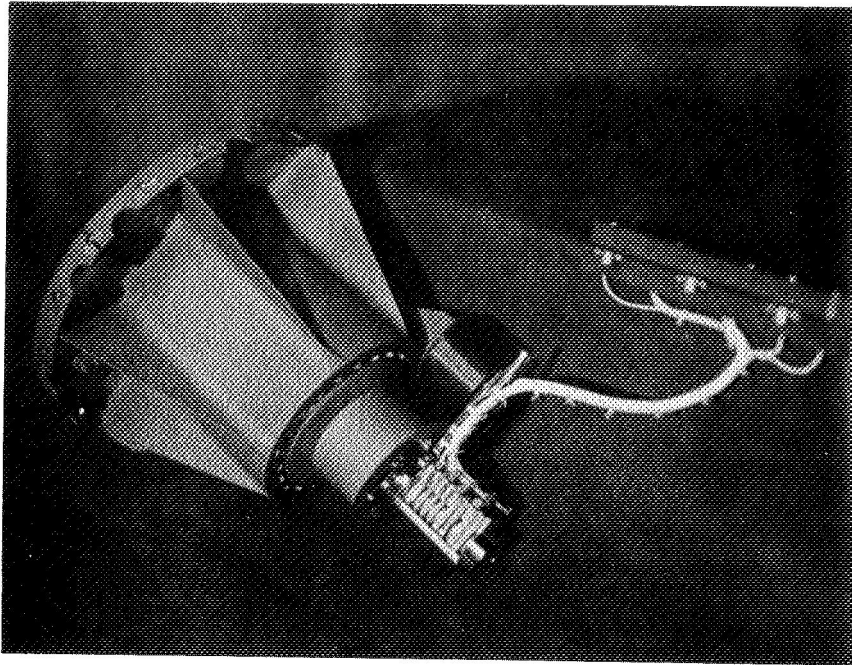


Figure 3.1-12 Inboard End Cap Assembly

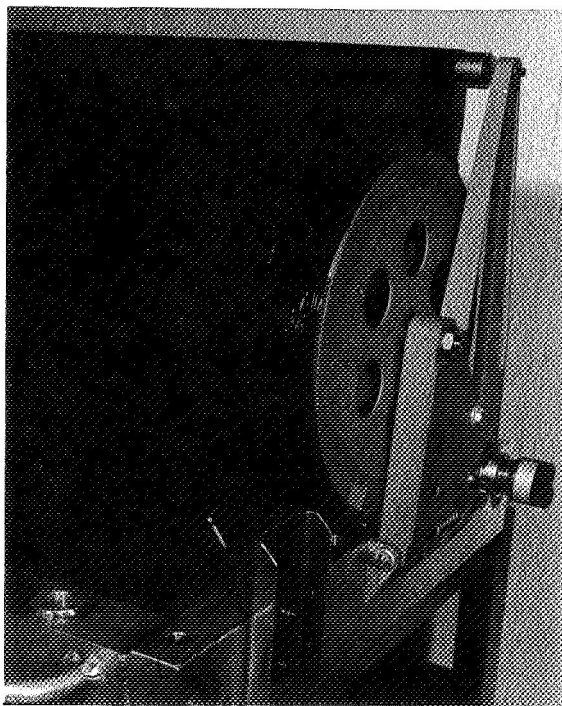


Figure 3.1-13 Outboard End Support (VF70157C)

the LEM functions to restrain the outer blanket wrap and to cage the BI-STEM boom element. The ends of the LEM are supported by the outboard end supports and the center section is supported from the actuator housing by two saddle-type brackets. With the exception of the stainless steel boom post, bearings, and associated spacers all parts are made from beryllium. The LEM is made up from two 50.1-inch-long cylinders fabricated from 0.020-inch beryllium sheet bonded with Epon 934. The two cylinders are inserted into a center fitting and bonded in place. This fitting also houses two instrument bearings which mate with the stainless steel boom post. These bearings decouple the array blanket from the BI-STEM boom for rotation about the boom axis. No bearing inserts are required because the surrounding material is steel and beryllium whose coefficients of thermal expansion are nearly the same.

3.1.5.3 Outboard End Support

The outboard end support, pictured in Figure 3.1-13, consists of the following major components:

1. Movable arm assembly
2. Hinge brackets
3. Separation nut
4. Bolt catcher
5. Hinge pin
6. Separation bolt
7. Spring

The movable arm assembly is a machined magnesium weldment. This arm carries the stainless steel tapered plugs which interface with the outboard end cap and leading edge member. Attachment of the movable arm to the vehicle-mounted bracket is through a hinge joint. The titanium hinge pin is dry-film-lubricated. A torsion spring which mounts on the hinge pin furnishes 100 in.-lb of torque in the stowed configuration. The release of the support is accomplished by a separation nut/separation bolt/bolt catcher combination. The 3/8-24 separation nut is attached to the movable arm and contains two electroexplosive pressure cartridges. Upon application of the required power pulse to the bridgewires of one or both of these cartridges, the nut will open and propel the separation bolt into the bolt catcher which is mounted on the stationary hinge bracket. The torsion spring forces the movable arm to rotate about the hinge pin through an angle of approximately 10 degrees. The storage drum and leading edge member are thus released to permit deployment of the BI-STEM actuator.

3.1.5.4 Center Support

The center support consists of a magnesium center tube, two machined magnesium end fittings and two magnesium face sheets. As shown in Figure 3.1-14, the center tube is pinned to the end fittings and the face sheets are riveted to the tube end fittings. One face sheet provides for the electrical connector installation, and together with the other face sheet, transmits shear loads. The end fittings provide the interface pads for the vehicle structure and the solar panel actuator (BI-STEM). Tolerances on all interface surfaces were selected in order to achieve reasonable alignment between the storage drums and the leading edge member and minimize end support vehicle interface adjustment at final installation. The center tube incorporates an access hole which allows either drum or the solar panel actuator to be disassembled from the center support without the removal of the

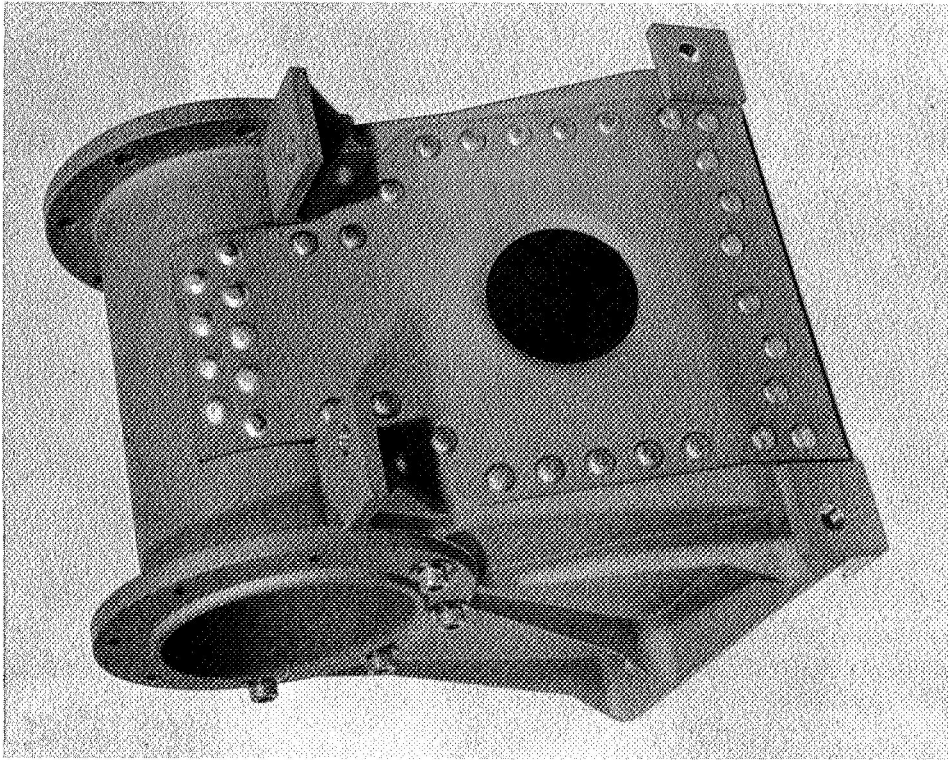
connectors from the harness. The five connectors shown in Figure 3.1-14 (b) carry array power from the slip rings, signals from the thermistors on the blankets, and power to the solar panel actuator.

3.1.6 MASS PROPERTIES SUMMARY

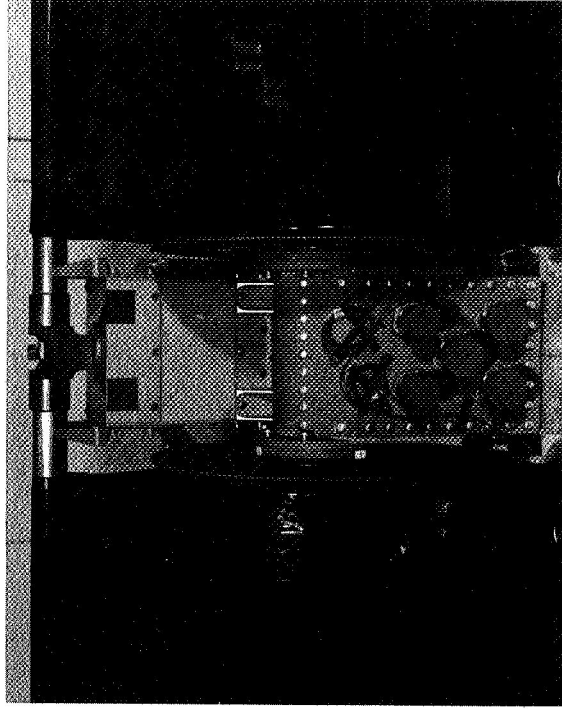
The actual weight breakdown for the engineering prototype model is shown in Table 3.1-4. The total weight of this model is 82.5 lb. Based on this weight, the array power-to-weight ratio is $2500/82.5 = 30.3$ watt/lb. For a flight model, this weight could be reduced to 79.3 lb (or 31.3 watt/lb.) by the implementation of the following changes as described in Reference 1-5.

1. Replace magnesium drum shells with beryllium.
2. Remove Schjel-Clad residual adhesive on the backside of the blanket. The flight weight also takes into account that the dummy glass simulated cells are slightly heavier than actual solar cells.

The calculated values for the center of mass and the moments and products of inertia are tabulated in Table 3.1-5.



(a) Component (VF7068)



(b) Assembly (VF70157B)

Figure 3.1-14 Center Support

Table 3.1-4. Actual Weight Summary (Prototype Model)

Nomenclature		Drawing No.	Unit Weight (lb)	Qty/Next Assy	Total Weight (lb)
RA250	Prototype Assembly	47E214519G2	-	-	82.5
	Center Support	47E218547	1.33	1	1.33
	Leading Edge Member	-	0.85	1	0.85
	Boom Actuator	-	11.73	1	11.73
	LEM Support Brackets	-	0.11	2	0.22
	Outboard End Support	-	2.05	2	4.10
	Movable Portion	-	1.31	1	-
	Fixed Portion	-	0.69	1	-
	Bolt	-	0.05	1	-
	Drum Assembly	47E218804 G3 & G4	8.80	2	17.60
	Guide Flange	47D218535 G3 & G4	0.38	2	-
	Drum Shell	47E218144G4	2.79	1	-
	Outboard End Cap Assembly	47E218194G3	0.45	1	-
	Inboard End Cap Assembly	47E218544 G1 & G2	4.80	1	-
	Mounting Hardware (Drum-to-Center Support)	-	-	-	0.13
	Prototype Array Blanket Assembly	475218819G1	23.22	1	23.22
	Prototype Array Blanket Assembly	47J218819G2	23.36	1	23.36

Table 3.1-5. Summary of Mass Properties

	Stowed	Deployed
Center of Mass (Inches)		
X	-0.2	+120.1
Y	0	0
Z	+0.9	+ 3.1
Moments of Inertia About Center of Mass (Slug-ft ²)		
I _{OX}	13.65	13.54
I _{OY}	0.46	338.89
I _{OZ}	13.63	352.69
Products of Inertia About Center of Mass (Slug-ft ²)		
P _{OXY}	0	0
P _{OXZ}	-0.008	+ 1.826
P _{OYZ}	0	0

The coordinate system is shown in Figure 1-1

3.2 SYSTEM PERFORMANCE

3.2.1 PREDICTED ELECTRICAL PERFORMANCE

The power-to-weight ratio of the RA250 system is based on generation of 2500 watts of raw array power while operating at 55°C under Air Mass Zero 1.0 AU illumination and orientation within ± 10 degrees of the sun. Cell efficiency is specified indirectly by the area performance criteria of 10 watt/ft² of gross module area. The cell is specified as 8 mil thick, 2 by 2 cm, with "bar contacts" (3.8 cm² active area per cell). Figure 3.2-1 shows the normal subsolar array I-V curve based on the published performance of these cells. This curve represents the expected beginning-of-life raw array characteristic and includes a six percent reduction in short circuit current to provide for coverglass transmission and other losses. The calculated maximum raw array power under these conditions is 2523 watts at 102vdc. To arrive at the maximum power available at the electrical interface on the center support, the following distribution losses must be accounted for:

1. Array blanket bus strip series resistance losses.
2. Slip ring series resistance losses including line losses within the storage drum and center support.
3. Solar cell interconnect series resistance losses.

The array blanket circuit bus strip series resistance losses were measured on the engineering prototype models blankets with the results shown in Table 3.2-1.

The effect of this combined series resistance is to reduce the maximum power by 51 watts at a 55°C operating temperature. The effective series resistance of the slip rings and associated harnessing within the drum and center support was

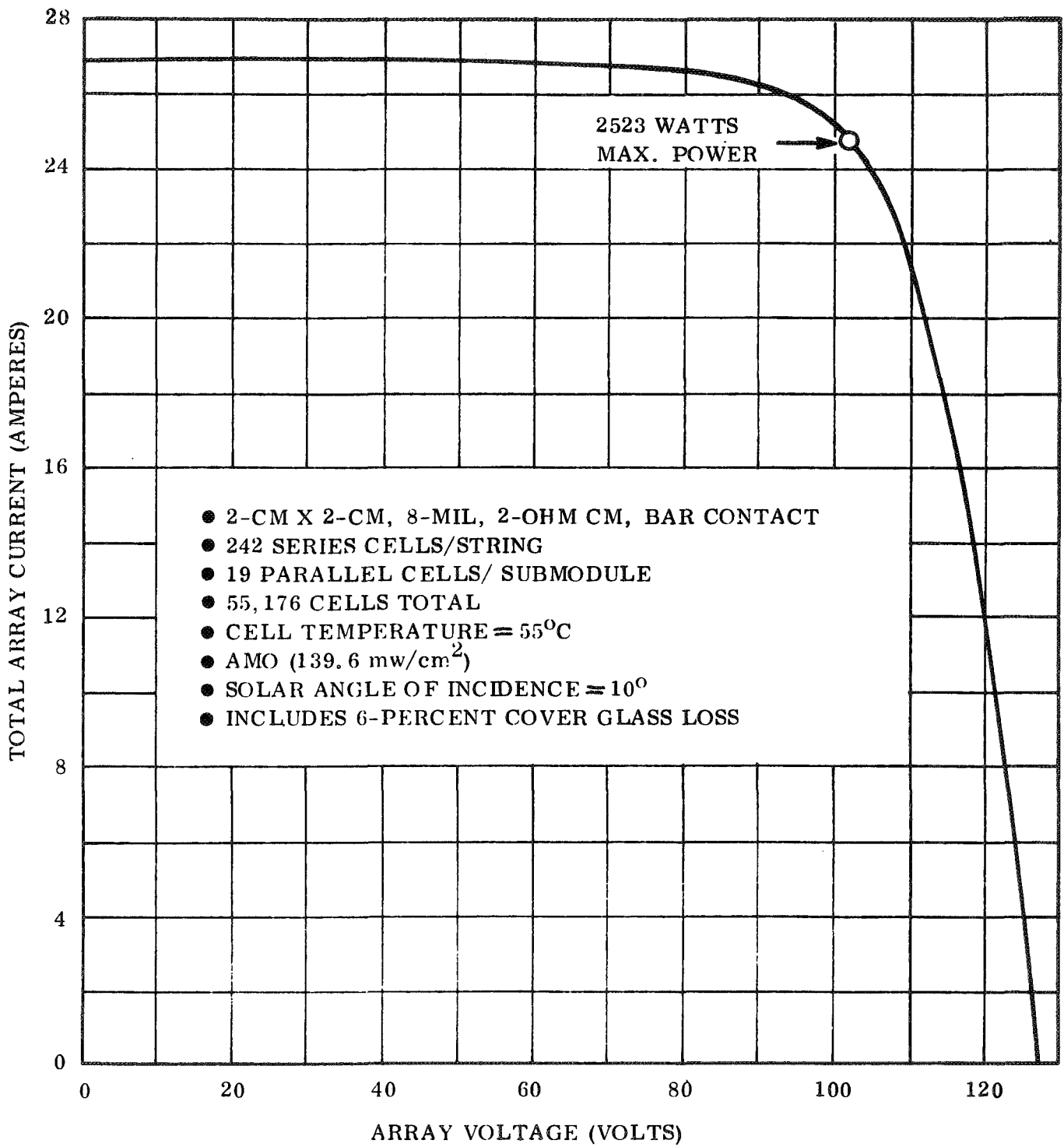


Figure 3.2-1. Nominal Subsolar Array I-V Curve

Table 3.2-1 Summary of Bus Strip Resistance Measurements

<u>CIRCUIT*</u>	<u>MEASURED RESISTANCE AT ROOM TEMPERATURE (OHMS)</u>	<u>RESISTANCE CORRECTED TO 55°C (OHMS)</u>
A	1.00	1.12
B	1.06	1.19
C	0.93	1.04
D	0.81	0.91
E	0.89	0.99
F	0.75	0.84
G	0.89	0.99
H	1.05	1.17
I	0.91	1.02
J	0.77	0.86
K	0.91	1.02
L	0.79	0.88

* See Figure 3.1-4 for circuit definition.

measured during the system test program. Based on these requirements, a value of 0.02 ohms is used as the combined series resistance of both power ring circuits of a slip ring assembly. Therefore, the total slip ring loss at maximum power is 6 watts for the entire array.

The series resistance losses associated with the solar cell interconnect will vary with the type of interconnect configuration utilized. For 2 mil thick silver expanded metal (2 Ag5-5/0) the calculated loss due to the interconnects is negligible compared to the other series resistance losses in the system.

Accounting for these various array losses, the maximum net power available at the electrical interface on the center support is 2466 watts.

3.2.2 PERFORMANCE DURING SYSTEM TEST CYCLE

3.2.2.1 General

The performance of the RA250 system was monitored periodically throughout the course of the system test program to check the status of the system after each environmental test. This inspection denotes a health check consisted of a detailed inspection of the array blankets for breakage, an inspection of the structural components for damage, the measurement of the electrical characteristics of each active solar cell module, and the deployment and retraction of the array to verify the performance of the BI-STEM actuator, slip ring assemblies, and drum bearing system. The first health check was performed after the RA250 final assembly and established the initial condition of the test specimen prior to any environmental testing.

3.2.2.2 Module Performance and Inspection

The electrical performance of the active modules is tabulated in Table 3.2-2. From the inspections conducted during the course of this program the maximum breakage which can be attributed to the environmental test program has been summarized in Table 3.2-3. This data is derived from Table 4.1-1 and Figure 4.1-9 of Volume II. Several observations can be made based on these results.

- The stowed vibration test caused the greatest breakage of cells and coverglass.
- The thermal vacuum test series caused the largest percentage of broken glass platelets.
- The total breakage numbers reflect that the glass platelets are significantly less vulnerable to breakage than either the cells or coverglass and that the cells are less vulnerable than the coverglass.

The fact that the thermal vacuum test was the most severe environment for the glass platelets may be explained by the fact that the areas of dummy glass were not temperature controlled during the deploy/retract cycles and therefore were colder than the solar cell modules. Also many localized areas of the dummy glass were affected by an overheating condition which occurred during the stowed high temperature test. Both of these factors could account for this disproportionate percentage of glass platelet breakage during this test.

The relatively high vulnerability of the coverglass is apparent from the inspection results. There is no breakage pattern to indicate a possible cause for this high proportion of damage, although there are a few examples of parallel adjacent coverglass within a module row which have cracked in a direction parallel to the axis of the storage drum. Two examples of this type of cracking pattern

Table 3.2-2. Maximum Power Measurement (Watts)

Module	Health Check No.								
	0	1	2	3	4	5	6	7	
K11	GE#1	18.3	18.0	17.8		18.0	17.6	18.3	18.4
H7	GE#2	18.5	18.25	18.5		17.7	18.1	18.6	18.4
E6	GE#3	16.6	16.2	16.3		15.6	16.2	15.7	15.4
G7	Heliolek	17.5	17.9	18.4		17.2	17.5	17.3	17.5
H1	Spectrolab	11.0	10.7	11.3		10.4	10.8	10.9	11.5
I7	Boeing	16.8	16.6	16.8		15.9	16.0	16.3	16.4
J6	EOS	16.9	17.3	17.2		13.0	13.5	13.4	12.2
K12	Centralab #1	17.4	17.2	17.5	No Measurements	17.4	17.1	17.6	17.5
	Subtotal	133.0	132.1	133.8		125.2	126.8	128.1	127.3
B12	Centralab #2	--	--	18.4		18.1	17.6	17.6	18.2
D11	Centralab #3	--	--	17.7		17.0	17.7	16.9	16.7
D12	Centralab #4	--	--	18.3	18.0	18.9	18.0	18.1	
	TOTAL			188.2		178.3	181.0	180.6	180.3

Event

Installation

Deployed Dynamics

3-31

Pyro Shock

Thermal Vacuum

Acoustic

Stowed Vibration

42 Deploy/Retract
Cycles

Table 3.2-3 Breakage Resulting from Environmental Test Program

Test Environment	Percent Broken* Glass Platelets	Percent* Broken Cells	Percent Broken Coverglass
Pyro Shock	0.043	0.025	0.100
Thermal Vacuum	0.213	0.400	0.825
Acoustic	0.084	0.325	0.225
Stowed Vibration	0.121	0.900	1.975
35 Ambient Deploy/Retract Cycles	0.008	0.100	0.125
TOTAL BREAKAGE	0.469	1.750	3.250

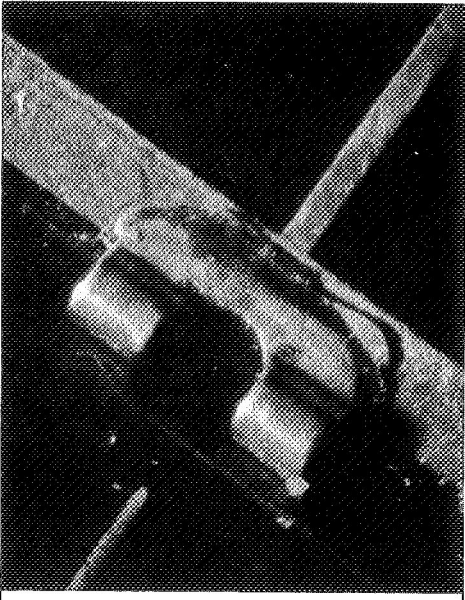
* Does not include damage known to be caused by handling and instrumentation installation and removal.

occurred on an inboard module (K12). This may be an indication of insufficient cushioning between the storage drum shell and the first wrap of solar cells.

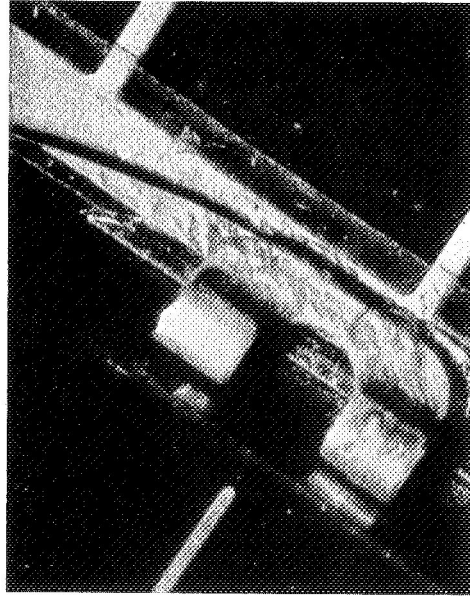
The results indicate that the cell/coverglass composite is not as resistant to damage as a corresponding glass platelet mass simulation which is .011 inches thick. The .003 in. thick coverglass cracked independently of the cell in many cases. The two modules with the most coverglass breakage are K12 and H1, located at the inboard and outboard ends of the -Y blanket, respectively. The H1 module also has the largest percentage of cell breakage. This would tend to indicate that the environment which produces breakage is more severe at both the inner and outer wraps of the stowed array. It is certain that the potential for handling damage is greater on the outer wrap.

Module J6 suffered extensive interconnect damage which was reflected by a 29.5 percent reduction in the maximum power. This damage occurred as a result of the thermal vacuum test series. Figure 3.2-2 shows examples of the various type of damage which occurred within this module. The majority of this damage occurred within the area of the module which was affected by the localized overheating during the stowed high temperature thermal vacuum test. The temperature in this area was high enough to melt the solder and cause the top contact feet to lift as shown in Figure 3.2-2 (d). The damaged pictured in figure 3.2-2 (a) and (b) is a silicon flake-out at the foot which is indicative of a low temperature failure mechanism. It is possible that the fractured conductor in (c) was caused by snagging on a cushioning button on the adjacent wrap.

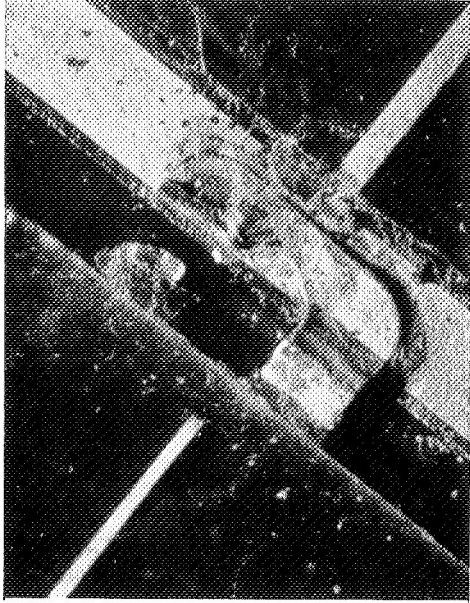
Some interconnect damage on the H1 module was observed after the stowed vibration test. Figure 3.2-3 shows examples of the types of failure. The lifted feet



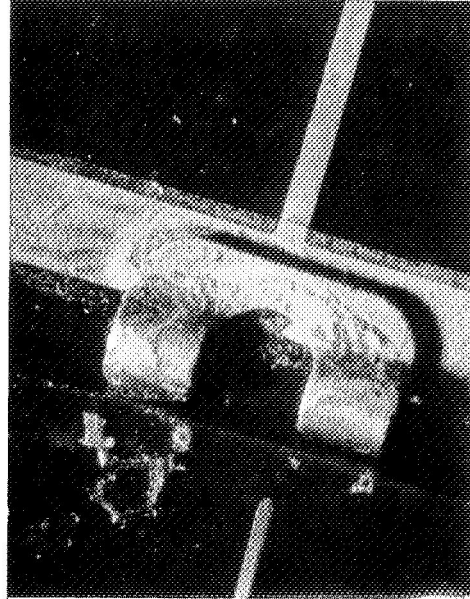
(a) Silicon Flake-out



(b) Silicon Flake-out and Splintering

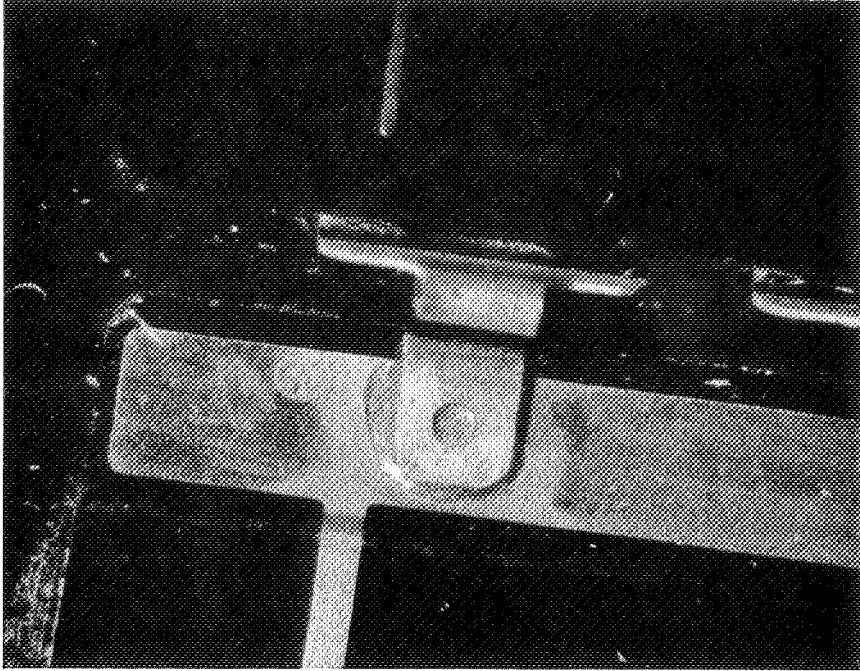


(c) Fractured Interconnect Foot

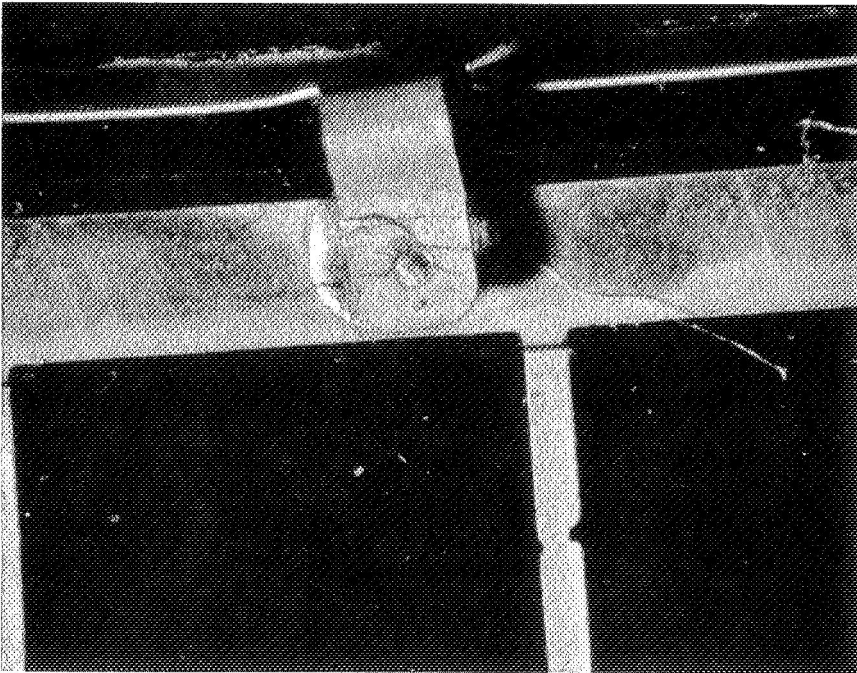


(d) Lifted Interconnect Foot

Figure 3.2-2. Damage in J6 Module



(a) Fractured Interconnect Foot



(b) Lifted Interconnect Foot

Figure 3.2-3. Damage in H1 Module

occurred adjacent to a cell which was not securely bonded to the substrate. The fractured conductor pictured in (a) was at the edge of the module.

One example of an interconnect related failure was also observed in the G7 Module following the stowed vibration test. This fracture of the cell around a top connection is pictured in Figure 3.2-4.

For comparison purposes results from two previous lightweight solar array development programs are summarized. Reference 1-8 summarizes the results of a program which included random and sinusoidal vibration environments and thermal vacuum tests of an array panel utilizing stretched fiberglass tape substrate and beryllium frames. Results are summarized in Table 3.2-4.

The second program is documented in Reference 1.9. The array assembly is a 50 square feet two boom Rollup Solar Array and it was subjected to stowed vibration and thermal vacuum tests. Results are summarized in Figure 3.2-5 and Tables 3.2-5 and 3.2-6.

3.2.2.3 BI-STEM Performance

The BI-STEM performed its function throughout the program. Problems associated with it are described in the following paragraphs. There are three microswitches within the BI-STEM actuator which perform the following functions:

- (1) Full retract limit switch - This switch is actuated by a ramp at the top of the rod to remove power from the motor when the rod reaches the fully retracted position.

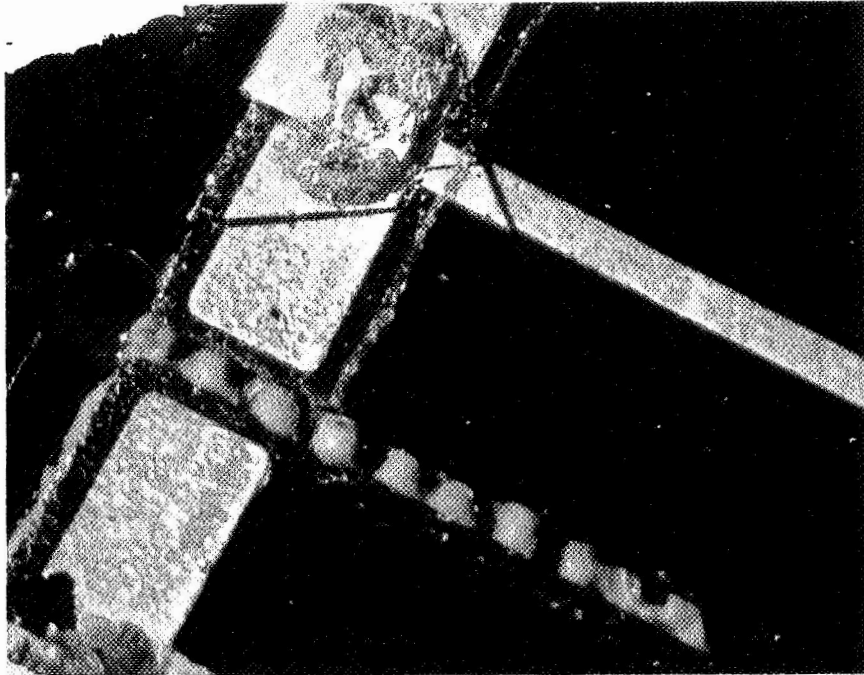


Figure 3.2-4. Fractured Cell at Foot in G7 Module

TABLE 3.2-4

TEST RESULTS FOR STRETCHED FIBERGLASS SUBSTRATE SOLAR ARRAY PANEL
 (From Boeing Lightweight Solar Panel Development Program)

A. ELECTRICAL PERFORMANCE

Test Module	Maximum Power - Watts Corrected to 55° C				
	3	4	5	6	7
3	23.5	24.7	24.7	25.1	23.3
5	25.3	24.7	25.1	24.0	23.9
7	25.2	25.0	24.9	24.2	24.2
9	24.5	24.6	24.4	23.8	23.8
10	24.1	23.9	24.1	24.0	24.0
11	24.4	24.6	24.2	24.1	24.0
Total	147.0	147.5	147.4	145.2	143.2

NOTE: Results from the first two tests were 25% low and could not be duplicated through controlled application of possible errors.

MODULE LOCATION (Back View)

8	7	6	5	4	3	2	1
9		10		11		12	

B. DAMAGE MAP

9 2CG 1C 2P		10 3CG 2C		11 2CG 1C 1P		12 3CG 3C	
8	7	6	5	4	3	2	1
5CG 3C	11CG 4C 3P	3CG	2CG 2P	4CG 4C	1CG 2C		2CG

Total 38CG - Coverglass Cracks
 20C - Cell Cracks
 8P - Pigtail Breaks

NOTE: There are 6480 each of cells and coverglasses on the panel.

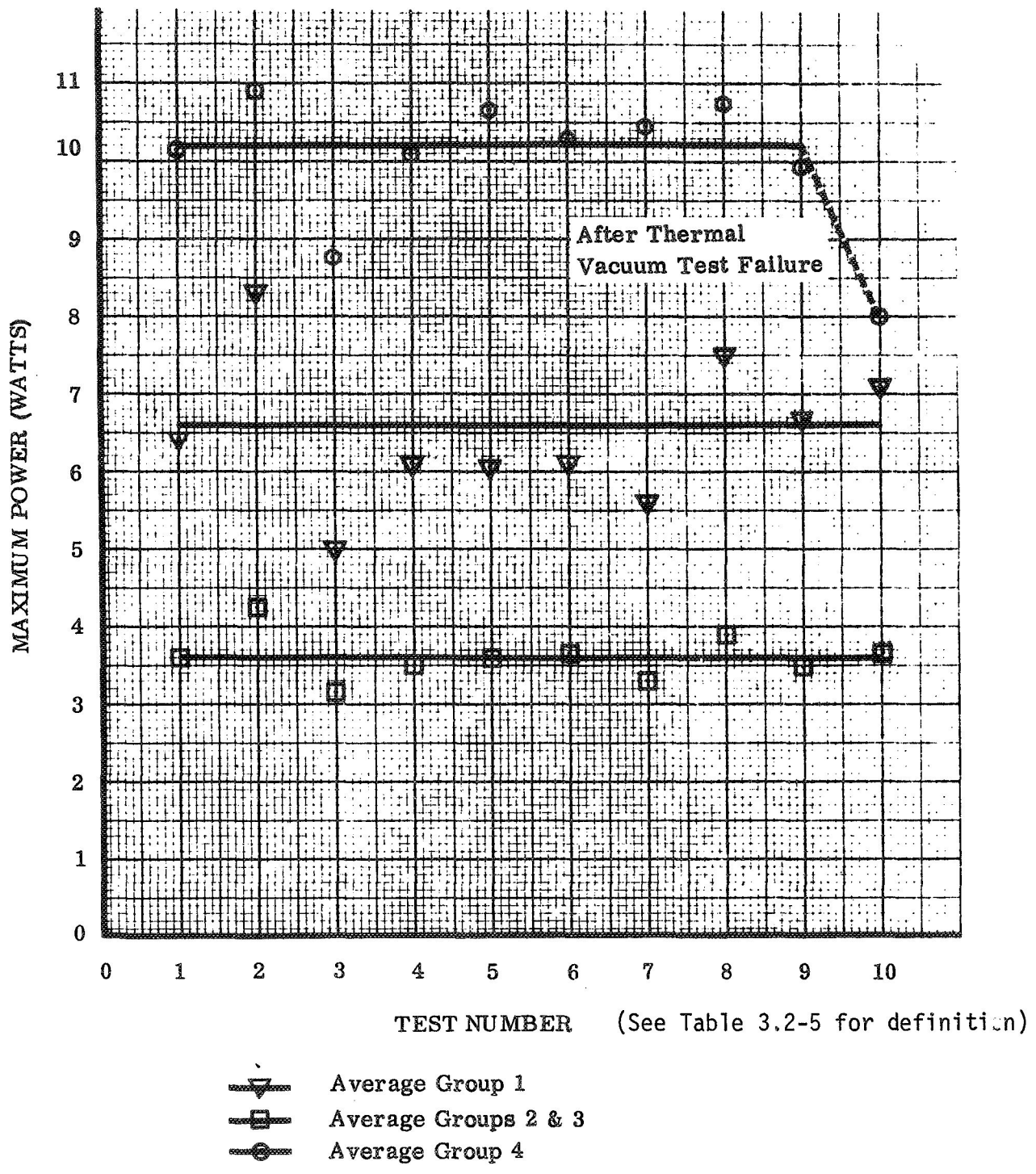


Figure 3.2-5. Electrical Performance (From Ryan Solar Array Program Report)

Table 3.2.5 Identification of Test Number

(Reference Figure 3.2-5)

<u>Test Number</u>	<u>Date</u>	<u>Test</u>
1	10-6-67	*After final assembly
2	10-6-67	After first retraction and deployment
3	10-18-67	After second retraction and deployment
4	10-18-67	After third retraction and deployment
5	10-20-67	After fourth retraction and deployment
6	10-20-67	After fifth retraction and deployment
7	10-31-67	Prior to sine vibration test
8	2-6-68	*Prior to random vibration test
9	2-16-68	*After random vibration test
10	4-11-68	*After thermal vacuum test

* Measured with center support rollers on fixture.

Table 3.2-6. Cracked Cells Per Matrix
(From Ryan Solar Array Program Report)

		CRACKED CELLS PER MATRIX																Total	Cracked During Test		
		MATRIX NO.	17	18	19	20	2	3	13	15	8	6	16	1	9	7					
EVENT		4	3	1	1	1	1	0	0	1	3	8	2	4	3	2	4	37			
Assembly		0	0	0	0	0	0	0	0	0	0	0	0	0	0	4	0	4	4		
1st Deployment		1	0	0	0	0	0	0	0	0	1	1	1	3	0	1	0	7	7	4	
2nd Deployment		0	0	0	1	0	0	0	1	0	1	0	0	0	0	0	0	3	3	3	
3rd Deployment		0	0	0	0	0	0	0	0	0	0	0	0	0	0	0	0	0	0	0	0
4th Deployment		0	0	0	0	0	0	0	0	0	0	0	0	0	0	0	0	0	0	0	0
5th Deployment		0	0	0	0	0	0	0	0	0	0	0	0	0	0	0	0	0	0	0	0
Install Instrumentation		0	0	0	0	0	0	0	0	0	0	0	0	0	0	1	0	1	1	1	8
Sine Vibration		3	0	1	0	0	1	0	0	0	0	0	1	1	0	0	1	8	8	8	
Rework		2	0	0	0	0	0	0	0	0	2	1	1	2	0	0	0	8	8	8	
Random Vibration		0	1	0	0	0	0	0	0	0	0	0	0	0	1	0	0	2	2	2	
1st Thermal Vacuum Test		1	0	0	0	0	0	0	0	0	0	0	0	0	0	0	0	1	1	1	
Rework		0	0	0	0	0	0	0	0	0	0	0	0	1	1		2	2	2		
2nd Thermal Vacuum Test		0	0	0	0	0	0	0	0	0	0	0	0	0	1	0	0	1	1	1	
Cold Deployment Damage		0	0	0	0	0	0	0	0	0	0	0	0	0	0	33	23	56	56	56	
TOTAL		11	4	2	2	1	1	1	1	4	11	6	10	8	41	28	130	130	130	82	

Total Cells per matrix 56

Total cells (14 matrices) 784

- (2) Orbital retract limit switch - This switch is actuated by a roller which falls into a slot in the rod element to remove power from the motor when the rod reaches the orbital retract position (approximately 4 inches from fully retracted).
- (3) Full extend limit switch - This switch is actuated by a roller which falls into a slot in the rod element to remove power from the motor when the rod reaches the fully extended position.

At the conclusion of the testing program none of these switches was operable. The full retract limit switch mounting bracket was out of adjustment as it became loose during the course of the testing program. Since its function was not vital to the actuation of the BI-STEM no effort was made to repair or adjust this switch. The orbital retract limit switch roller actuator broke off during an ambient deploy/retract of the BI-STEM on March 20, 1970. Figure 3.2-6 shows the location of this switch in the BI-STEM actuator housing. The roller which falls in the slot in the rod element is attached to a AZ31B-H24 magnesium bracket with a spring pin as shown in the detail sketch. This bracket is, in turn, riveted to a 302 stainless steel leaf spring which deflects to depress the microswitch button. The point of fracture was at the root of the bracket at the outermost rivet hole. The most probable cause of this failure is fatigue damage due to an inadequate section moment of inertia to accommodate the cyclic bending loads imposed during the component vibration test. The stress concentration at the rivet hole was probably a major contributing factor. A possible redesign of this roller bracket is shown on Figure 3.2-6 to illustrate that an adequate fix is not complicated. On June 5, 1970 an identical failure of the roller bracket on the full extend limit switch was discovered while attempting to deploy the BI-STEM following the Z axis stowed vibration test. This switch is located adjacent to the orbital retract limit switch and is actuated in exactly the same manner.

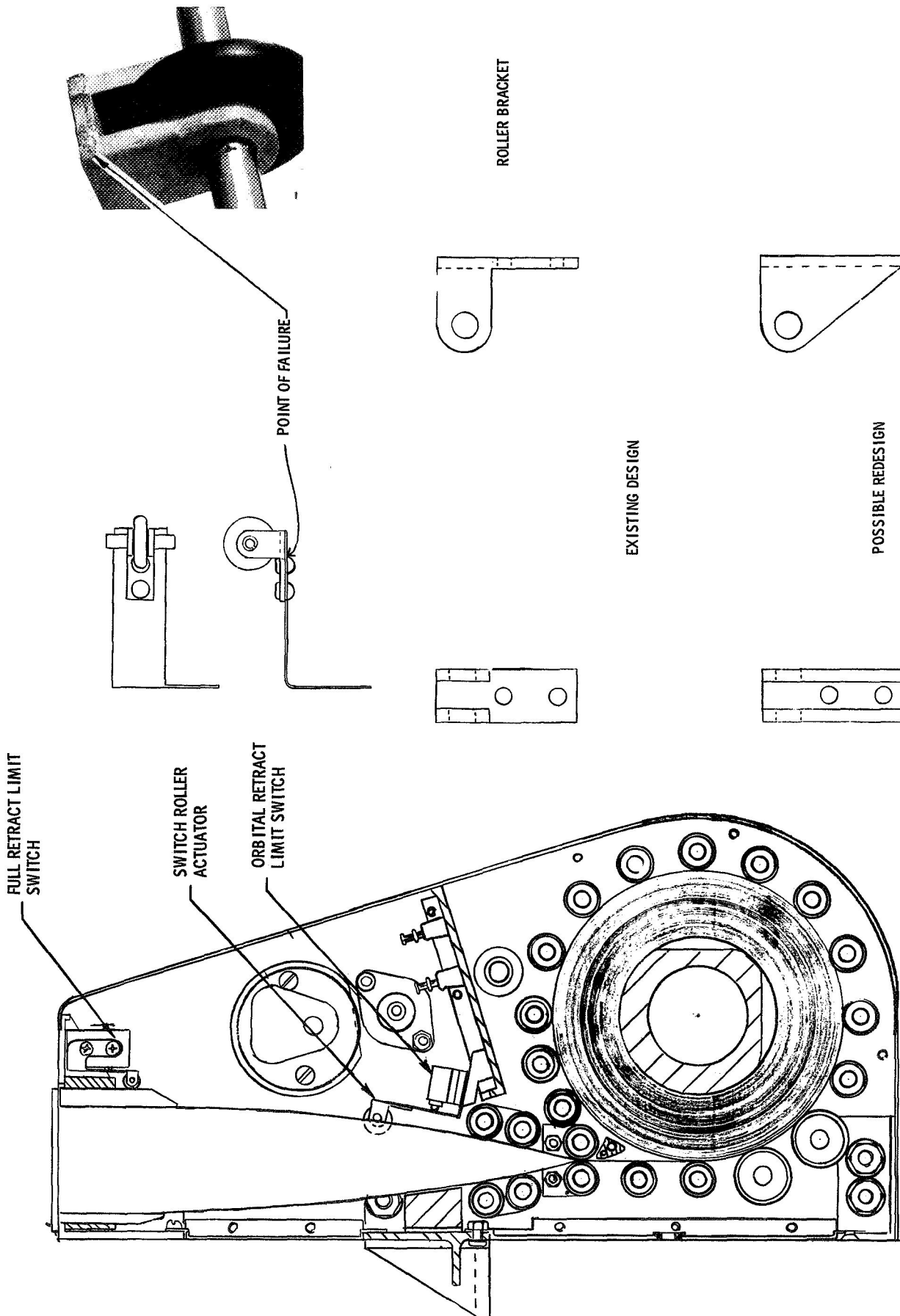


Figure 3.2-6 BI-STEM Limit Switch Actuator Problem

On June 17, 1970 a fatigue crack in the BI-STEM rod outer element was discovered while preparing for the 42 cycle life demonstration following the stowed vibration test. This 1/8 in. long crack is located approximately 7 1/8 in. down from the centerline of the leading edge member at the edge of outer element on the +Y side of the rod. No change was detected during and after the life demonstration. This crack did not affect the function of the BI-STEM. Except for the failure of the switch actuators, the BI-STEM performed its function in the system throughout the test program. There was a general increase in the noise level on the BI-STEM motor current as the program progressed.

The largest change occurred as a result of the thermal vacuum low temperature deploy/retract cycle. It is also apparent from the test data that the time to deploy or retract at ambient conditions increased as a result of the low temperature deploy/retract cycle. Since that increase, however, the total times to deploy or retract at ambient conditions have remained relatively constant.

3.2.2.4 Slip Ring Performance

At the beginning of the test program, the slip ring resistance remained constant as the storage drums turned during array deployment and retraction. Some slip ring dynamic resistance change was first recorded during the low temperature deploy/retract cycle. Similar fluctuations, along with a slight overall increase in resistance, were recorded during the high temperature deploy/retract cycle. The first ambient deployment following the stowed vibration test produced relatively large fluctuations in resistance with spikes which corresponded to the period of rotation of the storage drums. After 35 ambient deploy/retract cycles, the magnitude of these fluctuations in resistance had decreased substantially. The periodic nature of the changes in resistance indicates the possibility of

dirt on the power rings which was gradually removed by the brushes as the array was deployed and retracted during the 35 cycle life demonstration. There has been no significant increase in the static resistance of the power rings as a result of the environmental test program.

THINISTOR* type thermistors were bonded to the array substrate and used to monitor solar cell module temperature during the thermal vacuum test. These devices were selected as the transducer best suited for flight use but it was recognized this application was different from the normal use of this device. Review of the performance of the devices indicates they were damaged during installation in that a resistance change occurred which would alter the calibration. Further resistance changes occurred during the thermal vacuum test, probably because the ageing temperature was exceeded. At this time they are not an acceptable temperature transducer for this application.

* Trademark of Victory Engineering Corp., Springfield, N. J.

3.3 SYSTEMS TESTS

3.3.1 DEPLOYED DYNAMICS TEST

3.3.1.1 Introduction

The purpose of the deployed dynamics tests was to provide data on the dynamic characteristics of the deployed rollup array. It was to be used in a comparison with the analytical results to verify the mathematical models generated in earlier phases of the program or to provide information to improve the mathematical models. The linearity of the system response to different excitation levels was to be determined. Data on damping was to be obtained for use in future designs and analyses.

It was recognized that this test was unusual and that several problems had to be solved prior to testing. The effects of gravity were known to be large and had to be taken into account in the selection of the test approach. The large surface area of the array would produce significant aerodynamic forces. The natural frequencies of the system are below the operating range of conventional vibration test equipment and it was anticipated that very slow sweep rates would be needed to determine natural frequencies. Conventional accelerometers and other vibration instrumentation are not suitable for the low frequency, large displacement motion involved in this test and would affect the mass distribution of the test specimen.

A detailed discussion of this test is contained in Volume II, Section 4.3.

3.3.1.2 Test Approach

The approach to the test was to carry out an integrated effort involving the development of test techniques, the analysis of the array in the test configuration, the identification of instrumentation and equipment requirements, the procurement of new instrumentation and vibration test equipment, and the design and fabrication of the fixtures needed for the test. Development of the test techniques started in early 1968 and continued through the procurement and checkout of the new equipment. The test plan included the measurement of the natural frequencies, mode shapes, linearity, and modal damping for both in-plane and out-of-plane motion of the array.

It was concluded the best approach to the gravity forces was to test the system in a manner where the effects of gravity could be adequately included in the mathematical model. Correlation of the test results in gravity with a mathematical model that included gravity would provide confidence that the analysis could be extended to the zero gravity case with good results. The test arrangement was to deploy the array vertically downward and excite the system with motion at the center support. The deployed test length of 26 feet was determined by the work space below the lid of the vacuum chamber. This arrangement provided a free boundary condition at the leading edge member which is the boundary condition which will exist in an orbiting application. The blankets will have an increasing tension due to the force of gravity but are supported by the relatively rigid drums. The Negator spring motors were supplemented with support aids that individually applied torque to the drums to compensate for the weight of the blankets. The drums were allowed to rotate.

To eliminate aerodynamic effects, the tests were conducted in a vacuum chamber with an ambient pressure of less than 1mm Hg.

A DC coupled exciter suitable for vacuum operation was used for the test. Auxiliary equipment to provide stable sinusoidal motion down to 0.008 Hz and 0.0025 inches motion (double amplitude) was procured. A sweep rate capability down to 10^6 seconds per decade was included.

Array displacements were measured with Optron Model 800 optical trackers modified to allow operation in vacuum. The trackers have no physical contact with the test specimen and have the capability of measuring displacements in two directions over the frequency range from DC to 10 KHZ. The sensitivity of the units is a function of the lens system; the setup used for these tests had the capability of resolving motions as small as .001 inch. A total of eight trackers was used for the test. Two were focused on the ends of the leading edge member and were fixed. Six were mounted on a scanning bar which traversed the length of the system and could be positioned at ten equally spaced span locations. White paper targets were mounted on the cell side of the solar array blankets to provide the contrast needed for the operation of the trackers.

The physical arrangement of the test is shown in Figure 3.3-1 which is a sketch of the cross section of the setup in the 32 foot by 54 foot Space Simulator at the General Electric Valley Forge Space Center. The locations of the optical trackers are conceptual and are not specifically correct with respect to location or number. The array is suspended from the support fixture which includes a linear bearing system that can be arranged to provide motion in either of two

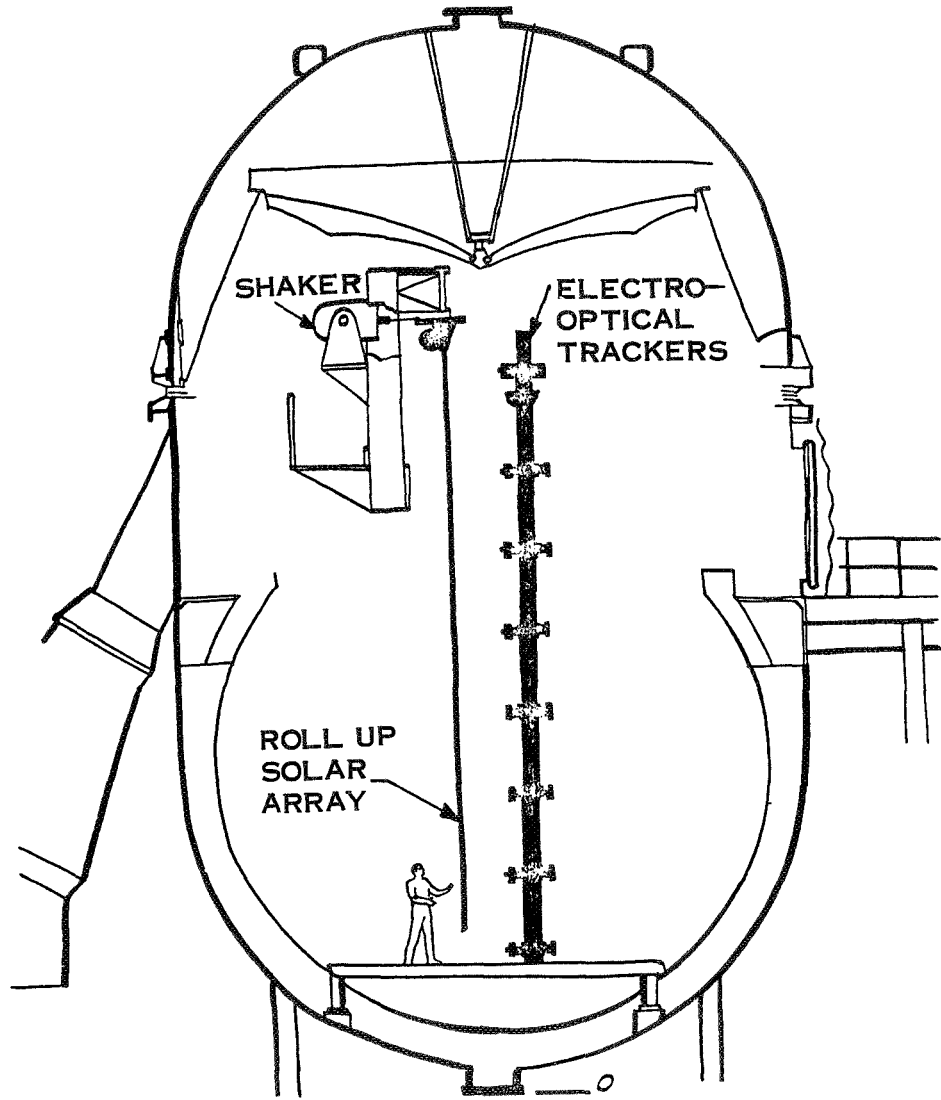


Figure 3.3-1. Deployed Dynamics Test Set-Up

directions in the horizontal plane or rotation about a vertical axis. The test data flow is shown in Figure 3.3-2.

3.3.1.3 Summary of Results

The sequence of tests is shown in Table 3.3-1. Testing was carried out initially in air to obtain preliminary data and then in vacuum. Resonant frequencies are summarized in Table 3.3-2. Mode shapes were determined with one example of the results shown in Figure 3.3-3. Experimental damping coefficients are tabulated in Tables 3.3-3 and 3.3-4.

Excellent agreement with analysis was obtained for the first bending mode of the system (out-of-plane symmetric excitation). Figure 3.3-4 shows the predicted response (for a damping ratio of 0.025) at 80% span and at the outboard edge of the blanket. A plot of data at this point for a slow sweep through this resonance is shown in Figure 3.3-5. The measured value of damping is approximately .003. Note the very long time required to sweep through this resonance (71 minutes). Very slow sweep rates are required for modal vibration tests of a lightly damped structure with a low natural frequency. Analytical and experimental data do not agree as well for the higher modes. Additional results are presented and discussed in Section 4.3 of Volume 2 of this report.

3.3.2 ENVIRONMENTAL TESTS

The RA250 Engineering Prototype Model was subjected to a rigorous environmental test program which included the following tests:

1. Pyrotechnic Induced Shock Test
2. Thermal Vacuum Test Series

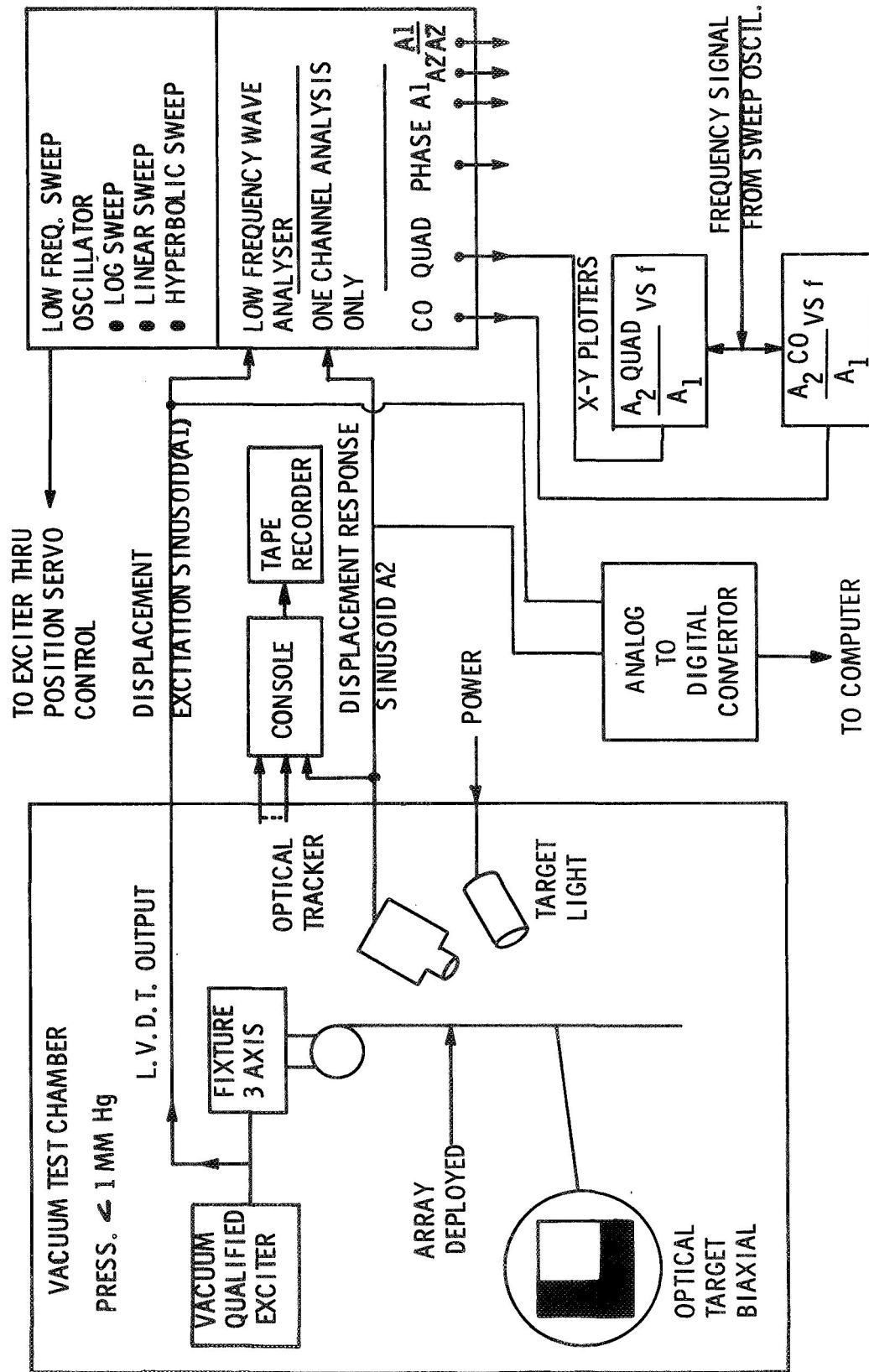


Figure 3.3-2 Deployed Dynamics Test Data Flow

Table 3.3-1 Testing Sequence

Test Axis	Test Description	Date
Out-of-Plane (Symmetric) Z-Axis Excitation	Ambient Sweep Test (0.1 Hz to 2.8 Hz)	3-30
	Sweep Test in Vacuum (0.13 Hz to 1.0 Hz)	3-31
	Resonance Dwells in Vacuum	4-1 & 4-2
	Linearity Checks and Damping Measurements in Vacuum	4-1 & 4-2
	Ambient Sweep Test with Leading Edge Member Removed	4-9
	Vacuum Sweep Test with Leading Edge Member Removed	4-10
	Vacuum Resonance Dwell with Leading Edge Member Removed	4-10
Out-of-Plane (Antisymmetric) Torsional Excitation About X-Axis	Ambient Sweep Test (0.05 Hz to 1.0 Hz)	4-3
	Sweep Test in Vacuum (0.15 Hz to 1.0 Hz)	4-4
	Resonance Dwell in Vacuum	4-6
	Narrow Band Sweep Tests in Vacuum	4-7
	Linearity Checks and Damping Measurements in Vacuum	4-7
	Movies of Resonance Dwells	4-8
	Ambient Sweep	4-8
	Ambient Sweep Modified Tension Distribution at the Leading Edge	4-8
In-Plane Motion Y-Axis Excitation	Ambient Sweep Test (0.1 Hz to 2.3 Hz)	4-8
	Sweep Test in Vacuum (0.6 Hz to 1.6 Hz)	4-9
	Ambient Sweep with Drums Locked	4-9
Static	Mapping of Static Shape of System	4-9

TABLE 3.3-2

SUMMARY OF RESONANT FREQUENCIES
FROM DEPLOYED DYNAMIC TESTS

A. Out-of-Plane		Frequency (Hz)					
		M O D E			N U M B E R		
Symmetric Excitation		Measured			Predicted*		
		1	2	3	1	2	3
Ambient		.16	.55			**	
Vacuum		.252	.632	.781	.248	.55	.94
B. Out-of-Plane							
Ant-Symmetric Excitation							
Ambient		.12	.50	.99		**	
Vacuum		.174	.65	.74	.232	.58	.96
C. In-Plane Excitation							
Ambient		1.00				**	
Vacuum		1.015			.38		

* Blanket membrane modes omitted

** No analysis was made which included aerodynamic effects

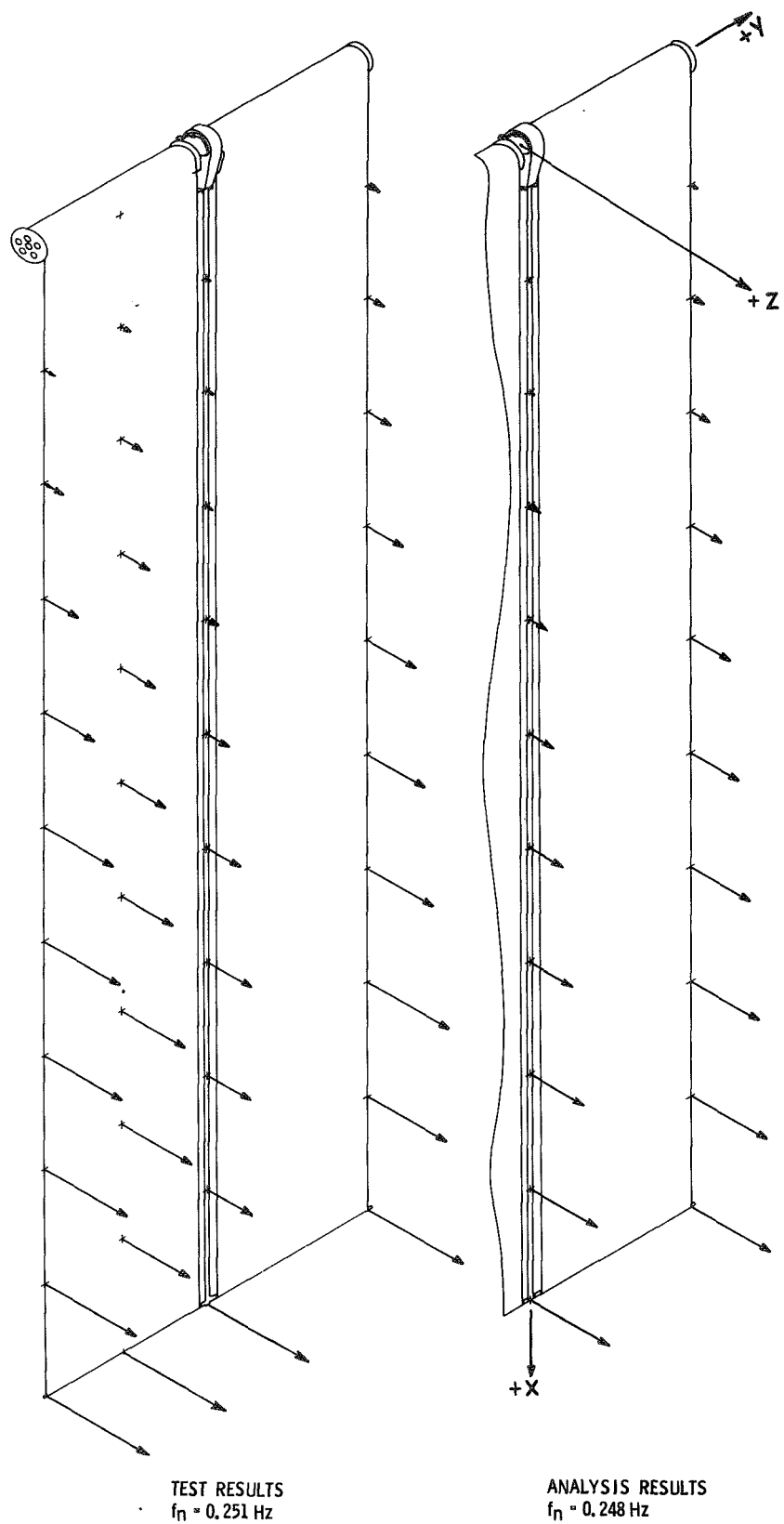


Figure 3.3-3 Mode Shape - First Mode-Out-of-Plane Symmetric Excitation

TABLE 3.3-3

DAMPING COEFFICIENTS FOR OUT OF PLANE MODES -
SYMMETRIC EXCITATION

Modal Frequency (Hz)	Damping Coefficients				
	Method 1		Method 2		Method 3
	a	b	Input Level in. DA		
0.251	.003	.0042	.025	.003	.0055
		.0053	.050	.0055	
0.632	—	—	—	—	—
0.781	—	—	0.10	.0275	—
			0.20	.0226	

Notes: Method 1 determined from decay of motion. a is decay from response to step input and b is decay from dwells at a natural frequency.

Method 2 is determined from frequencies of peak in-phase response to a slow sinusoidal sweep.

Method 3 is determined from comparison of response with analytical responses.

TABLE 3.3-4

DAMPING COEFFICIENTS FOR OUT OF PLANE MODES -
ANTI SYMMETRIC EXCITATION

Mode Frequency (Hz)	Damping Coefficients			
	Method 1 a	Method 1 b	Input Level in D.A.	Method 2
.178		.0060	0.0025	
.178	.0069	.0054	0.0050	
.65			0.01	.010
		.037	0.05	.010
		.043	0.10	.011
			0.25	.012
.74			0.01	.015
			0.05	.015
			0.10	.018
			0.25	.019

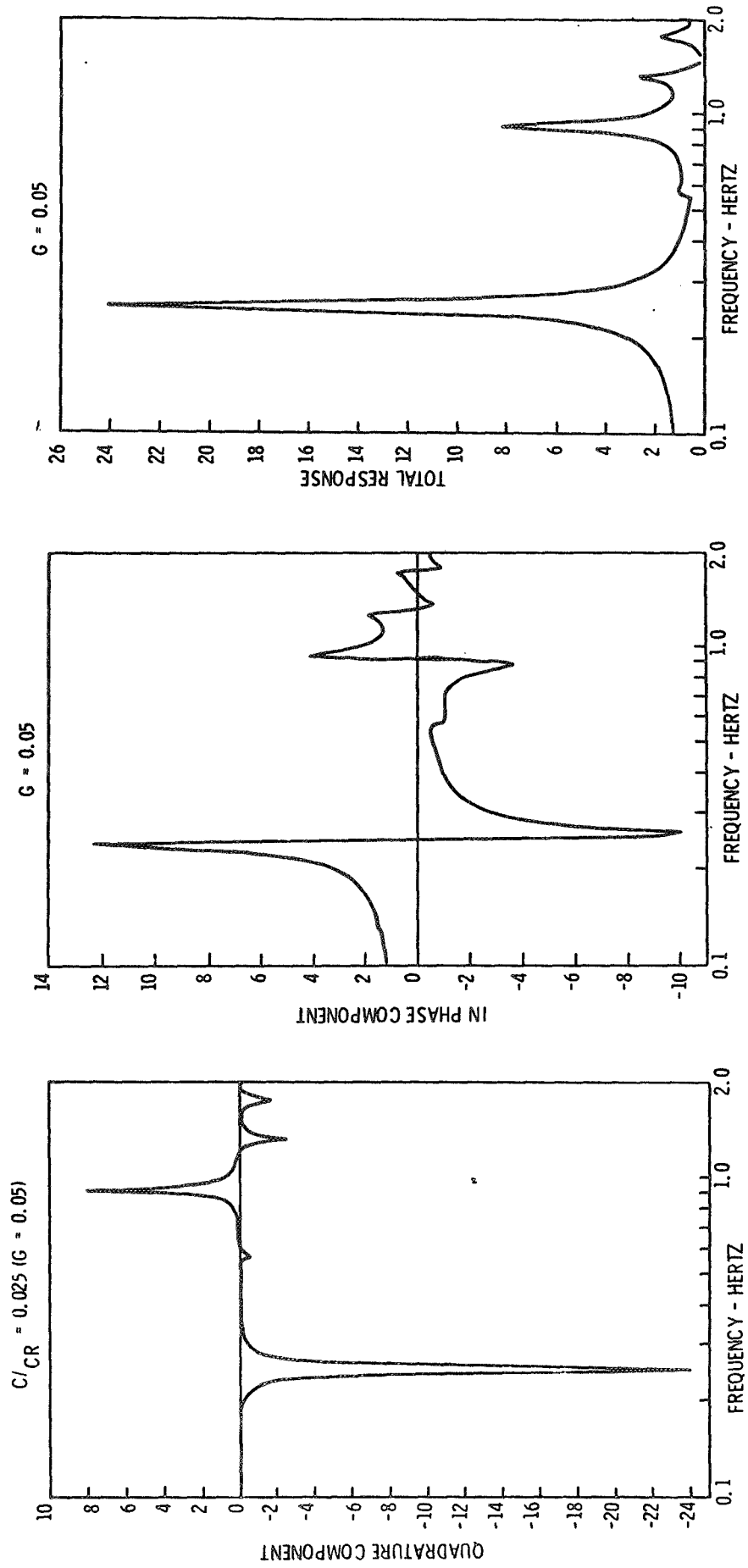


Figure 3.3-4. Predicted Response at Outboard Edge of Blanket (80% Span) Out-of-Plane Symmetric Excitation

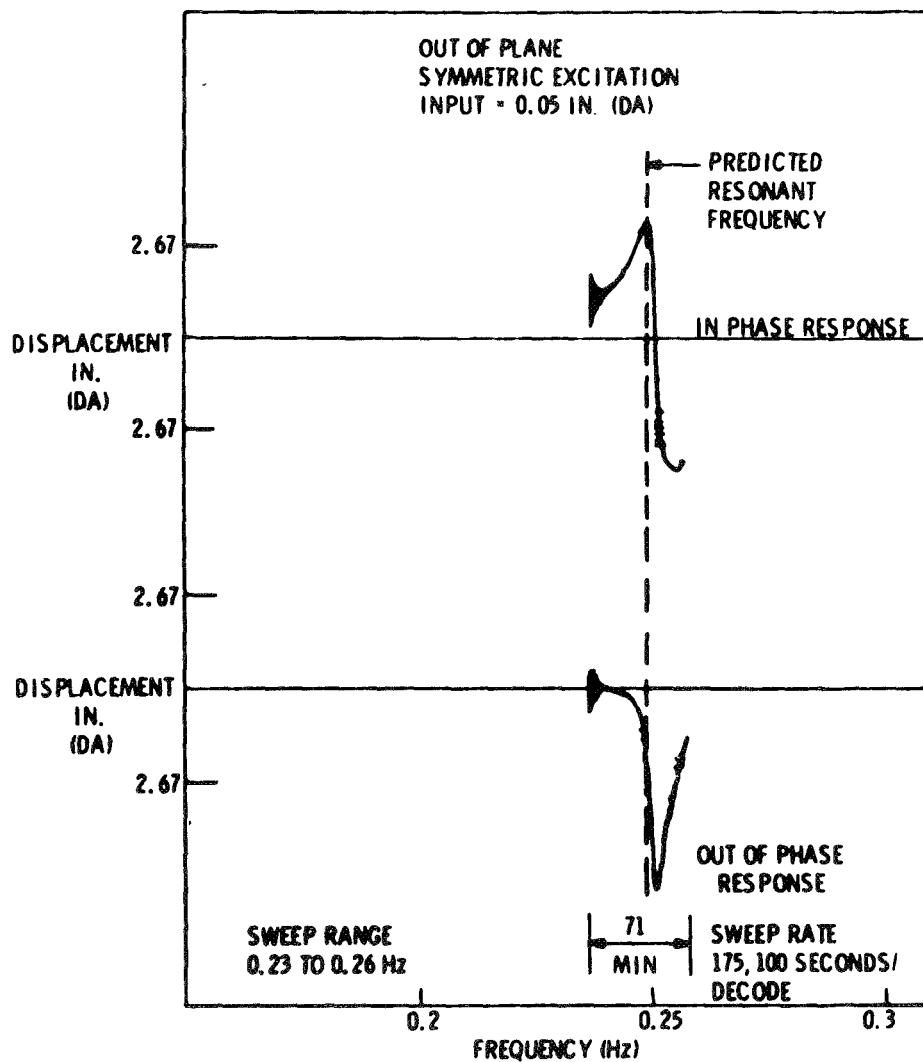


Figure 3.3-5. Results of Narrow Band Frequency Sweep
3-59

3. Acoustic Noise Test
4. Stowed Vibration Test

These tests were performed in the order listed, with intervening health checks as shown in Figure 1-2.

3.3.2.1 Pyrotechnic Induced Shock Test

3.3.2.1.1 Introduction

The pyrotechnic induced shock test was conducted by simultaneously firing both separation nuts (each armed with two active squibs) on the outboard end supports. The response of the system was determined through the use of shock spectra analysis to determine the necessity for further shock type testing to synthesize the specified shock pulse shown in Figure 3.3-6.

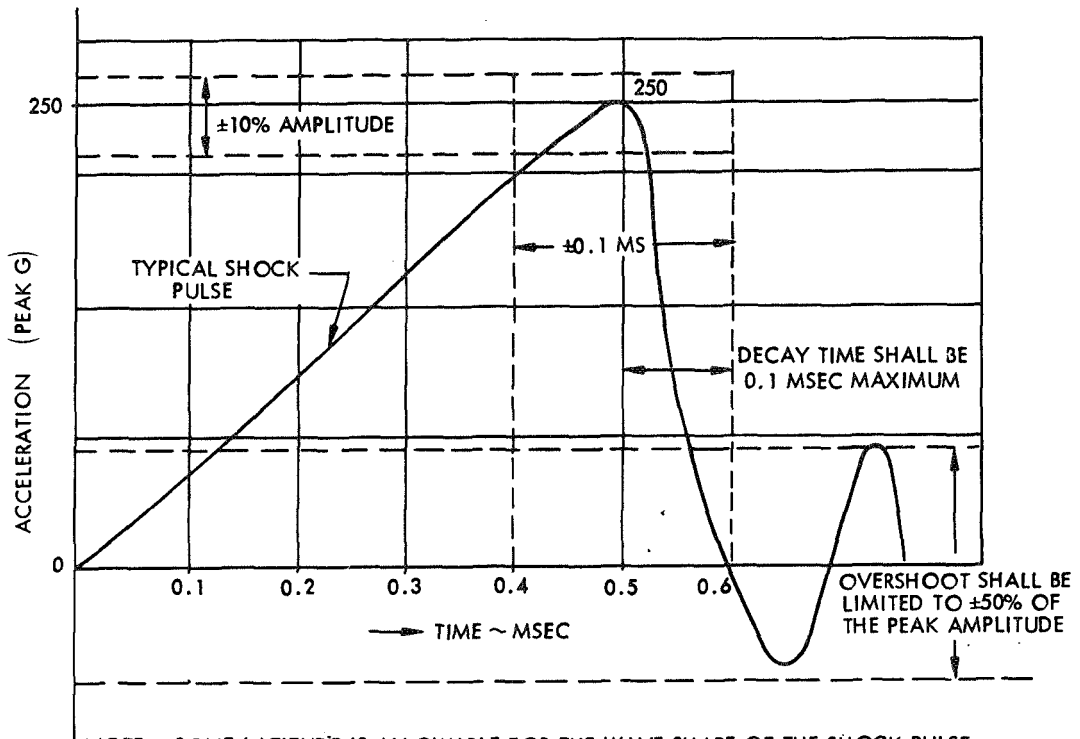
A detailed discussion of this test is contained in Volume II, Section 4.4.

3.3.2.1.2 Summary of Results

The array structure suffered no visible or operational damage as a result of this shock environment. The results of the health check are discussed in Volume II, Section 4.2.

3.3.2.1.3 Discussion

The highest accelerations were measured on the movable arms four inches from a separation nut assembly. Acceleration levels of 6,000 and 2,500 G (O-P) were recorded. These levels were approximately equal to shock levels measured on the



NOTE: SOME LATITUDE IS ALLOWABLE FOR THE WAVE SHAPE OF THE SHOCK PULSE. HOWEVER, IT IS DESIRABLE THAT THE SHAPE CONFORM TO THAT OF A TERMINAL PEAK SAWTOOTH AS NEAR AS PRACTICAL.

Figure 3.3-6. Shock Pulse

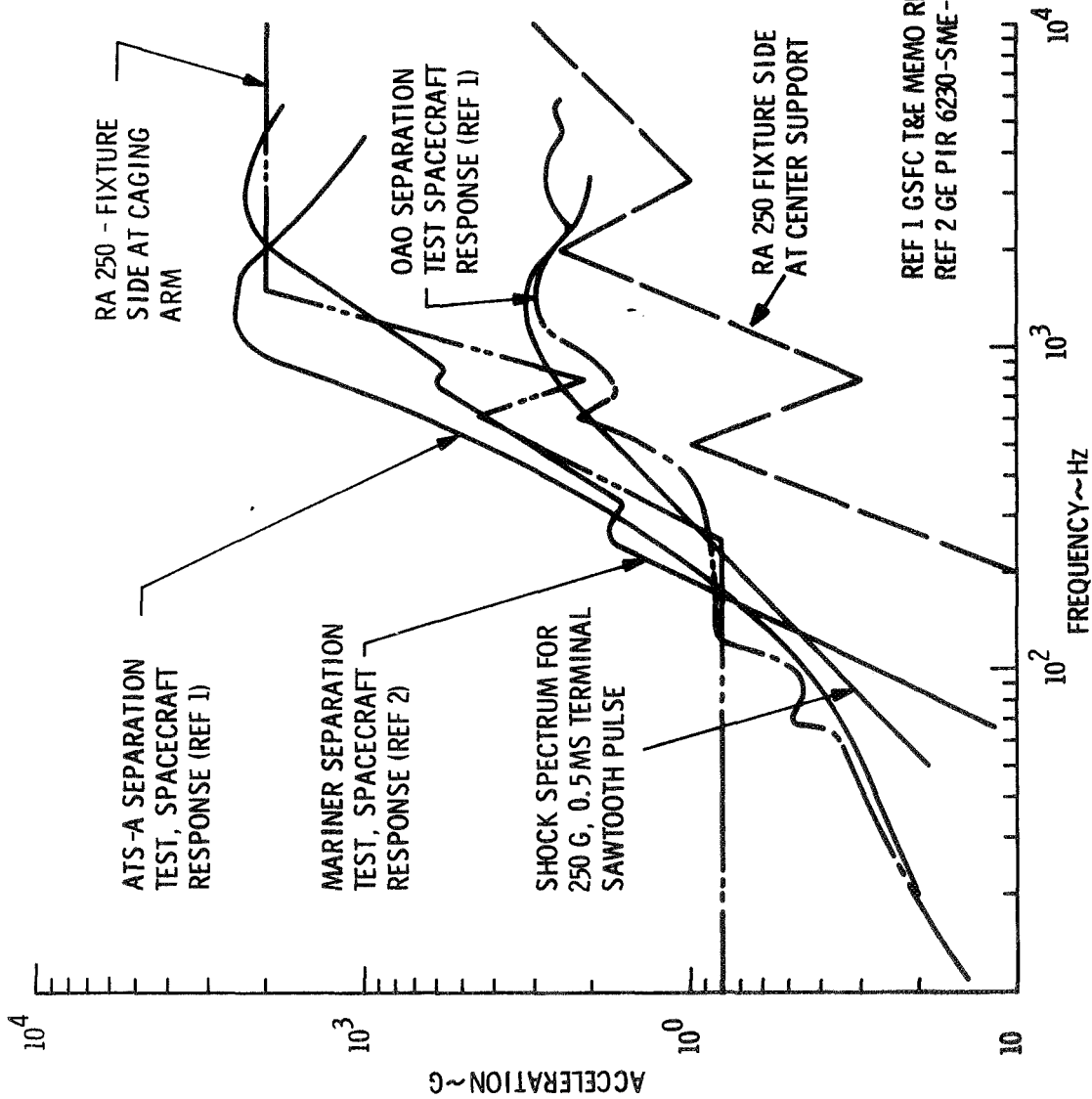
array handling frame interface with the outboard end supports. The shock level rapidly decreased in magnitude with distance from the shock source. Shock levels on the drums at 100% span (near pyrotechnics) were 1365 G (O-P) and at 0% span (near the outer support) dropped to 124 G (O-P). The blanket outer wrap (about 4 in. from the outboard end), the center support structure and the drum bearing support shaft all experienced acceleration levels of 125 G (O-P) or less. This attenuation results from the lack of high frequency transmissibility across the soft blankets and the distance between the shock source and the response points monitored on the center support.

As shown in Figure 3.3-7 the RA250 separation nut firings induce acceleration loads which are comparable to those induced in spacecraft structures by the firing of other pyrotechnical release devices. At the outboard end supports, the shock spectrum of the array pyrotechnics is higher than that resulting from the 250 G, 0.5 millisecond terminal saw tooth pulse defined in Reference 1-7. In the center support region, the shock spectra from the separation nut actuation is approximately equivalent to the spectrum of the saw-tooth pulse above 2000 Hz and approximately 50% of the spectrum of the saw tooth below 2000 Hz.

3.3.2.2 Thermal Vacuum Test Series

3.3.2.2.1 Introduction

The RA250 engineering prototype model was subjected to a series of thermal vacuum tests which consisted of the following segments as defined in the JPL specification (Reference 1-2):



REF 1 GSFC T&E MEMO REPT NO. 671-18 DTD OCT 9, 1967
 REF 2 GE PIR 6230-SME-190 S. M. KAPLAN DTD MAY 2, 1968

Figure 3.3-7. Comparison of Various Spacecraft Separation Shock Spectra with the RA250 Specification and Realized Shock Spectra

<u>Test No.</u>	<u>Description</u>
1	Deployed Transient
2	Low Temperature Stowed
3	Low Temperature Deploy and Retract
4	Stowed Transient and High Temperature Soak
5	High Temperature Deploy and Retract

A detailed discussion of this test series is contained in Volume II, Section 4.5.

3.3.2.2.2 Summary of Results

The following anomalies occurred as a result of this series:

1. Both separation nuts fractured at the mounting flange during the outboard end support release immediately prior to the low temperature deploy/retract cycle.
2. The array blankets failed to rewrap properly on the storage drums during the low temperature retraction test. Post test inspection showed that a pull-away thermocouple wire had tangled with the Y drum.
3. A localized heating condition occurred during the high temperature stowed test. This anomaly is attributed to a "greenhouse" phenomenon which resulted when visible and near-infrared energy from the

heating lamp array was transmitted through the dummy glass and trapped inside, causing localized high temperatures on inside wraps of the stowed array blankets. This condition would not have occurred if the array blankets were completely covered with solar cell modules instead of optically transparent dummy glass platelets.

3.3.2.2.3 Discussion

The deployed array transient test was performed without incident. An example of the temperature vs. time histories for two active solar cell modules are shown in Figure 3.3-8. All active solar cell modules had similar transient response temperature histories. In all cases, the warm-up to +284°F was performed by first turning on the lamps at a very low voltage to allow the filaments to heat up before applying full voltage. This procedure was necessary to avoid blowing fuses as a result of the high inrush current associated with the cold lamp filaments. This turn on procedure caused the step-like appearance of the temperature rise plots for active solar cell modules.

During the low temperature stowed test, it became apparent that the specified low temperature extreme of -202°F (-130°C) on the control thermocouple (located on the H1 module) could not be reached within a reasonable period of time. Therefore, this phase of the test was discontinued when the control thermocouple reached -172°F.

The low temperature deployment of the array was initiated by the simultaneous firing of both squibs in each separation nut. The temperature recorded on a thermocouple located on the outboard end support adjacent to the -Y separation

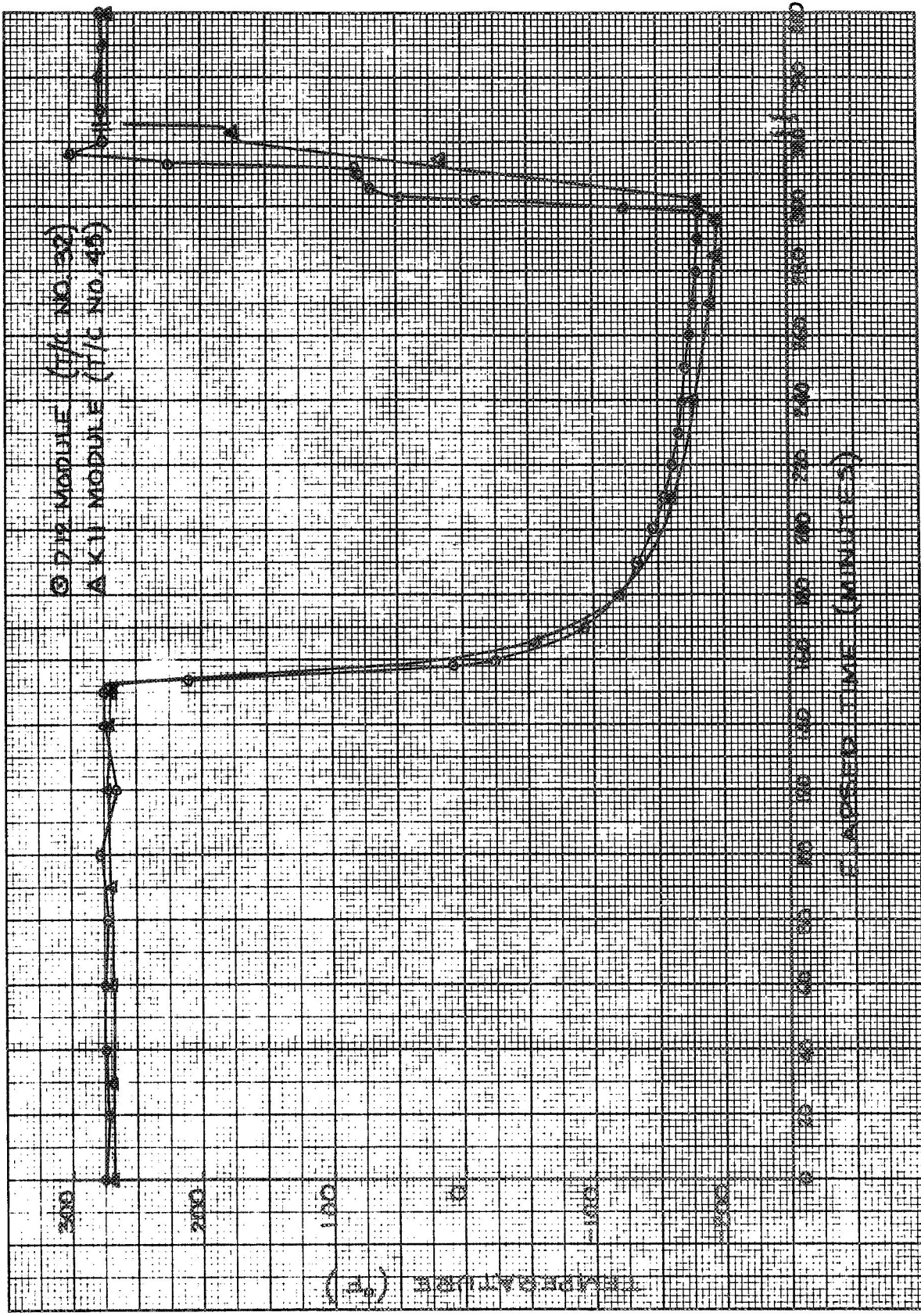


Figure 3.3-8 Deployed Transient Temperature History

nut was -76°F at the time of firing. An audible report was heard in the control room and a flash was seen on the closed circuit T.V. screen. Outboard end support release was verified by the signal from the microswitches at each end. Post test inspection of the test specimen revealed that both separation nuts had completely fractured at the mounting base (see Figure 3.3-9) and had been propelled against the cryopanel. The loose parts of the separation nuts (see Figure 3.3-10) were found in the bottom of the chamber completely detached from the electrical harness.

Deployment of the BI-STEM element was accomplished without incident. The motor temperature was -63°F immediately prior to deployment with a 37°F rise recorded during the deployment. The BI-STEM was retracted from the fully extended position, but the retraction was stopped 77 inches short of the fully stowed position because of an apparent billowing of the +Y blanket as viewed via the closed circuit T.V. camera. At the end of this retraction, the motor temperature was -7°F . Upon entering the chamber to examine the test specimen, the major portion of the -Y blanket was found draped on the chamber cryopanel. The +Y blanket was discovered in a billowed condition, but the movement of personnel in the chamber was enough to cause the +Y drum to rotate and rewrap this blanket in its normal stowed configuration. More detailed examination of the -Y blanket revealed that a pull-apart thermocouple connector was lodged in the wrapped blanket in such a way as to prevent the drum from rotating. The failure to secure this connector to the BI-STEM housing had evidently caused much of the -Y blanket rewrapping problem. However, this test condition should not have influenced the billowing of the other blanket.

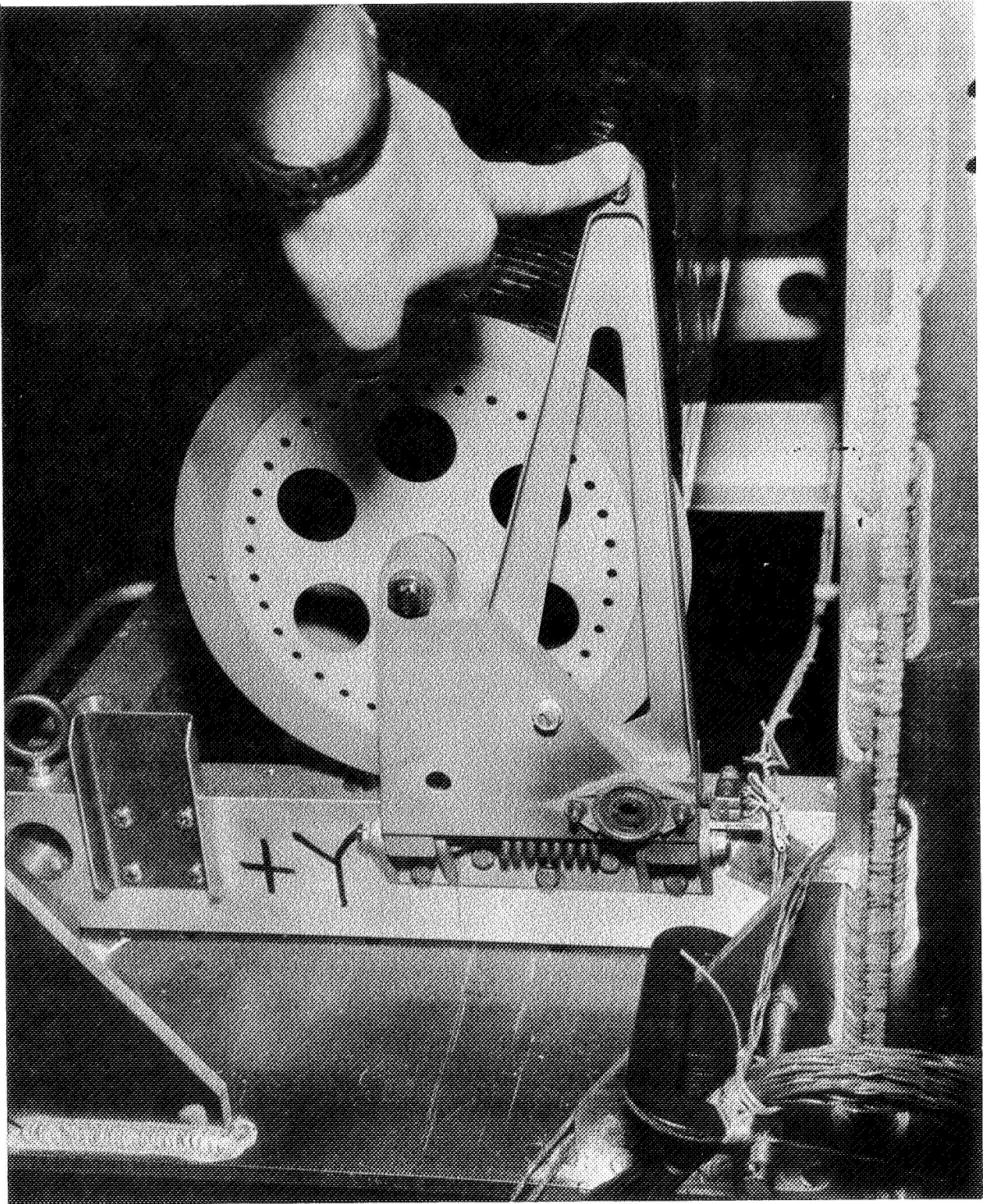


Figure 3.3-9. Outboard End Support Showing Fractured Separation Nut Mounting Base (VF 70224B)

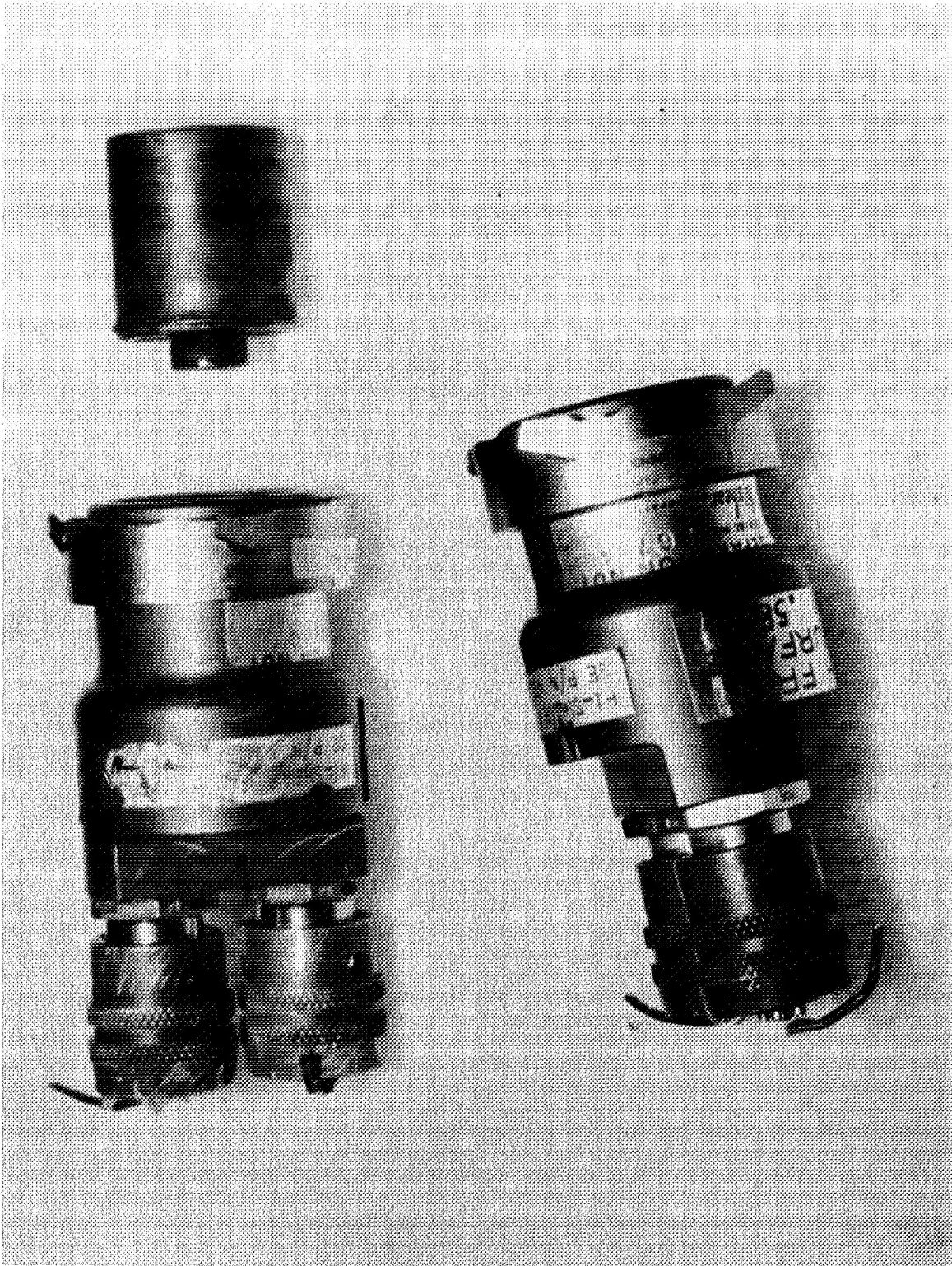


Figure 3.3-10. Both Separation Nuts with Fractured Mounting Bases (VF 70244C)

Some typical results of the stowed transient test are shown in Figure 3.3-11. Subsequent post test inspection of both array blankets revealed that localized heating of the blanket had occurred as a result of the high temperature stowed test. Areas of scorched adhesive were indicative of temperatures in excess of 350°F. Two active solar cell modules were situated within an overheated area at the same longitudinal station on the blankets. One of these modules (J6) suffered extensive lifting of the interconnect top contact feet due to solder melting in the overheated area. The cause of this overheating is discussed in Volume II, Section 4.4.5.6.

The high temperature deployment and retraction of the array was performed satisfactorily.

3.3.2.3 Acoustic Noise Test

3.3.2.3.1 Introduction

The stowed array was to be exposed to 60 seconds of random incidence, reverberant sound with an overall sound pressure level of 150 db. During the test runs, the acoustic environment was monitored at various locations in and around the array and the response of the system was monitored. A detailed discussion of this test is contained in Volume II, Section 4.6.

3.3.2.3.2 Summary of Results

The RA250 engineering prototype model survived exposure to the specified acoustic test environment. The results of the post test health check are presented in Volume II, Section 4.2. The response of the system indicates that an acoustic test of this type should be retained as a system test environment for future

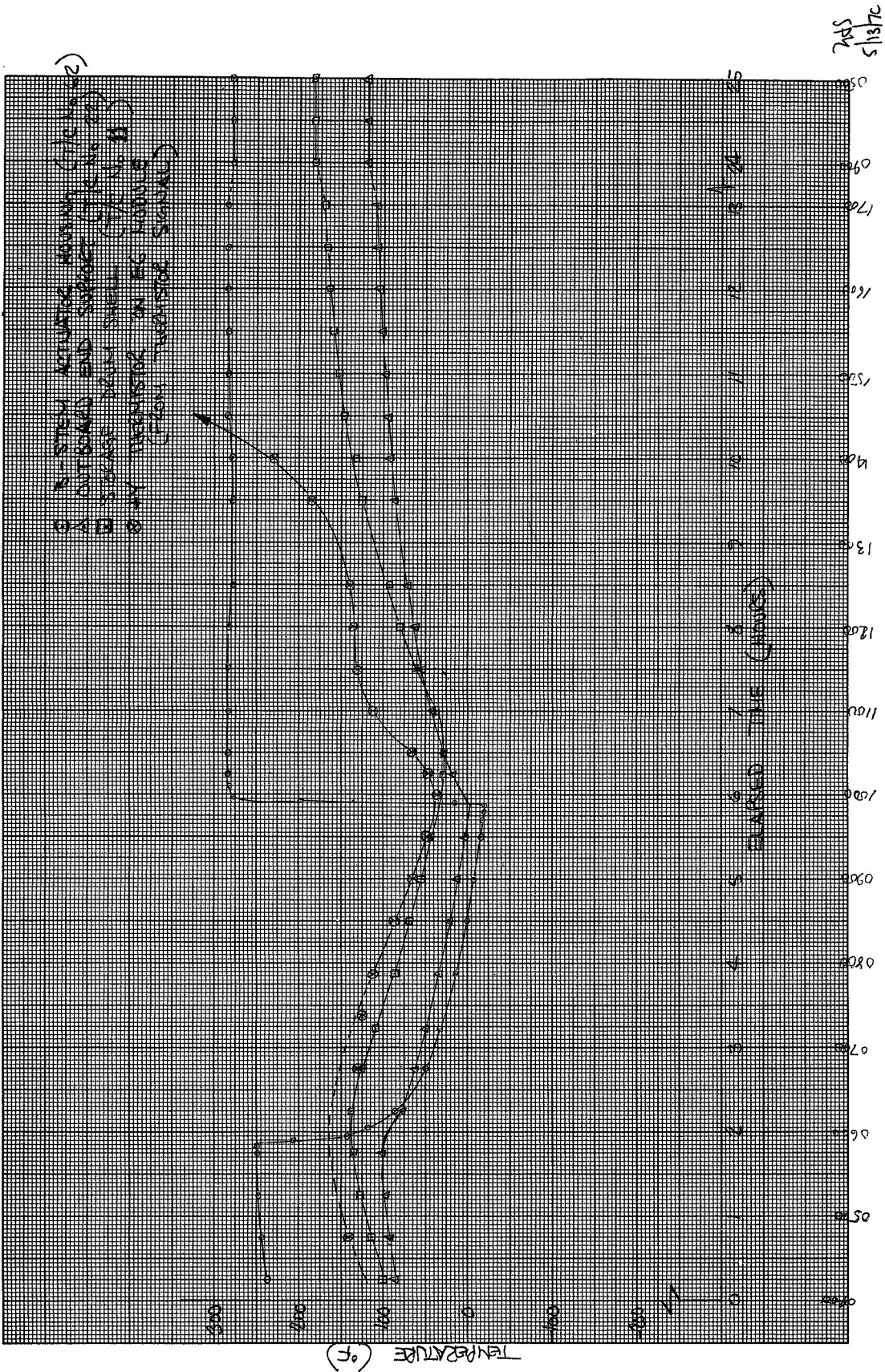


Figure 3.3-11. Stowed Transient Temperature History

light weight solar array assemblies to provide high frequency excitation of the solar cell blankets.

3.3.2.3.3 Discussion

The RA250 test specimen, fully instrumented and secured to its holding fixture, was suspended from a spreader bar using shock (or bungee) cord so that the natural frequency of the suspension system was less than 5 Hz. The positioning of the test specimen with respect to the horns on the chamber is as shown in the photograph of Figure 3.3-12. A first test run at 130 db overall was made to check the spectrum shape with the actual test specimen in place. The second and third test runs of 30 seconds each were at full level. The test environment during these runs is shown in Figure 3.3-13. Note that the test environment follows the lower limit of the specified environment. Since the test level could not be increased without extensive effort, a 30-second penalty run resulted in a 147 db overall SPL, so a second 30-second penalty run was performed. The overall level of each transducer is summarized in Table 3.3-5.

3.3.2.4 Stowed Vibration Test

3.3.2.4.1 Introduction

The object of this test series was to subject the stowed array to qualification levels sinusoidal and random vibration spectra as defined in Figure 3.3-14. In addition, low level sinusoidal sweeps were performed to locate stowed array resonant modes below 100 Hz. A detailed discussion of this test is contained in Volume II, Section 4.7.

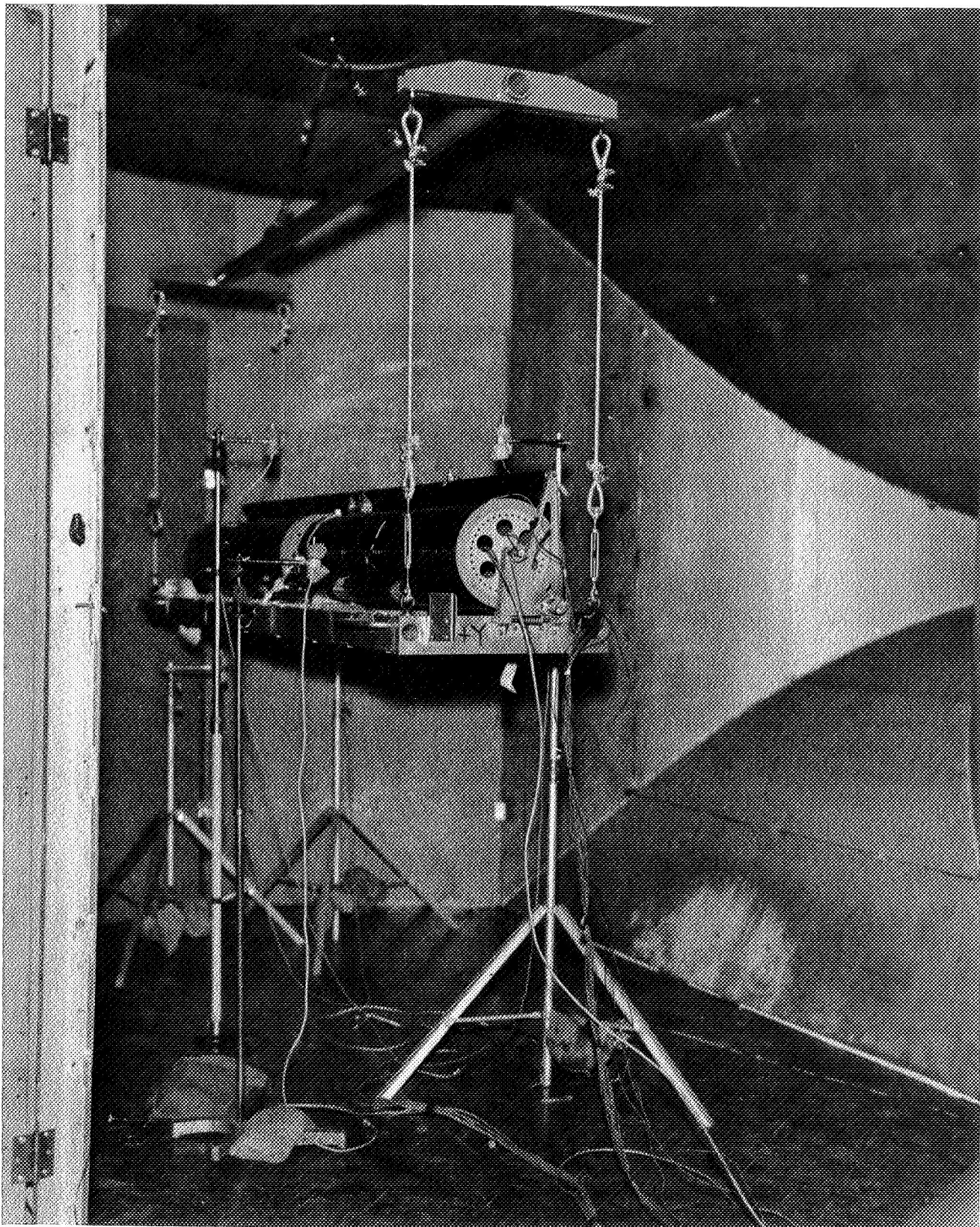
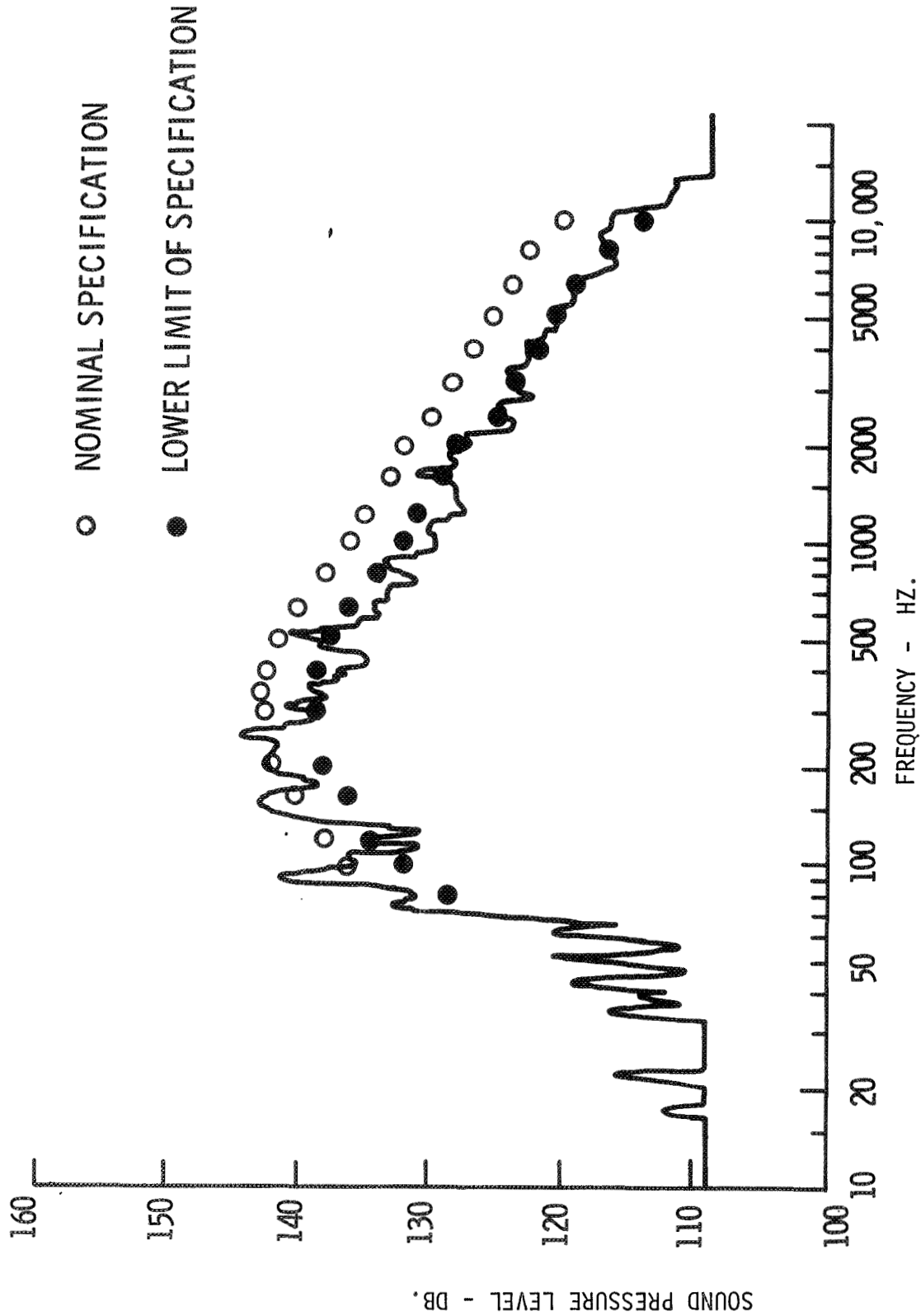


Figure 3.3-12. View of the Rollup Solar Array Installed in the Acoustic Chamber (C 70-0115-A)



Identification R371
 Outside +Y Drum
 0% Span
 0 =

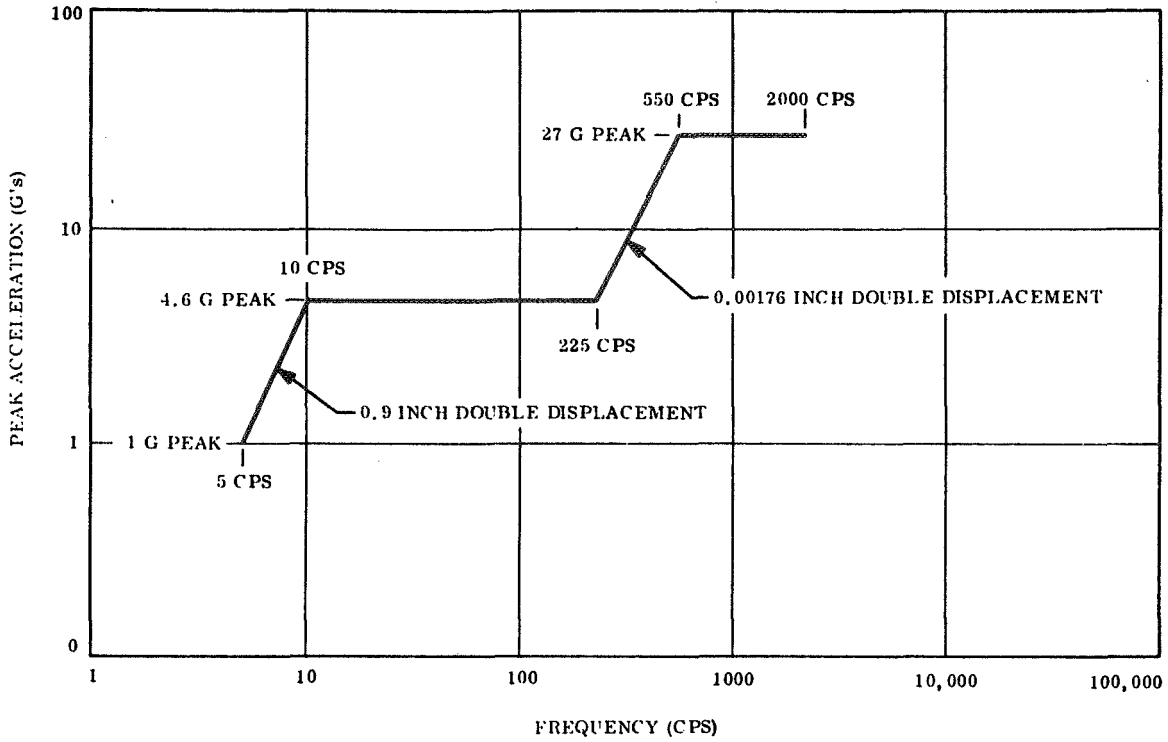
Run No. 3
 Date 5/15/70

Figure 3.3-13 Spectrogram of Input Acoustic Field During Run 3

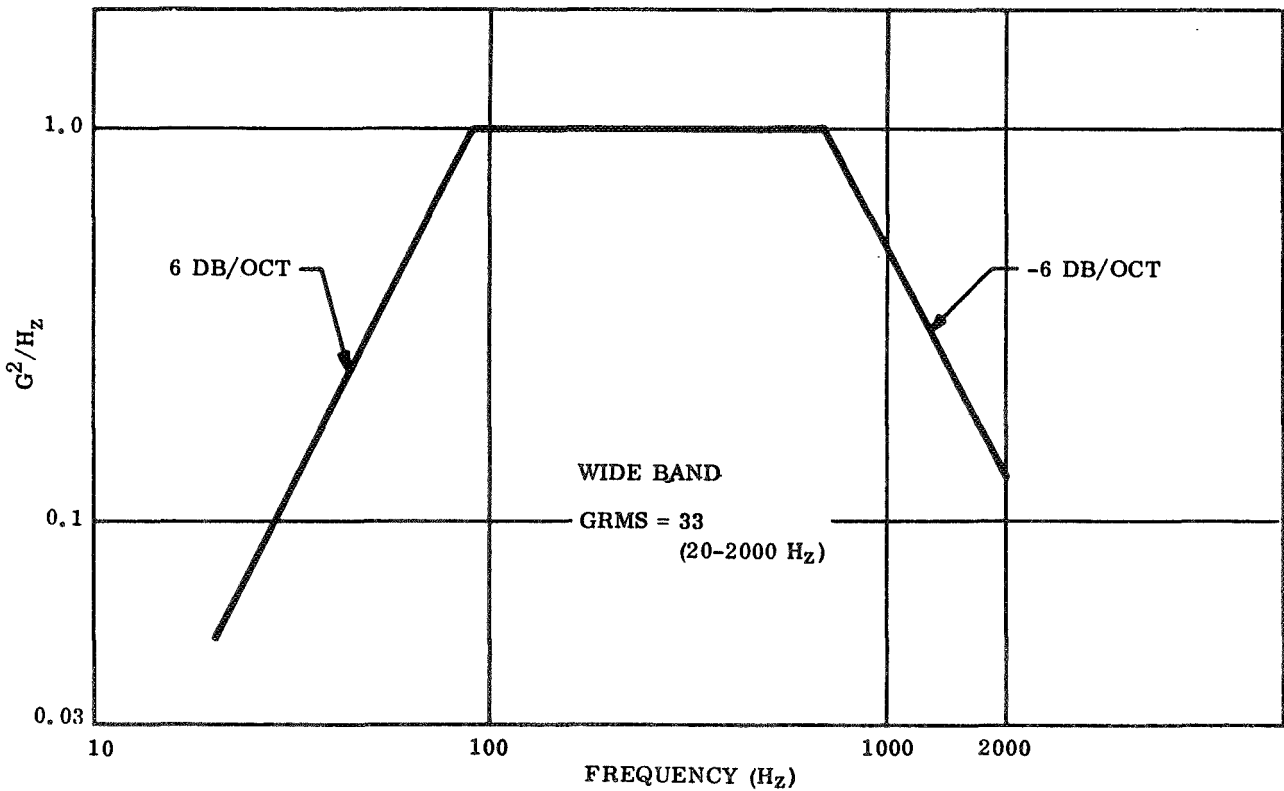
TABLE 3.3-5

TRANSDUCER LOCATIONS AND LEVELS

<u>ITEM NO.</u>	<u>TRANSDUCER</u>	<u>STA. NO.</u>	<u>LOCATION</u>	<u>RUN</u>	<u>OVERALL LEVEL</u>
1	Microphone	D, Trk 3	Outside +Y Drum, 50% Span $\theta=0^\circ$	3	149.0 db
2		B, Trk 6	Outside +Y Drum, 50% Span $\theta=90^\circ$	3	150.0
3		C, Trk 1	Outside +Y Drum, 0% Span $\theta=0^\circ$	3	150.0
4		F, Trk 4	Outside -Y Drum, 100% Span $\theta=180^\circ$	3	147.5
5		A, Trk 5	Outside -Y Drum, 100% Span $\theta=270^\circ$	3	150.5
6	Microphone	E, Trk 2	Inside +Y Drum, 50% Span on Y Axis	3	151.5 db
7	Accelerometer	2X	LEM +Y Side Center Coup.	3	7.4 GRMS
8		2Z	LEM +Y Side Center Coup.	3	4.8
9		4X	LEM 50% Span +Y Side	5	8.0
10		4Z	LEM 50% Span +Y Side	5	5.5
11		7Y	+Y End Support on Drum Plug	5	3.6
12		11Y	+Y Blanket 100% Span 180°	3	5.6
13		11Z	+Y Blanket 100% Span 180°	3	10.2
14		13X	+Y Drum 100% Span 90°	5	3.3
15		14Y	+Y Drum 100% Span 180°	5	2.8
16		14Z	+Y Drum 100% Span 180°	5	5.2
17		15X	+Y Bearing Housing	3	1.5
18		15Y	+Y Bearing Housing	3	0.9
19		15Z	+Y Bearing Housing	3	1.4
20		16X	+Y Blanket 50% Span 0°	3	10.5
21		18Z	+Y Blanket 50% Span 90°	3	15.6
22		24X	+Y Drum 50% Span 0°	3	4.0
23		26Z	+Y Drum 50% Span 90°	3	4.9
24		36Z	+Y Blanket 0% Span 0°	3	6.3
25		37Z	+Y Blanket 0% Span 90°	3	6.6
26		38Z	+Y Drum 0% Span 0°	5	14.3
27		40Y	+Y Drum 0% Span 180°	5	2.1
28		41Y	+Y Blanket 0% Span 180°	3	3.6
29		42X	-Y Blanket 50% Span 0°	3	10.0 GRMS



(a) Sinusoidal Vibration



(b) Random Vibration Noise Plot

Figure 3.3-14 Specified Qualification Level Vibration Environments (from Reference 1.2)

3.3.2.4.2 Summary of Results

1. No significant structural modes were noted below 100 Hz.
2. Pure blanket modes were not discovered during this test.
3. Blanket slack was generated at the outer wraps during the course of the Y axis (first axis of test) runs.
4. The array structure survived the test environment in all axes. The BI-STEM experienced a failure of the "fully extended" limit switch roller actuator. In addition, a fatigue crack in the BI-STEM outer rod element was discovered after the vibration test. Both of these anomalies are discussed in Section 3.2.2.3. Results of the health check following the vibration environment are discussed in Volume II, Section 4.2.

3.3.2.4.3 Discussion

The stowed vibration test was performed first in the Y axis (coincident with the storage drum axis), then in the Z axis (normal to the plane of the deployed array surface), and finally in the X axis (parallel to the axis of the deployed BI-STEM rod). For each of these orientations, the testing was substantially identical and consisted of the following:

1. Several low level sinusoidal sweeps at 0.46G at 1 octave/minute from 5 Hz to 2 kHz. These sweeps were run to set initial recording

gain factors and to obtain array response to a constant level base excitation input to determine amplification factors. During these runs, the array was visually observed under strobe lighting to obtain an appreciation of blanket motion. Selected channels for the low level sweeps were analyzed for colinear and quadrature response for identification of blanket and structural modes occurring below 100 Hz. In addition, selected strain or accelerometer channels were analyzed to determine the risk of damage as the input levels were progressively increased to the qualification level.

2. An acceptance level sinusoidal sweep at two thirds of the specification level was performed to evaluate linearity of system response and as a final assessment of the risks associated with the full level qualification input.
3. The sinusoidal qualification sweep was performed with selected channel responses reviewed during preparations for subsequent random testing.
4. Random testing followed the same sequence of low level, acceptance level, and qualification level testing. Selected strain channels were evaluated as the test proceeded to assess the risk of damage during subsequent higher level inputs.
5. On completion of any axis vibration testing, the array structural components were visually inspected and the BI-STEM actuator was operationally checked.

Table 3.3-6 lists the array resonant amplification factors and frequencies. The dynamic loads developed in the stowed vibration test were low. Consequently the material stress were low and no structural damage was experienced. The response of the array blankets was low and the blankets provided dumping for the entire system.

3.3.3 BI-STEM LIFE DEMONSTRATION

At the conclusion of the environmental testing program, the array was subjected to a series of 35 consecutive deploy/retract cycles under ambient conditions to demonstrate the ability of the BI-STEM actuator to perform many array extensions and retractions in orbit. All of these cycles were performed without incident. At the start of this sequence there was a relatively high fluctuation in the slip ring apparent dynamic resistance as the drums turned. These fluctuations had the period of the drum rotation. As the number of deploy/retract cycles increased, the magnitude of these fluctuations in power slip ring resistance decreased. This tends to indicate a wear-in period required to remove dirt or tarnish which may have collected on the rings.

3.4 DEVELOPMENT TESTS

During the course of this program several subsystem or component level development tests were performed. These tests are summarized in this section.

3.4.1 BI-STEM THERMAL BENDING TEST

The objectives of the thermal bending test was to check analytical predictions of maximum tip deflection of 35.68 inches for a deployed length of 33-1/3 feet. All thermal bending testing was performed by NASA/GSFC using boom samples provided by GE.

The thermal vacuum chamber utilized in investigating boom thermal bending behavior, Figure 3.4-1, consists essentially of a vertical cylinder approximately 1 foot in diameter and 13 feet high, incorporating a liquid N₂ shroud, and illumination that provides an intensity equivalent to one solar constant over the full length of a 10 foot boom length with an intensity uniformity of better than ±5 percent.

The chamber incorporates provisions for rotating the suspended test specimen relative to the fixed I.R. heat source. The degree of bending can be recorded photographically as well as by optical means. Samples were removed from the test specimen to measure their solar absorptance necessary to correct the observed bending, for the differences in spectrum of the sun as it was and the essentially I.R. source.

Over the past two years, NASA/GSFC has employed this facility in the development of a technique for measurement of gravity gradient rod deflections under the influence of solar heating. The RA250 BI-STEM is one of many boom configurations tested by NASA/GSFC. Results of the entire boom deflection study will be published by NASA/GSFC on completion of this program of boom investigations.

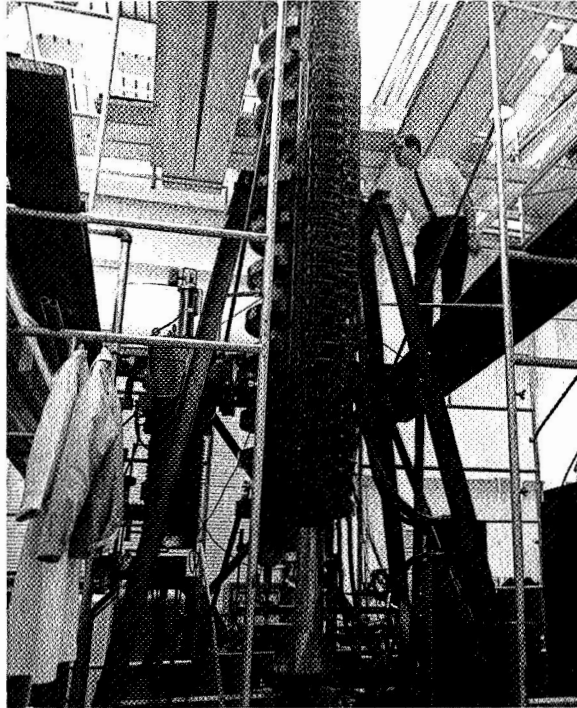


Figure 3.4-1 Thermal Bending Test Setup (NASA G-69-4536)

Two silver plated 1.34 inch diameter BI-STEM boom configurations were evaluated. The first of these had the elements mechanically decoupled at the free end, and the second had the two elements welded together at the free end. The latter configuration more accurately represents the RA250 application which incorporates a tip plug. Figure 3.4-2 presents smoothed deflection curves for the 10 ft. test rod configurations. Figure 3.4-3 results from extrapolation of test data to a 33.5 ft. deployed boom length in a zero gravity field. The derivation of the transfer functions to extrapolate results from the measured 10 ft. rod to the 33.5 ft. rod in zero gravity field is developed in Reference 1-5 and is represented by:

$$S_{IP, OP} = 18.9 S \text{ measured}$$

where S is displacement in inches and
IP is in sun plane,
OP is out of sun plane (normal)

Inspection of Figure 3.4-3 reveals that in position 11 (300° boom rotation), the welded test specimen exhibited a negative bending toward the sun. This condition is generally considered to be unstable and could result in thermal "flutter". The amount that the welding technique contributed to this negative bending is unknown at this time. After welding, it was noted the outer element was displaced along its edges from the inner element at some points.

When the maximum absolute value of the zero-g thermal deflections indicated on Figure 3.4-3 are added to the BI-STEM vertically deployed tip deflections measured during SPAR actuator acceptance tests, the following apparent maximum total tip deflections occur:

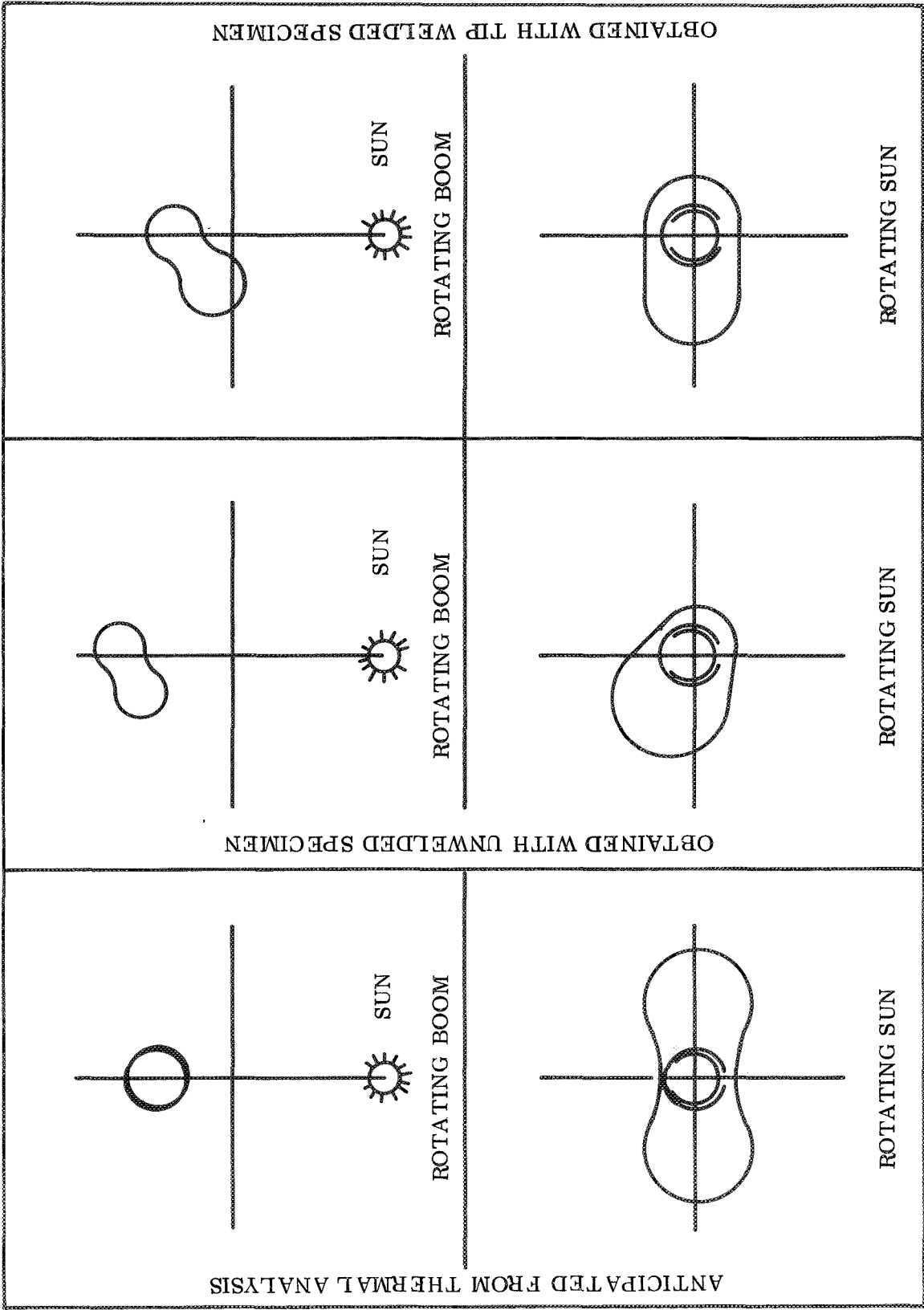


Figure 3.4-2 Idealized Tip Deflection Patterns

TEST CONFIGURATION
 1.34 IN. DIA BI-STEM SILVER PLATED OD
 10 FT LONG, 301 STAINLESS ELEMENTS
 NOT WELDED AT TIP

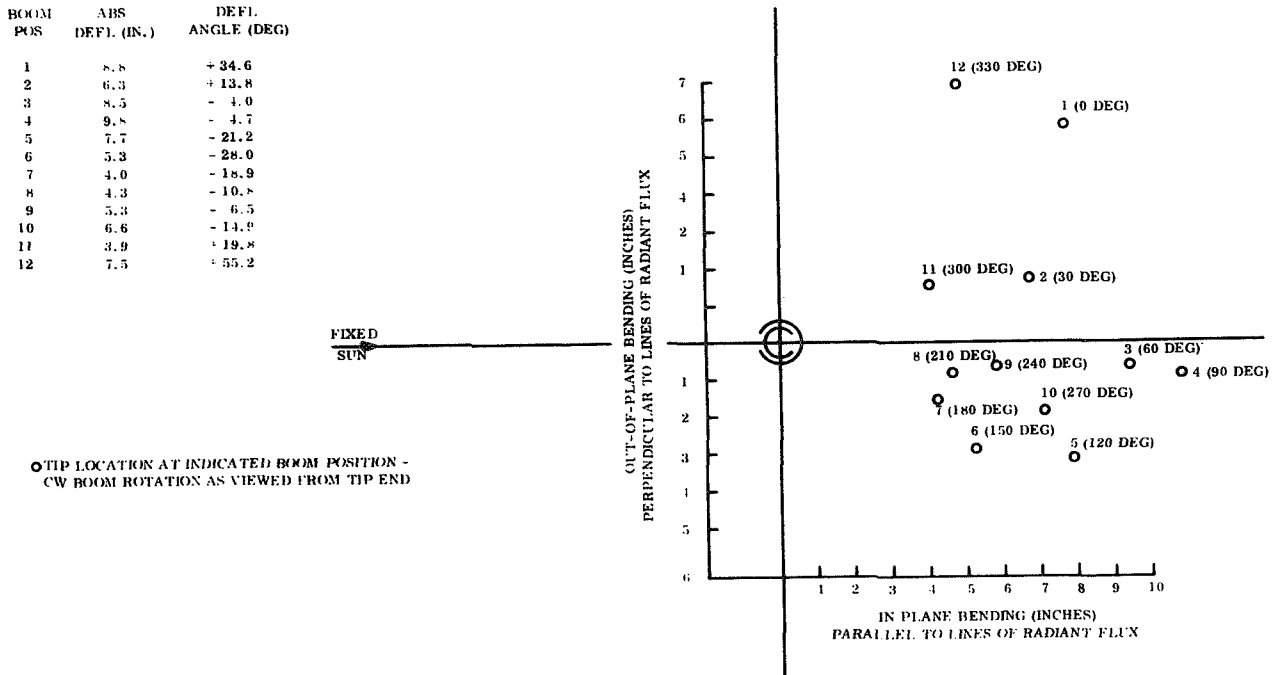


Figure 3.4-3 Extrapolated Absolute Zero-G Bending at 33.5 Ft.²

Tip Welded (in.)

Boom deflection for vertical deployment	8.0
Deflection due to 5.2 lb. load	11.0
Absolute thermal deflection (maximum)	<u>13.4</u>
Maximum Total Apparent Deflection	32.4

Analysis of the rod deployed condition indicated that with a temperature gradient of 43.9°F, a blanket tension of 4.0 pounds, and a solar illumination at 260 mw/cm² intensity (1.5 suns), a rod tip deflection of 35.68 inches could be expected. The maximum total apparent deflections above did not exceed the predicted deflections.

3.4.2 MODULE THERMAL CYCLING TEST

Three sample solar cell modules (two 4 x 4 and one 5 x 7) were thermally cycled 34 times between -200°F and +285°F. These modules were fabricated utilizing the

JPL furnished solar cells and coverglass. The cells were interconnected with silver expanded metal per drawing number 47C218187. The three modules were bonded to a Kapton substrate with SMRD-745. The rear side of the substrate had cushioning buttons installed as on the prototype blanket. A copper strip was also etched on the rear of the substrate to simulate the bus strip network. This copper strip was insulated with 1-mil Kapton silicone pressure sensitive tape, as on the prototype blanket.

Figure 3.4-4 shows the three modules mounted on the common substrate suspended in front of an array of 500 watt Quartzline lamps which provided the heat input to the vacuum chamber. In addition to this active module substrate, a module of dummy glass platelets was placed in the same test so that the thermal cycling effects on the dummy glass modules could be determined.

Figure 3.4-5 shows a typical active module temperature profile during one 50-minute cycle.

A detailed visual examination of the solar cell modules revealed a failure which might be attributed to this thermal cycling test. The expanded metal interconnect strands were fractured in localized areas. This type of failure occurred only in areas where the interconnect loop had been deformed (or scored) by the mesh forming tool. Similar failures were found in formed interconnects prior to their use in assembly. The cause of this deformation was corrected by rework of the forming tool and subsequent 100 percent visual inspection of each strand after forming. Thus it is likely the interconnect failures were not related to thermal cycling.

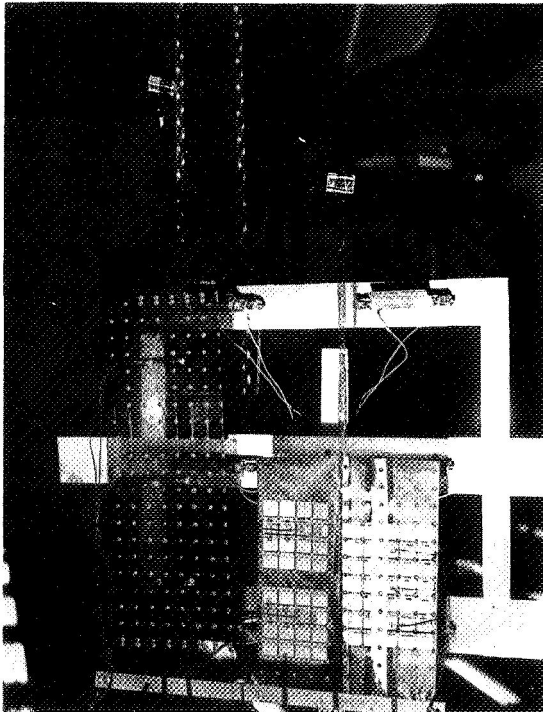
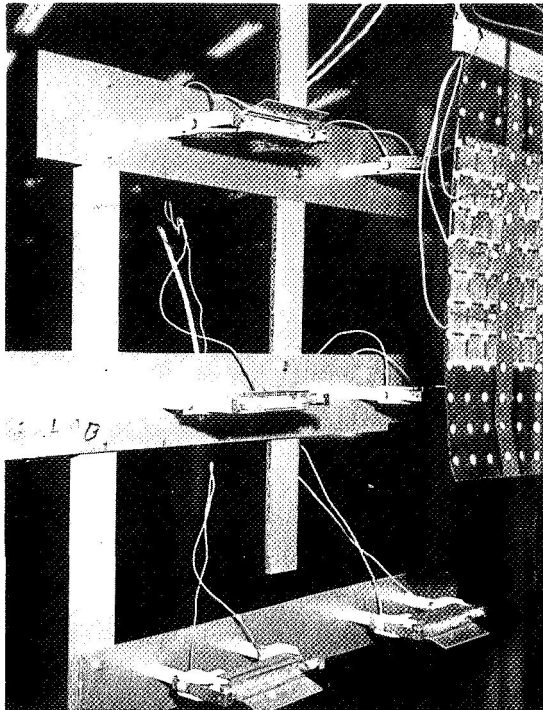


Figure 3.4-4. Thermal Cycling Module Test Set-Up

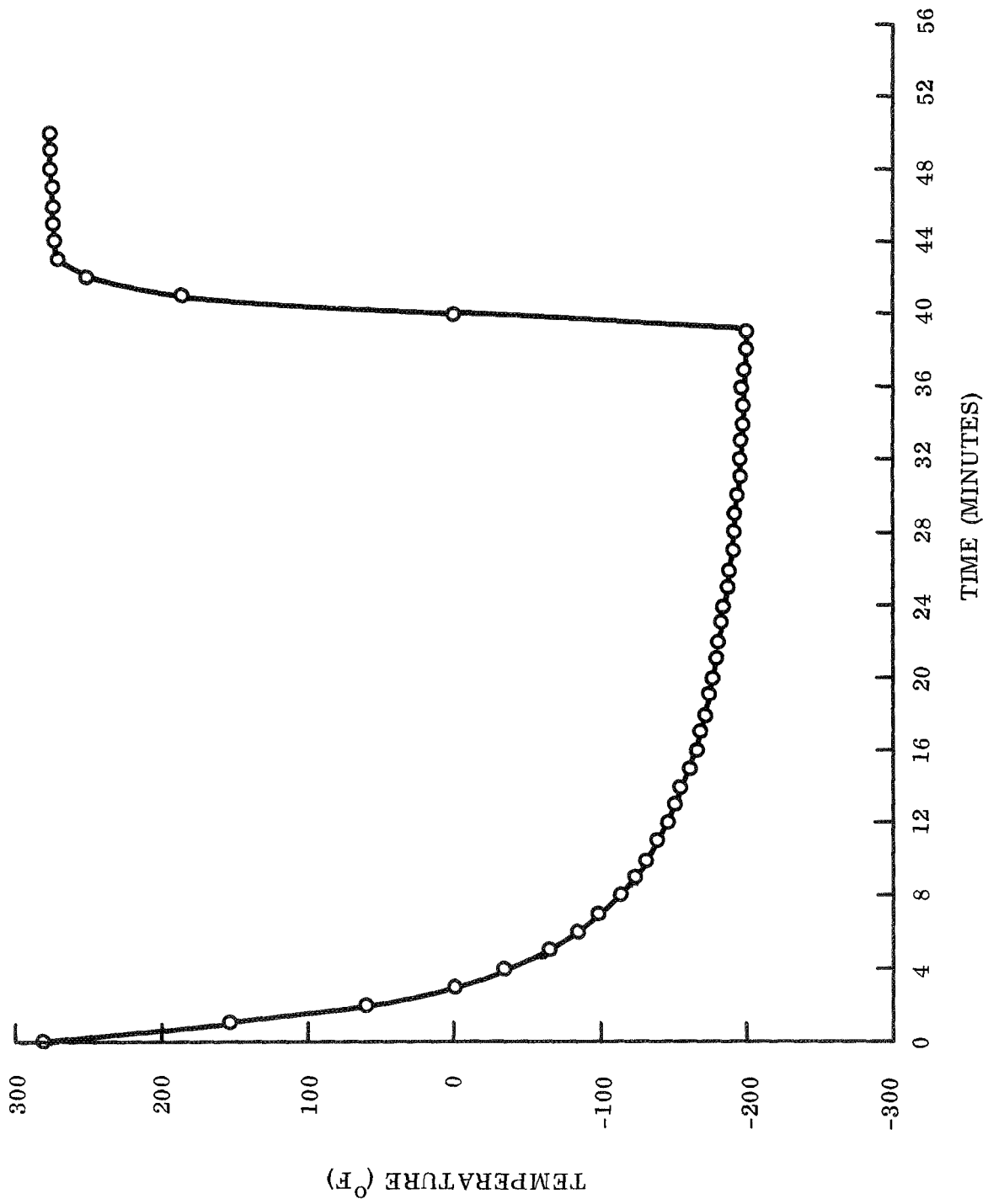


Figure 3.4-5 Typical Active Module Temperature Profile

3.4.3 BLANKET TRACKING WITH A LATERAL OFFSET

At the completion of the 35 cycle BI-STEM life demonstration, an array blanket tracking experiment was performed by displacing the array, with respect to the upward deployment aid, along the Y (storage drum) axis in 2-inch increments to check the ability to rewrap satisfactorily during retraction. At each shift increment, the array was deployed and retracted, and the blanket rewrap was observed. This procedure was continued until the total lateral displacement (in Figure 3.4-6) was 10 inches. During the deployment and retraction at this displacement, the inboard blanket edge on the -Y side was observed to rub against the leading edge member saddle which is mounted on top of the BI-STEM actuator.

During this experiment, the edge guides served to redirect the rewinding blanket so that it restowed properly on the drums. As shown in Figure 3.4-7, as the blanket began to ride up over the flange, it was forced to slide down the ramp of the edge guide. The majority of the force required to produce this sliding action comes from the weight of the blanket wrap itself as it turns over the top of the storage drum. In a zero g environment, this same sliding action would be aided by a stronger Negator spring system in the drums.

3.4.4 ARRAY STRUCTURAL LOAD DEFLECTION TEST

The objectives of this test was to determine array drum bearing flexibility coefficients for incorporation in the analytical mode of the stowed RA250 solar array assembly. Flexibility coefficients were obtained for the bearing assembly, center support assembly and end support caging arms. Figure 3.4-8 presents a list of loading tests performed and Figure 3.4-9 presents a sketch of the test setup. Loads were applied in 5 lb. increments from zero to ± 20 lbs. and deflections measured by dial indicators located as shown in Figure 3.4-9. All data was published in Reference 1-6.

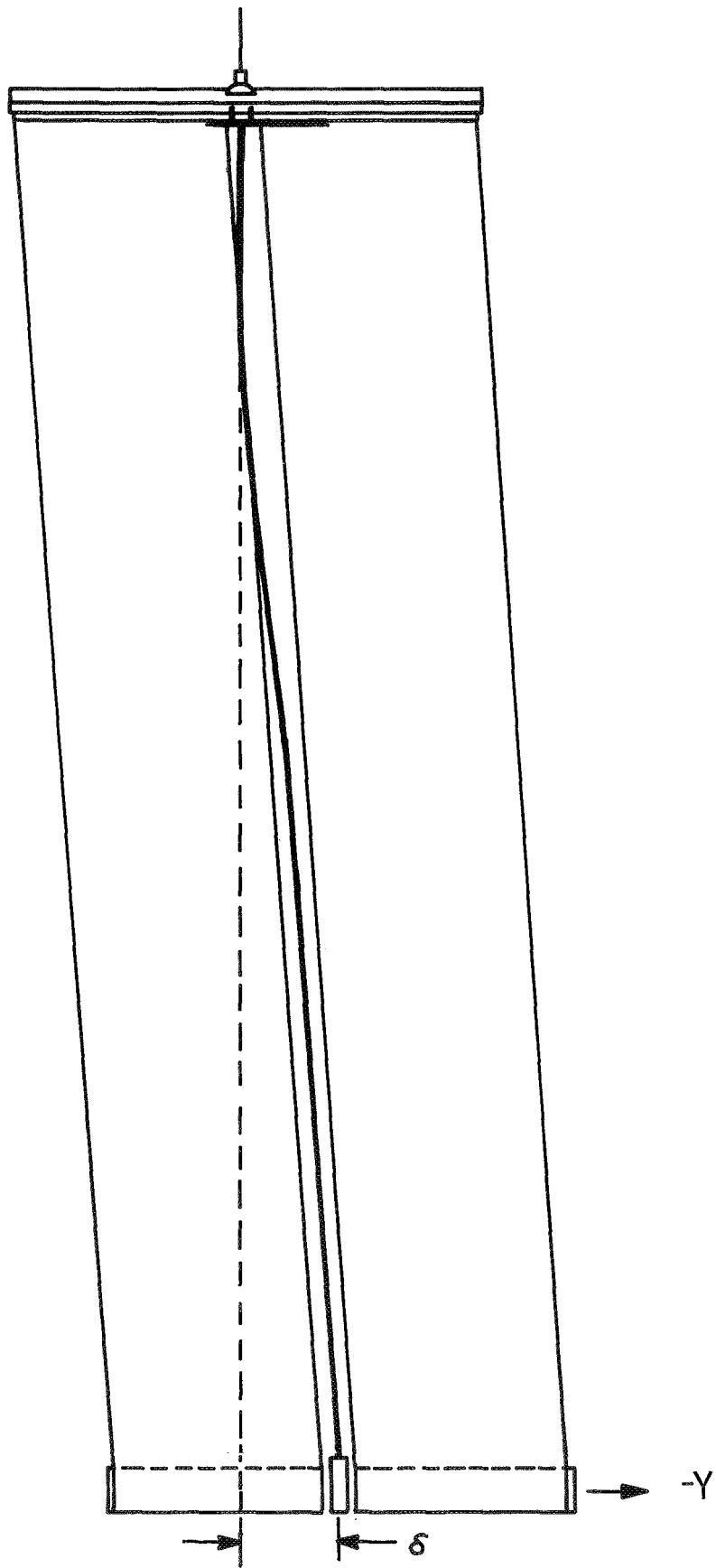


Figure 3.4-6. Schematic of Tracking Demonstration Test Set-Up

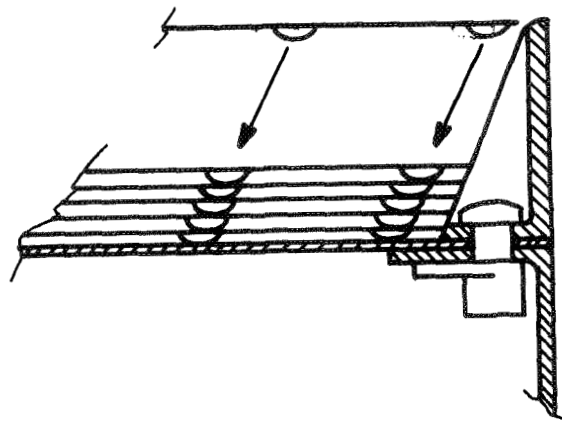
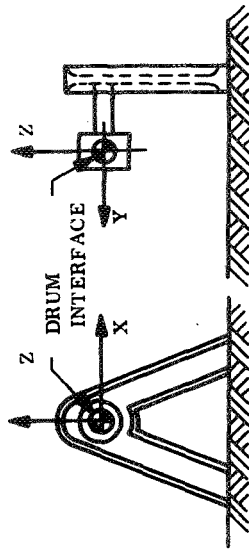

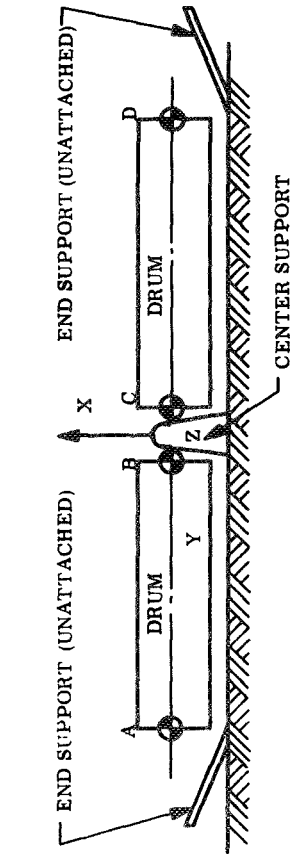


Figure 3.4-7. Rewrap Against Edge Guide



(a) DRUM DEFLECTION TEST GEOMETRY

NOTE: A BULLSEYE  DENOTES A POINT OF LOAD APPLICATION AND/OR DEFLECTION MEASUREMENT; THE CAPITAL LETTER, I.E., B, ADJACENT TO IT IDENTIFIES THE POINT.



(b) END SUPPORT TEST GEOMETRY (SIMPLIFIED)

TEST NO.	RUN NO.	TEST DESCRIPTION	LOADING AND DEFLECTION DATA		
			TEST AXIS	LOADING DESCRIPTION APPLIED AT	DEFLECTIONS MEASURED AT
1	a	Loads @ Drums - Outboard	X	Symmetrical	A, D
1	b	Loads @ Drums - Inboard	X	Symmetrical	B, C
2	a	Loads @ Drums - Outboard	X	Antisymmetrical	A, D
2	b	Loads @ Drums - Outboard	X	Antisymmetrical	B, C
3	a	Loads @ Drums - Inboard	Z	Symmetrical	A, D
3	b	Loads @ Drums - Inboard	Z	Symmetrical	B, C
4	a	Loads @ Drums - Outboard	Z	Antisymmetrical	A, D
4	b	Loads @ Drums - Inboard	Z	Antisymmetrical	B, C
5	a	Loads @ Drums - Outboard	Y	Symmetrical	A, D
6	a	Loads @ Drums - Inboard	Y	Antisymmetrical	A, D
7	a	End Support Deflection	-	Z-Force	At Drum Interface
7	b	End Support Deflection	-	X-Force	$\delta_x, \delta_y, \delta_z$ At Drum Interface
7	a	End Support Deflection	-	Y-Force	

Figure 3.4-8. Load Deflection Tests

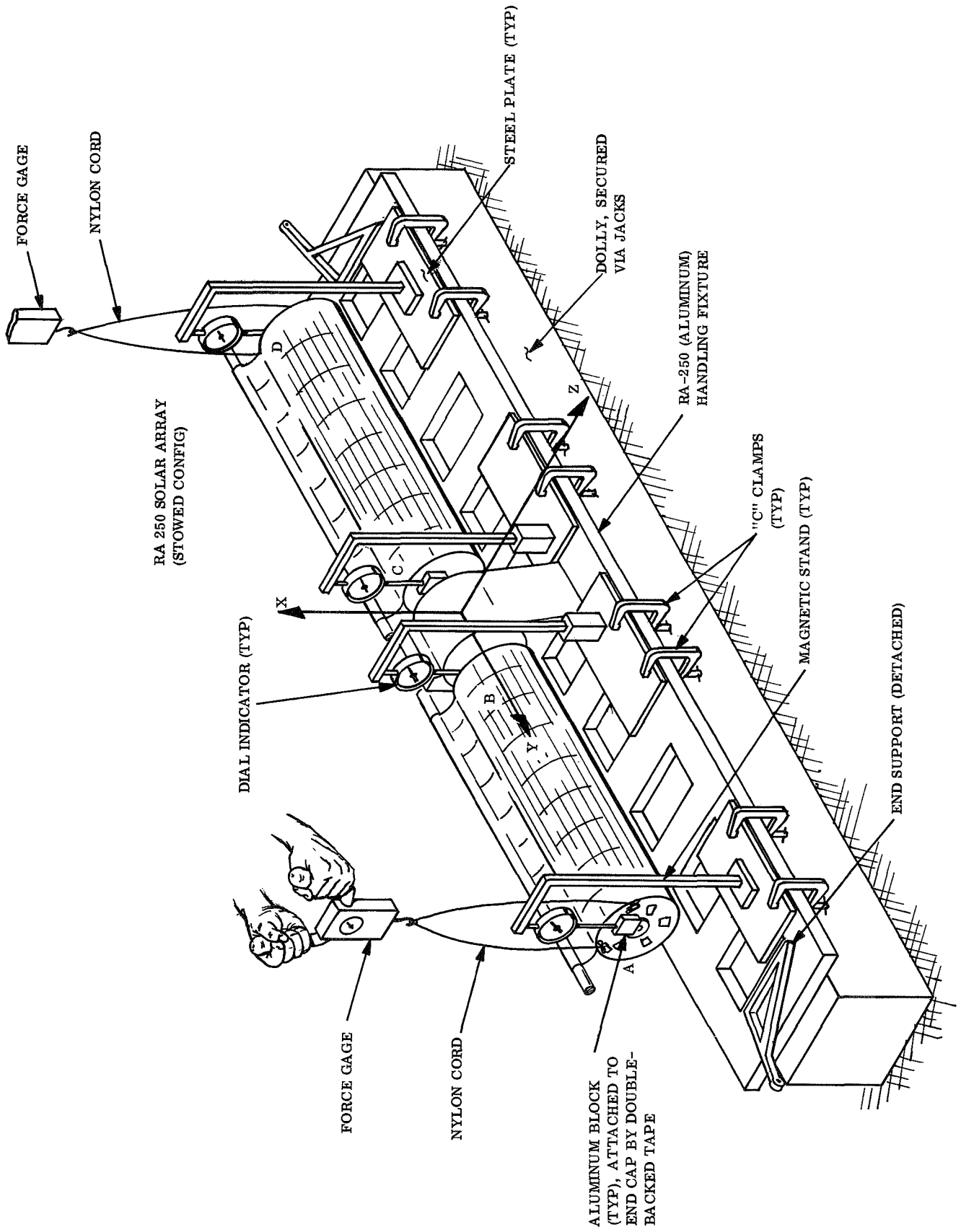


Figure 3.4-9. Test Arrangements

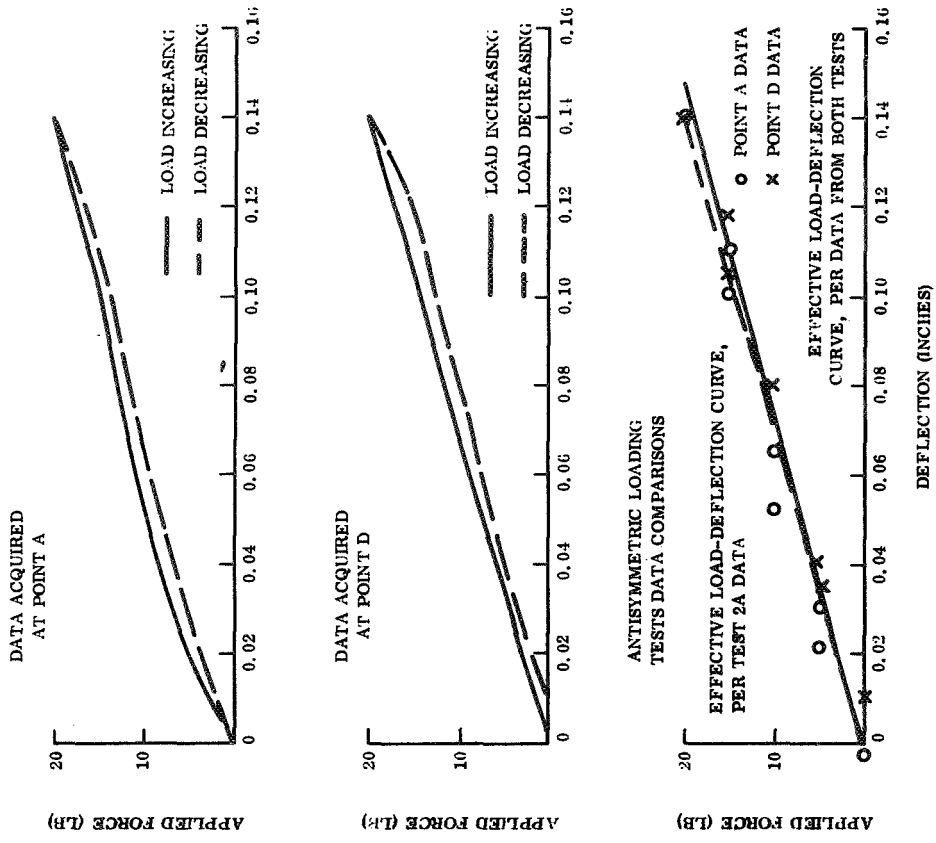


Figure 3.4-11. Results of Test 2A, Antisymmetric Loading in X Direction

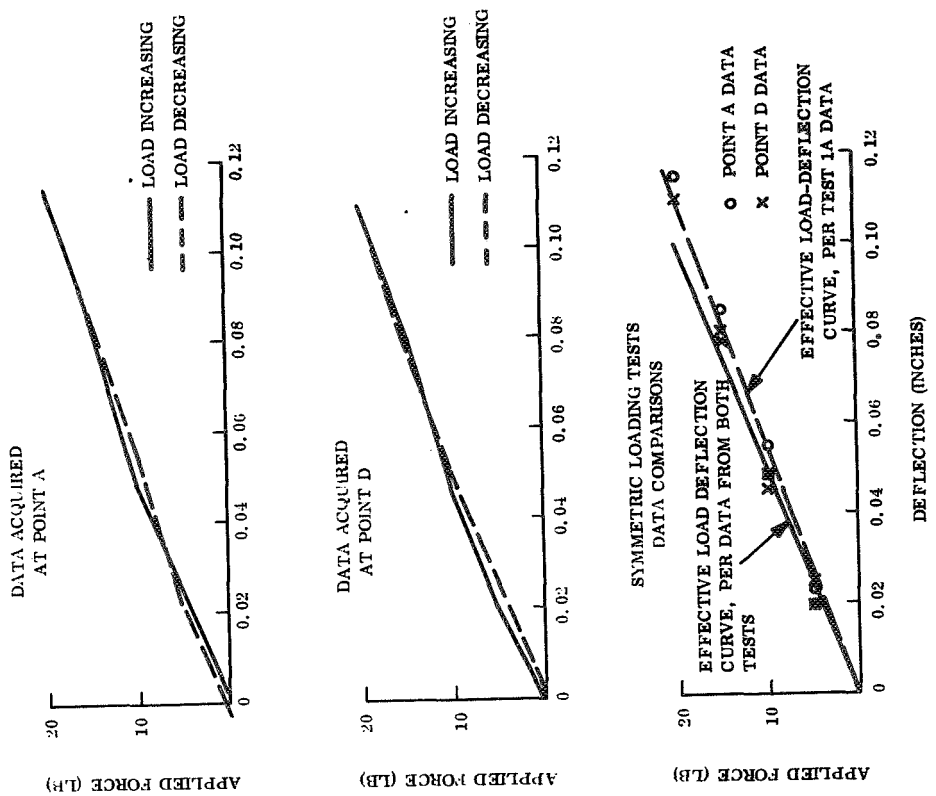


Figure 3.4-10. Results of Test 1A, Symmetric Loading in X Direction

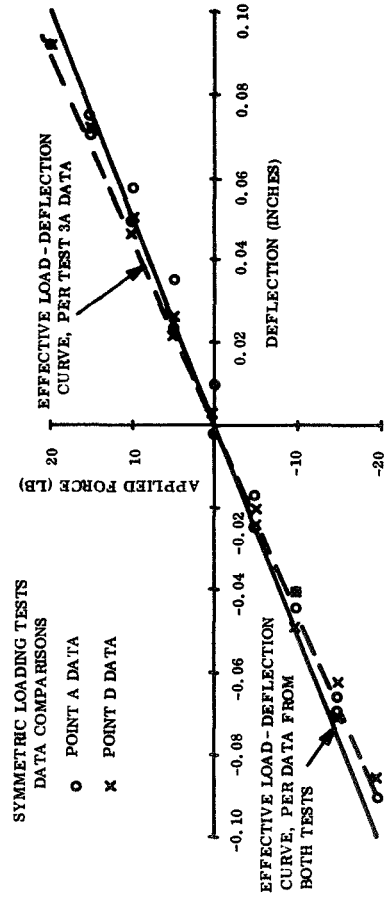
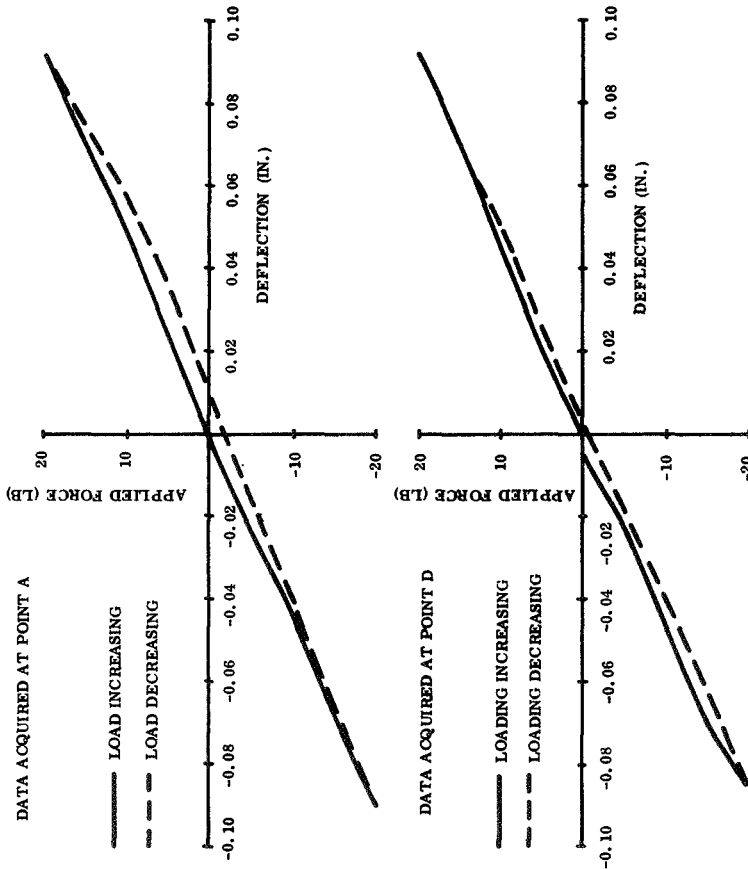


Figure 3.4-12. Results of Test 3A, Symmetric Loading in Z Direction

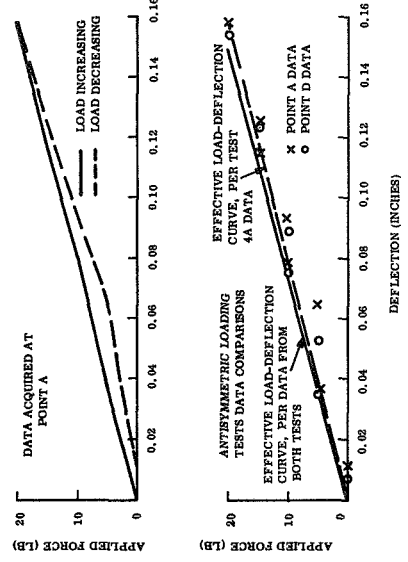
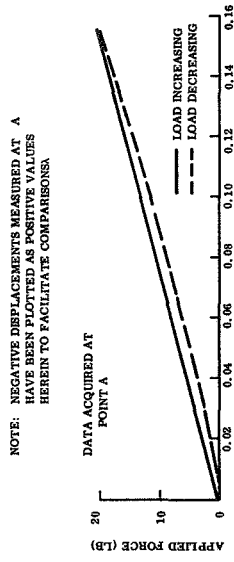


Figure 3.4-13. Results of Test 4A, Antisymmetric Loading in Z Direction

Figure 3.4-10 thru 3.4-13 present deflection of drum outboard points A and D as a function of symmetric and antisymmetric outboard loading. Deflections measured at the inboard drum faces points B and C were zero for all loading conditions run. The symmetric loading conditions yielded the torsional moment flexibility coefficient for the drum bearing, and the antisymmetric loading yielded the coefficient for the center support structure. The displacement force rate coefficient for the outboard movable support (caging) arms was determined in test 7a. Test runs 7b and c were not performed due to need for extensive adaption hardware.

This short test provided the following flexibility coefficients for incorporation into the deployed and stowed array dynamic models.

1. Drum bearing X and Z axis rotation - moment coefficient

$$C_{\theta, M} \quad B = 2.4 \times 10^{-6} \text{ radians/inch-pound}$$

2. Center support X and Z axis rotation moment coefficient

$$C_{\theta, M} \quad \text{C.S.} = 0.5 \times 10^{-6} \text{ radians/inch-pound}$$

3. Drum and center support displacement - force coefficients

$$C_{\xi, F} \quad B = C_{\xi, F} \quad \text{C.S.} = 0$$

4. Drum and center support displacement - moment and rotation - force coefficients.

$$C_{\xi, M} = C_{\theta, F}; \quad \& \quad C_{\theta, F} \quad B = C_{\theta, F} \quad \text{C.S.} = 0$$

5. Caging arm force displacements coefficient

$$C_{\xi, F} \quad \text{C.A.} = 5.3 \times 10^{-3} \text{ inches/pound}$$

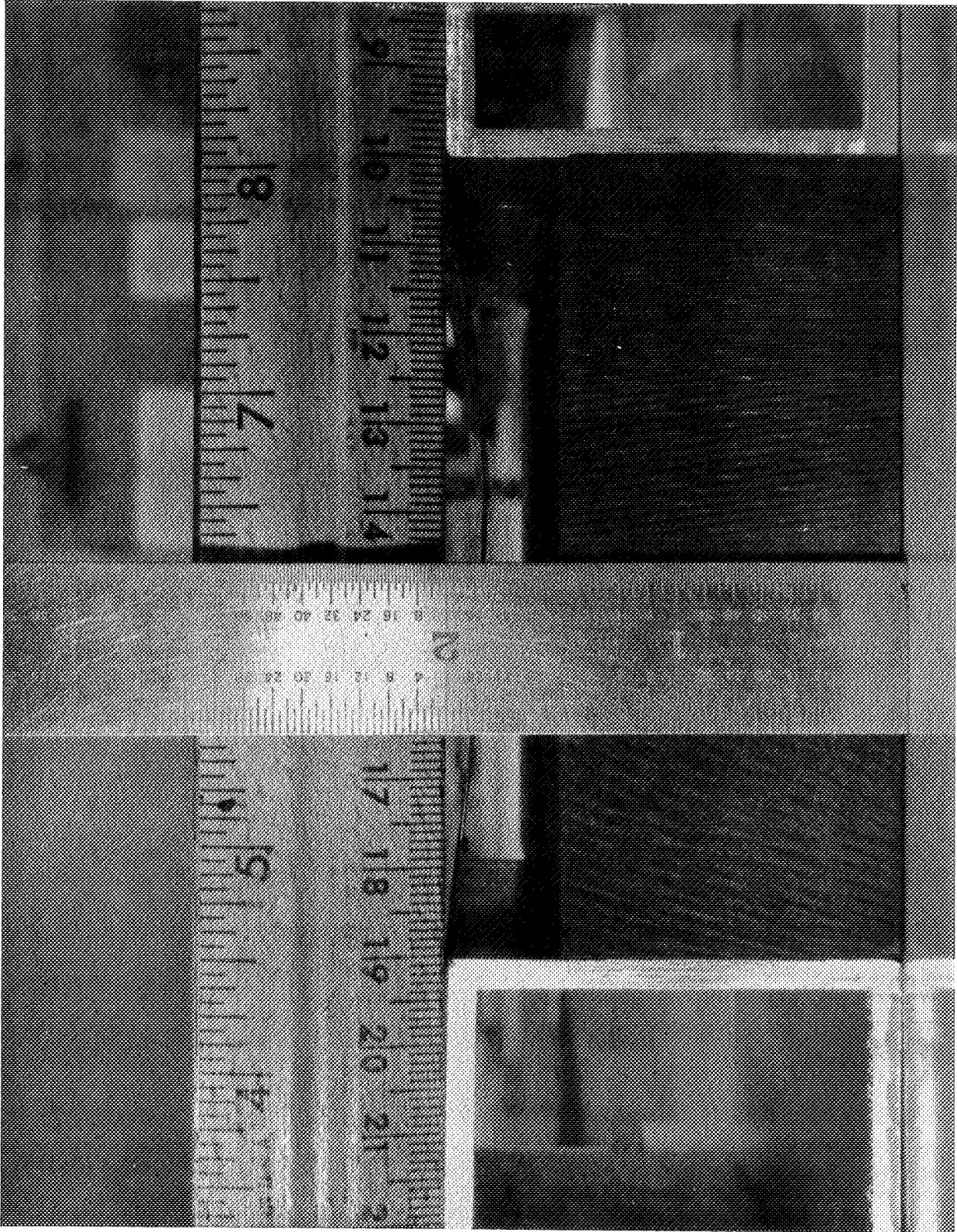


Figure 3.4-14. Solar Cell Module Deflection Test Set-Up

3.4.5 DUMMY CELL MODULE STIFFNESS EVALUATION

The prototype subsolar array which was assembled and tested during this program had only seven percent of its surface covered with active solar cells. The remaining area was to be covered with dummy cells. A preliminary development test was performed to determine if the physical characteristics of the proposed construction was appreciably different from that of solar cells mounted on the typical rollup array substrate of Kapton and cushioning buttons.

Two configurations of solar cell-interconnection substitute units were assembled and evaluated for degree of stiffness simulation. Both of these dummy module configurations simulate the cell by a chip of glass 0.013 inch thick by 0.75 inch square. The dummy interconnection for Configuration 1 is the silver mesh interconnection used with solar cells, bonded to span the gap between chips with SMRD 745. For Configuration 2, the dummy interconnection is a 2 mil strip of Kapton the same width as the silver interconnection (0.26 inch). It is similarly bonded across the gap with SMRD 745.

Five cell by five cell modules were constructed for each configuration and checked for stiffness against comparable solar cell modules. The test modules included Configurations 1 and 2 and a module without simulated interconnections.

Figures 3.4-14, -15, and -16 show the deflection test set up and modules undergoing deflection testing in both the "face up" and "face down" directions. Figure 3.4-17 and -18 are graphs of the data obtained during the deflection tests. The area of most relevance is along the "0" grams load line where the units were being supported at the edges and deflected only by their own weight. Both dummy configurations approximate the no-load stiffness of the solar cell assemblies, and the wide

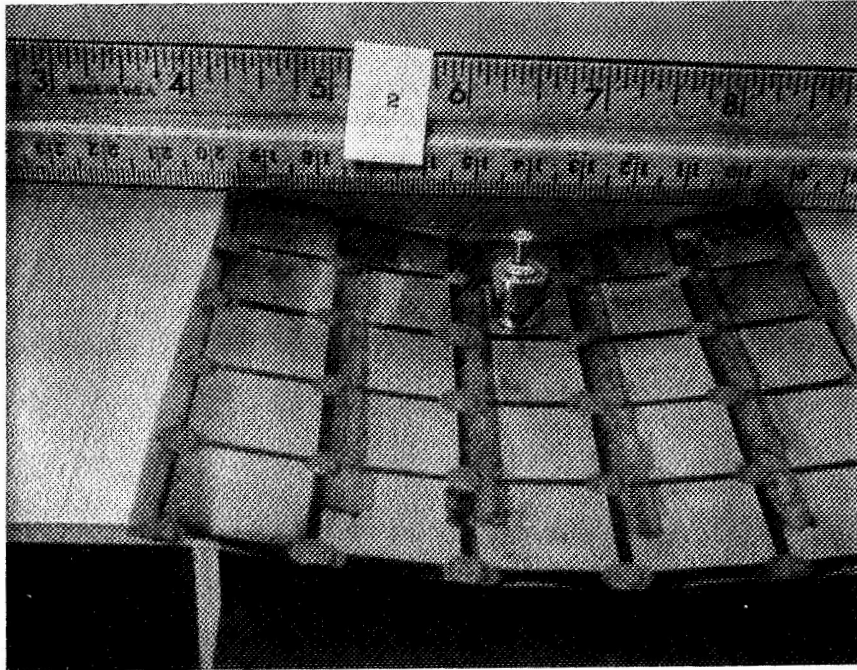


Figure 3.4-15. Face-Down Deflection Test - Active Solar Cell Module No. 1
With 5 gram load.

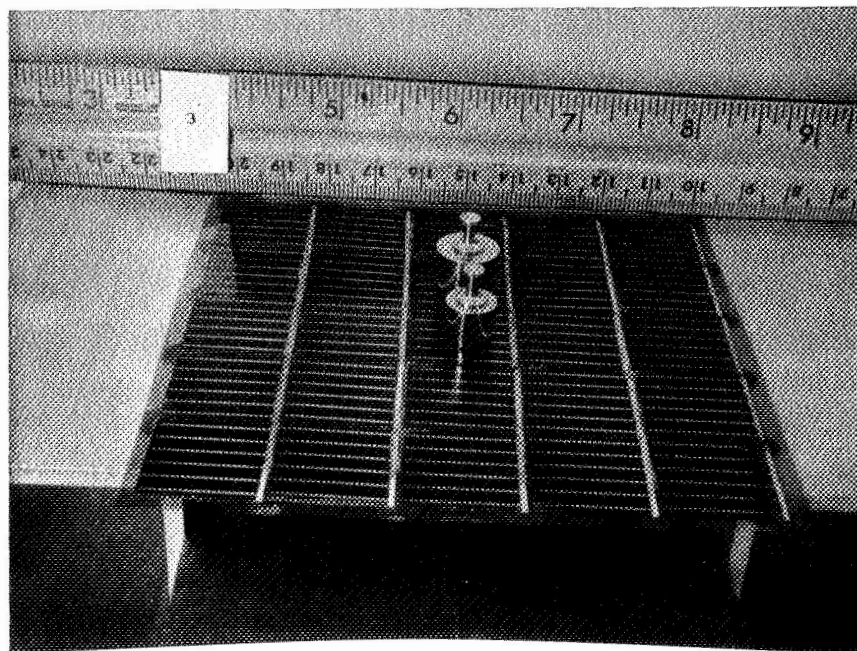
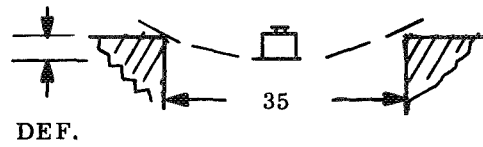
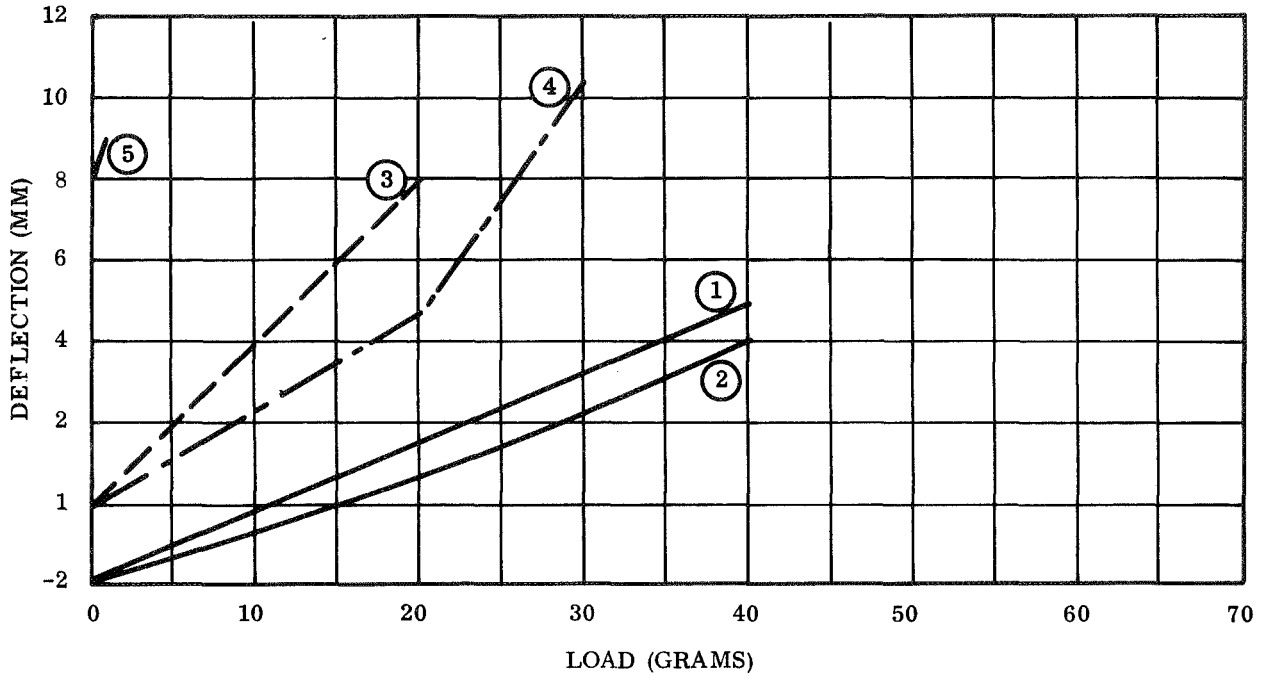


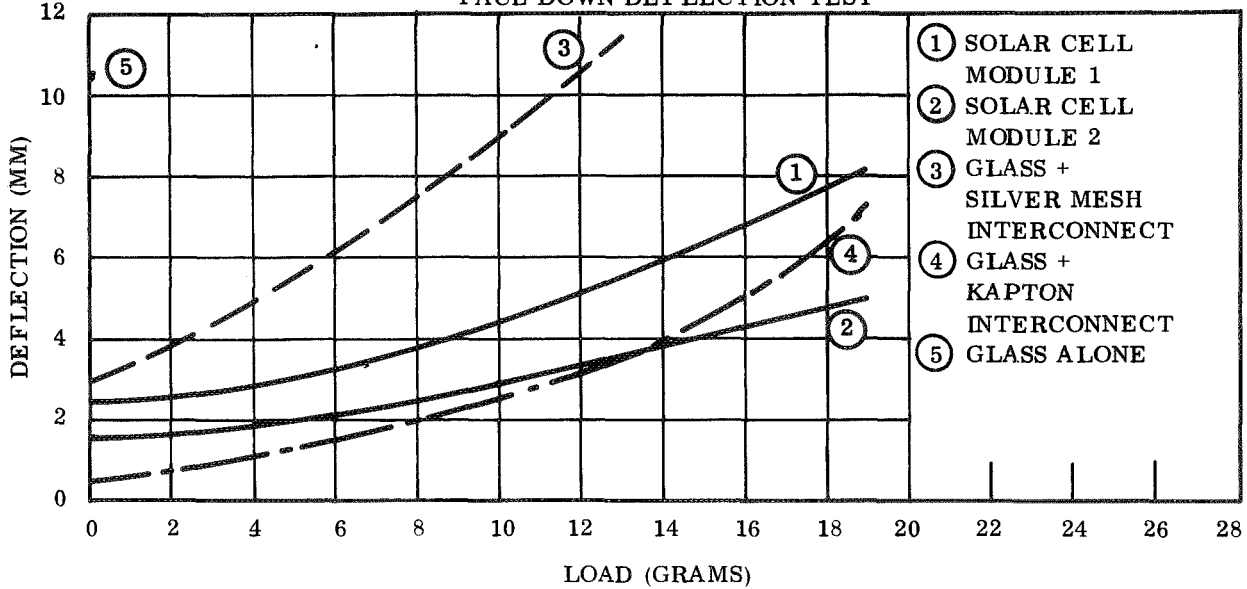
Figure 3.4-16. Face Up Deflection Test - Active Solar Cell Module No. 1
With 15 gram load.



FACE UP DEFLECTION TEST



FACE DOWN DEFLECTION TEST



- ① SOLAR CELL MODULE 1
- ② SOLAR CELL MODULE 2
- ③ GLASS + SILVER MESH INTERCONNECT
- ④ GLASS + KAPTON INTERCONNECT
- ⑤ GLASS ALONE

Figure 3,4-17 Load Deflection Curves

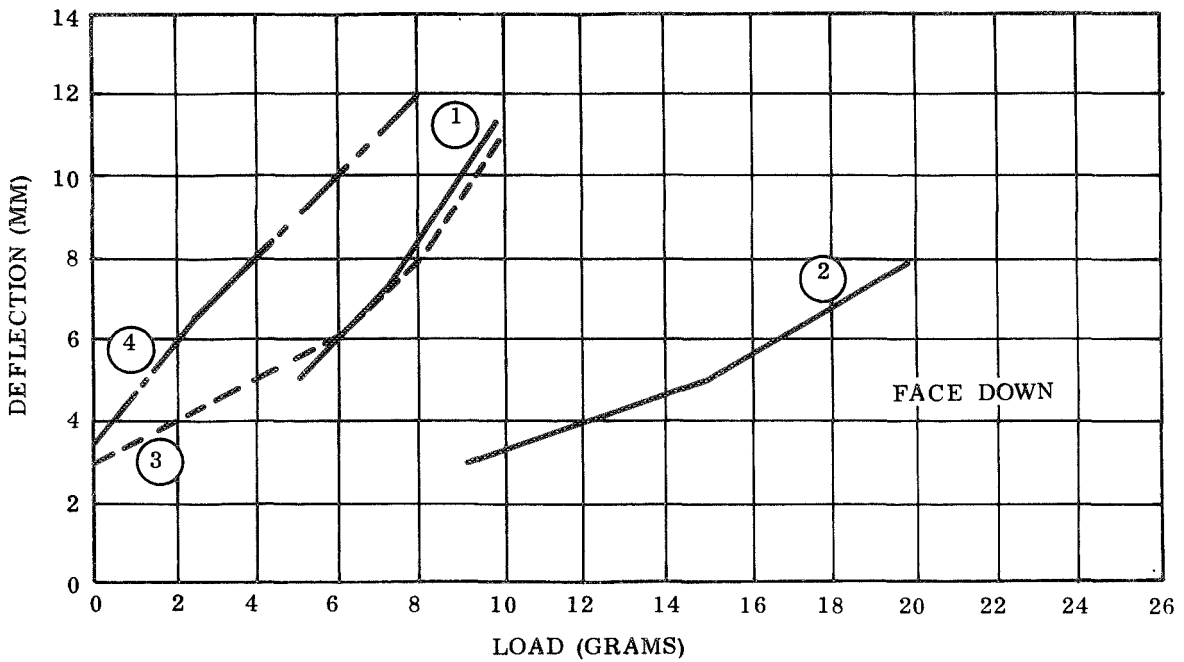
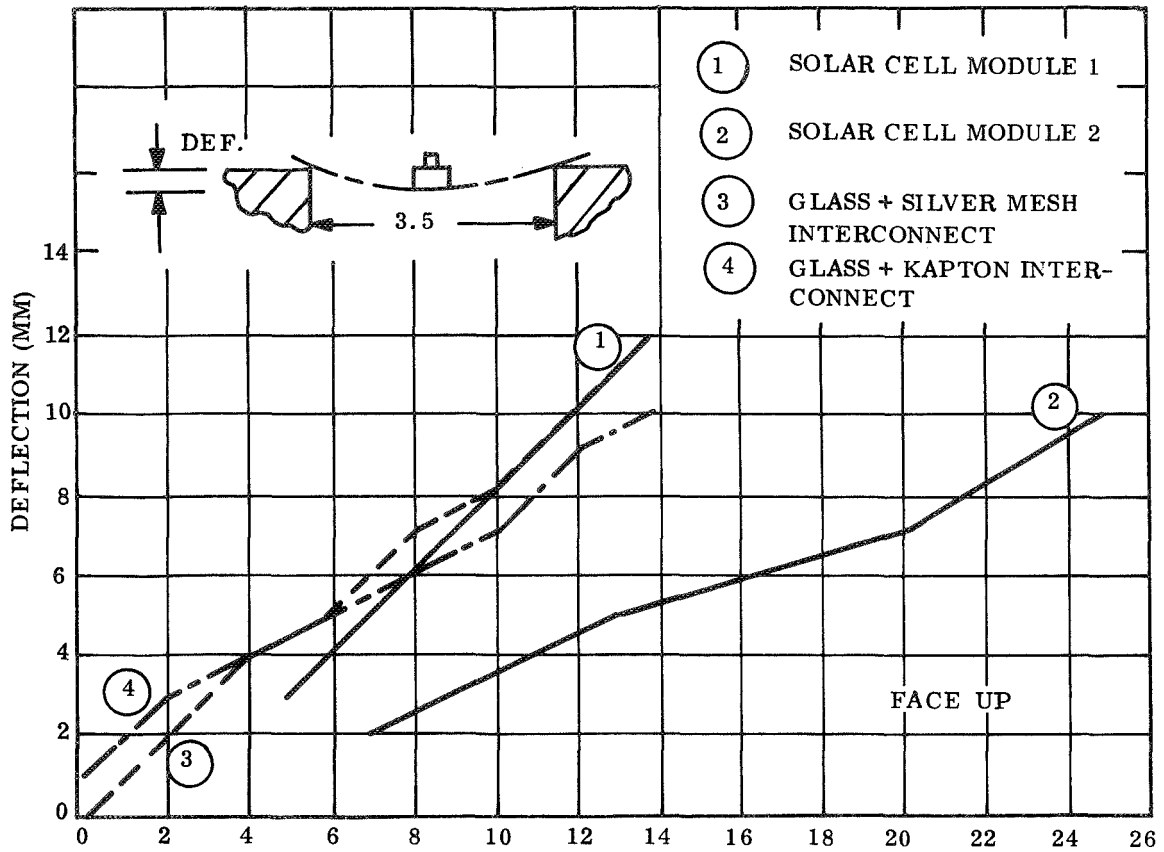


Figure 3.4-18 Load Deflection Curves - Transverse Curvature

margin separating the group from the "glass only" module highlights the need for inclusion of a simulated interconnection.

Additional load-deflection data was obtained in the transverse direction (with the interconnections perpendicular to the supporting edges). These data are shown in Figure 3.4-18. There is an appreciable variation in the stiffness of the two solar cell modules which is probably due to a variation in the bonding process. Both types of dummy construction using interconnection simulation (silver mesh and 2 mil Kapton strips) closely correlate with solar cell module No. 1.

The Kapton strips are considered to provide the best simulation of the stiffness of the solar cell modules, and these strips were incorporated into the dummy modules on the solar cell blanket for the test unit.

3.5 PROBLEMS AND LESSONS LEARNED

The intent of the program was to develop lightweight solar array technology and document results so they could be utilized. Program results are given in the five reports (Four Quarterly plus a final report) and were published as they were obtained. The major results are readily available in the reports. However, a careful reading of the reports is necessary to identify and understand some of the important, but smaller scale, results. In order to provide maximum benefit to future lightweight array programs the following items (not included in

Section 4 - Conclusions) were identified:

1. Structural Bonding - During fabrication of the magnesium drums it was found that the bond strength of the DOW 17 finish to the base material was less than the adhesive (EPON 934) bond strength. Test coupons, made up of the anodized coupons, exhibited lower shear strengths than can be achieved with EPON 934 on properly treated bare metal. The structural bonds had adequate strength for this application but other applications using bonded magnesium structures should take this into account.

2. Boom Thermal Bending Tests - The results obtained on this program are another example of the difficulty in resolving the thermal bending aspects of deployable booms. It is difficult to understand and apply the test results even though they were obtained in a facility that has been utilized for this type of testing for several years. It may be that the behavior of the deployable booms is erratic and the major source of the difficulty. In any case it should be recognized that measuring the thermal bending characteristics of deployable booms is difficult and that accurate analytical techniques for predicting this phenomena are not available.

3. Assumption of Symmetry - Symmetry was assumed in the selection of sensor locations for the deployed dynamics testing. The non-symmetry in the engineering model was sufficient to eliminate purely symmetric and anti-symmetric response. If the test were to be repeated, the sensor arrangement would be modified to measure the response of both blankets and not rely on obtaining symmetric (and anti-symmetric data). This experience should be factored into test planning for future programs.

SECTION 4
CONCLUSIONS

The following conclusions were derived from the results of the program:

1. It is possible to design a 250 square foot rollup solar array which exceeds a baseline performance of 30 watts per pound for space applications. Detailed manufacturing drawings for such an array were produced; the design was verified by analysis; the weight and performance were verified by building a full-scale engineering model; and the design integrity was established by a series of environmental tests.
2. Design performance predictions of slip ring and solar cell blanket bus network resistance were verified by measurement.
3. Performance data on six different solar cell module configurations candidates for rollup solar array applications were obtained. These configurations range from those being used on current solar panel production to configurations intended specifically for rollup solar array applications. All configurations can be considered feasible for this application though significant differences in weight, temperature range capability, and flexibility exist.

4. Results of array retraction tests on this program shows that blanket tracking can be achieved by careful alignment during installation. Special control devices to aid blanket tracking during retraction should not be needed.
5. The more than fifty complete deployment/retraction cycles provides assurance that the design has a multi-cycle life capability. The life limiting item in the design with respect to deployment/retraction cycles is considered to be the BI-STEM actuator. Life tests on the BI-STEM alone would provide more insight on the system deployment/retraction life capability.
6. The array system demonstrated excellent structural integrity in severe mechanical environments (sine and random vibration, acoustic noise, and mechanical shock). The dynamic response of the solar array blanket mass was low which resulted in low structural loads and stresses. An indication of the structural capability is that extra runs (at least 10) of sinusoidal excitation (5 to 100 Hz) at Qualification Level were made without causing structural failures. These runs were made to observe and photograph blanket motion.
7. The array system was shown to perform in thermal vacuum conditions though the low temperature retraction test results are clouded by a fouled thermocouple wire. The design margin in the Negator spring

at low temperatures is small and may even be negative. The predicted thermal transients of the array blanket were verified by test. The stowed thermal characteristics were found to be approximately as predicted though analytical predictions and test results did not agree in all details. The integrity of the solar cell modules with silver mesh interconnects over the range of -130C to +140C was demonstrated in a 34 cycle test.

8. Solar cell and dummy glass breakage during the program exceeded the goal of zero. Breakage can be attributed to a number of reasons and no specific gross failure mode was identified. Handling and instrumentation installation (and removal) caused a significant fraction of the failures. Special handling techniques and strict observance of the established procedures are required for a flight hardware program. The solar cell end coverglass breakage resulting from the environmental testing program was significantly greater than the dummy glass platelet breakage. The relative percentage of breakage follows the relative difference in individual element thickness with the 3 mil coverglass at 3.25 percent total breakage, the 7 mil solar cells at 1.75 percent, and the 11 mil dummy glass platelets at 0.47 percent. Based on this data, it appears that the coverglass and solar cell breakage due to the environmental test program can be reduced by increasing the thickness of these items.

The most severe environment with respect to coverglass and solar cell breakage was the stowed vibration series. The distribution of active module breakage on the blankets indicates that the most severe environment occurs on both the inner and the outer wraps of the stowed array. Handling is perhaps the most damaging of all environments. The edges of the blanket and the outer wrap of the stowed array are particularly vulnerable to damage. It was impossible to account for all handling and instrumentation damage and separate it from damage which occurred as a result of the actual test environments. Special handling procedures and strict observance of established handling procedures will be required in a flight program.

- 9.9. The solar cell damage cited in Conclusion 6 did not result in a corresponding reduction in electrical performance.
10. The array blanket design and fabrication process used to produce the engineering prototype model do not yield a product which meets accepted standards for appearance. Voids in the adhesive between the cells and the substrate resulted from the wrinkles which were inherent in the copper clad substrate material where the majority of the copper was etched away.
11. New techniques of low frequency structural dynamics testing were demonstrated. These included frequency sinusoidal excitation, slow sweep rates, a hyperbolic sweep rate for efficient testing, electro-

optical methods of measuring displacements, and low frequency vibration data analysis.

12. The dynamic characteristics of the deployed array were measured and the results compared with analysis. Excellent agreement was obtained from the lowest out-of-plane symmetric mode. Agreement for the higher out-of-plane modes was fair. The experimental results for the in plane motion differed from the analytical predictions.

13. As a result of specific failures the following design modifications are required for a flight design:
 - a. Redesign of limit switch follower in BI-STEM actuator.,
 - b. Specification of a different material for the separation nut mounting flanges (if low temperature operation is required).
 - c. Selection of a different temperature transducer on the blanket.

14. With respect to mechanical environment tests, it was found the high frequency mechanical vibration environment is not representative of a spacecraft application. Even with a 600 pound vibration fixture high frequency excitation is not adequately transmitted from the shaker to the array structure and certainly not to the blankets. Acoustic excitation provides the best means of introducing high frequency to the solar array blankets though the admittance is low.

Pyrtotechnics provide a means of obtaining a reasonable simulation of the shock environment to be expected on a spacecraft.

15. The test program provided some unanticipated results. These included:
 - a. A greenhouse heating effect in the stowed solar array blankets.
 - b. Low dynamic response of solar cell blankets.
 - c. High first natural frequency resonant (in-plane mode)
 - d. Blanket slack during stowed vibration

16. New data of general applicability to rollup array and other programs includes:
 - a. BI-STEM thermal deflection data
 - b. Solar array blanket stiffness data
 - c. Damping characteristics of deployed array

SECTION 5

RECOMMENDATIONS

The following recommendations are based on the results of this program. In general, the recommendations address the additional effort which is applicable to the use of rollup solar arrays for flight applications.

With respect to rollup solar array technology applicable to the design and application of different sizes and configurations, the following activities are recommended:

1. An investigation of the wrap tension needed to stabilize the blankets during stowed vibrations should be accomplished.
2. An investigation of the dynamic loads caused by stowed solar array blankets during launch vibrations be carried out to provide design data for techniques used in this program produced grossly conservative results.
3. A study of the in-plane structural characteristics to determine the effects of blanket tension forces on the structural characteristics be made. This information can be used to upgrade mathematical models of in-plane dynamic characteristics.
4. Long term thermal cycling tests of various module configurations are recommended to form the basis for selection of the best interconnect approach for possible earth orbiting mission applications.
5. Additional environmental tests which would reduce unknowns for future applications include: acceleration, launch depressurization, a repeat of the low temperature retraction cycles, and long term thermal cycling tests.
6. Design concepts which provide modularization of the blanket assembly should be investigated. These would allow replacement of sections of the array in the event of accidental damage and would facilitate manufacturing and assembly.

7. Fabrication methods/blanket redesigns which would eliminate the wrinkles (and resulting adhesive voids) in the blanket substrate should be investigated.

For the 250 square feet design configuration, the following design changes should be made prior to a flight application:

- a. Redesign the limit switch followers in the B1-STEM actuator.
- b. Select a new temperature transducer (if temperature is to be measured).
- c. Specify a different material for the mounting flanges of the pyrotechnic nuts (if low temperature deployment is needed).
- d. Investigate the design margin in the Negator spring motors at low temperature (if low temperature retraction is required).
- e. Specific unusual mission requirements must be individually evaluated.

SECTION 6
NEW TECHNOLOGY


No items of new technology have been reported during the course of this contract.

,

SECTION 7

REFERENCES

- 1-1. Feasibility Study 30 Watts Per Pound Rollup Solar Array Final Report
Report No. 68SD4301, 21 June 1968, JPL Contract 951970, General Electric Company, Philadelphia, Pa.
- 1-2. Detail Specification for 30 Watts Per Pound Rollup Solar Cell Array, Rev. E, JPL Specification SS501407.
- 1-3. Quarterly Report No. 1, Rollup Subsolar Array. Report No. GE-SSO-69SD4282, 12 June 1969. JPL Contract 952314. General Electric Company, Philadelphia, Pa.
- 1-4. Quarterly Report No. 2, Rollup Subsolar Array. Report No. GE-SSO-69SD4351, 15 September 1969. JPL Contract 952314. General Electric Company, Philadelphia, Pa.
- 1-5. Quarterly Report No. 3, Rollup Subsolar Array, Report No. GE-SSO-69SD4373, 15 December 1969. JPL Contract 952314. General Electric Company, Philadelphia, Pa.
- 1-6. Quarterly Report No. 4, Rollup Subsolar Array. Report No. GE-SSO-70SD4225, 13 March, 1970. JPL Contract 952314. General Electric Company, Philadelphia, Pa.
- 1-7. Hok, Gunnar, "Response of Linear Resonant Systems to Excitation of a Frequency Varying Linearly with Time", Journal of Applied Physics, August, 1947.
- 1-8. Final Program Briefing - Lightweight Solar Panel Development Program. 15 July 1970. JPL Contract 952571. The Boeing Company, Seattle, Wash.
- 1-9. Deployable Large Area Solar Cell Array Testing. Report No. 20869-4. JPL Contract 951107. Ryan Aeronautical Company, San Diego, California.

GENERAL  ELECTRIC
SPACE DIVISION
SPACE SYSTEMS ORGANIZATION